國立交通大學

電信工程研究所

博 士 論 文

中繼站輔助細胞網路之系統設計與最佳化

On the System Design and Optimization of Relay-Assisted Cellular Networks

研 究 生：林香君

指導教授：黃家齊　教授

沈文和　教授

中 華 民 國 九 十 九 年 三 月

中繼站輔助細胞網路之系統設計與最佳化

On the System Design and Optimization of Relay-Assisted Cellular Networks

研 究 生： 林香君　　Student： Shiang-Jiun Lin

指導教授： 黃家齊　　Advisor： Chia-Chi Huang

沈文和　　Wern-Ho Sheen

國 立 交 通 大 學

電 信 工 程 研 究 所

博 士 論 文

A Dissertation

Submitted to Institute of Communication Engineering

College of Electrical and Computer Engineering

National Chiao Tung University

in Partial Fulfillment of the Requirements

for the Degree of Doctor of Philosophy

in

Communication Engineering

March 2010

Hsinchu, Taiwan, Republic of China

中華民國九十九年三月

中繼站輔助細胞網路之系統設計與最佳化

研究生：林香君　　指導教授：黃家齊 博士

沈文和 博士

國立交通大學

電信工程研究所

中文摘要

下一世代行動通訊系統中，中繼站輔助細胞網路架構被視為一可行且具有潛力的網路架構。此架構佈放中繼站在傳統蜂巢式網路中，以多躍方式協助基地台與使用者之間的訊號傳輸。它提供一個以較低成本之佈建方式來改善細胞覆蓋，提昇使用者傳輸速率，提高細胞系統容量，以及減少使用者的上行傳輸功率。

發展中繼站輔助細胞網路之重要關鍵即是需從理論與實務等方面進行系統效能之全面性評估。本論文考慮在一般的系統配置下，探索中繼站輔助細胞網路之系統設計與優化。文中主要分為三大部份進行探討：

在第一部分研究中，我們針對中繼站輔助細胞系統在多細胞環境下之下行性能進行研究。綜合考量影響系統效能之系統參數：中繼站之佈放位置、使用者之路徑選擇、頻譜資源重用、資源配置等，以及考慮兩種使用者體驗品質，即固定頻寬分配與固定傳輸速率分配，我們提出以基因演算法為基礎之演算法進行中繼站輔助細胞網路之系

統效能之優化。實驗結果顯示，相較於傳統網路架構，中繼站輔助細胞網路之下行細胞容量以及使用者之傳輸速率大大地被提昇。

在論文的第二部分，我們提出中繼站輔助細胞之上行效能之設計與最佳化。在上行效能中，使用者平均傳輸功率消耗以及上行系統的頻譜利用效率是兩個重要的效能指標。文中考慮中繼站的佈放位置、頻率重用模式、使用者之路徑選擇以及資源分配等系統參數進行系統設計。利用基因演算法搭配一個多重存取干擾估算演算法對中繼站輔助細胞系統進行效能之優化。實驗結果表明，中繼站輔助細胞網路之上行細胞容量獲得提昇，以及使用者之上行傳輸功率消耗獲得改善。

在第三部分研究中，我們考慮在似曼哈頓式環境中，多跳躍式中繼網路的傳輸排程問題。利用似曼哈頓式環境中的高遮蔽效應，搭配在基地台與中繼站之指向性天線，文中提出有效率之傳輸排程方法以提昇此環境下之細胞系統容量。實驗結果指出，在似曼哈頓式環境中，基地台與中繼站搭配指向性天線，可有效提升系統頻譜效能。

本論文從理論與實務兩方面，針對中繼站輔助細胞網路進行研究。我們考慮在不同的系統配置下，中繼站輔助細胞網路之上行與下行之設計優化與理論效能。我們亦考量在似曼哈頓環境中，中繼站輔助細胞網路之實際的傳輸排程問題。綜合實驗結果說明，中繼站輔助細胞網路可提昇使用者傳輸速率，提高細胞系統容量，以及減少使用者的上行傳輸功率，並且提供似曼哈頓環境中較好的細胞覆蓋。

On the System Design and Optimization of Relay-Assisted Cellular Networks

Student：Shiang-Jiun Lin　　Advisor：Dr. Chia-Chi Huang

Dr. Wern-Ho Sheen

Department of Communication Engineering

National Chiao Tung University

Abstract

Deploying fixed relay stations (RSs) in traditional mobile cellular networks is widely recognized as a promising technology in next generation mobile communication systems to improve cell coverage, user throughput and system capacity, to save transmit power of a mobile station (MS) in the uplink, and to provide a low cost deployment for coverage extension.

One crucial step toward developing such a relay-assisted cellular network is to fully evaluate its performance from both theoretical and practical points of view. In this dissertation, we aim to explore the system design and the optimization of relay-assisted cellular networks in multi-cell environment by considering general system configurations.

In the first part of this dissertation, we aim to investigate the downlink performance

limits of a general relay-assisted network with optimized system parameters in a multi-cell environment. Two types of quality of end-user experience (QoE), i.e., fixed bandwidth allocation and fixed throughput allocation, along with two path selection methods, i.e., spectral-efficiency based and signal-to-noise-plus-interference ratio based are investigated. A genetic algorithm (GA) based method is proposed for joint optimization of system parameters, including the number of RSs and their locations, frequency reuse pattern, path selection and resource allocation so as to maximize the system spectral efficiency. Numerical results show that significant improvement on the system spectral efficiency and the user throughput are achieved in the relay-assisted cellular network.

In the second part, the aim is to study the uplink performance of a relay-assisted cellular network. Two performance measures, average power consumption of mobile stations and uplink system spectral efficiency, are optimized by jointly considering the system parameters of RSs' locations, reuse patterns, path selections and resource allocation. GA-based method along with a method of MAI (multiple access interference) estimation is applied to solve the optimization problem. Numerical results show that with proper deployment of RSs both power consumption of MSs and the system capacity are remarkably improved in the uplink.

In the third part, we investigate the important issue of resource scheduling for multi-hop relay networks in the Manhattan-like environment. New resource scheduling methods are proposed for the multi-hop relay network with directional antennas equipped at both the base station and relay stations. By taking advantage of the effect of high degree shadowing in the Manhattan-like environment, the system throughput can be largely increased by the proposed methods as compared to the system with omni-directional antennas.

In this dissertation, the theoretical performance in both downlink and uplink with general configurations in relay-assisted cellular networks is presented. The practical issues of resource scheduling of relay-assisted cellular networks in the Manhattan-like environment is also addressed. With comprehensively evaluations, we can conclude that a relay-assisted cellular system is with the benefits to improve the system capacity and the user throughput, to save transmit power of an MS in the uplink, and to provide better coverage in the Manhattan-like environment with the optimized system parameters.

To my family

Acknowledgements

It is a great pleasure to thank those who made this dissertation possible. First of all, I heartily thank my advisors, Professors Chia-Chi Huang and Wern-Ho Sheen. In addition to the solid research training, they also set a good example for me to be positive and optimistic toward every challenge. With their guidance, advice and encouragement, it was in the end what made this work accomplished.

Special thanks to Professor Dr.-Ing. Bernhard Walke in RWTH Aachen University, Aachen, Germany and Professor Jenq-Neng Hwang in University of Washington, WA, USA, who broadened my perspective of thought and made me more confident during my visit with their research groups. Thanks also go to my doctorial committee members, Professors Chung-Jr Chang, Jhy-Horng Wen, Ching-Yao Huang, Ray-Guang Cheng, and Yuh-Ren Tsai, for their valuable comments and suggestions to make this work more complete.

I would also like to show my gratitude to my lab mates in both the Wireless Communication Lab and Broadband Radio Access System (BRAS) Lab. Their company made my Ph.D. life more wonderful and joyful.

This dissertation is dedicated to my family — my parents, my brother, and my husband — for their love, support and understanding; this great power encourages me deeply and endlessly.

Last but not least, I offer my regards and blessings to all of those who supported me in any respect during the completion of my graduate studies.

Contents

中文摘要 i

Abstract iii

Acknowledgements vii

Contents viii

List of Figures xii

List of Tables xv

Acronyms xvi

Chapter 1 Introduction 1

1.1 Evolution of Cellular Communication Systems 2

1.2 Requirements of IMT-Advanced Systems 3

1.3 Key Technologies toward IMT-Advanced Systems 6

1.3.1 Transmission Technology and Multiple Access Scheme – OFDMA 6

1.3.2 Carrier Aggregation 7

1.3.3 Multiple-Input Multiple-Output Antenna Technology 7

1.3.4 Coordinated Multi-Point Transmissions and Receptions 8

1.3.5 Relaying Technology 9

1.4 Overview of Relay-Assisted Cellular Networks 9

1.4.1 Classifications of Relay Stations 10

1.4.2 Relay Operation Modes 11

1.5 Problem and Motivation 12

1.6 Organization of the Dissertation 14

Chapter 2 Downlink Performance and Optimization of Relay-Assisted Cellular Networks in Multi-cell Environments 15

2.1 Background 16

2.2 System Setups 17

2.2.1 Cell configuration 17

2.2.2 Relaying technology 18

2.2.3 Propagation Models 21

2.2.4 Antenna Configurations 23

2.2.5 Power Setting of BS and RS 23

2.2.6 Path Selection 25

2.2.7 Frequency Reuse over RS-MS Links 25

2.3 Optimization of System Parameters 26

2.3.1 Objective Function 26

2.3.1.1 Fixed Bandwidth Allocation 27

2.3.1.2 Fixed Throughput Allocation 29

2.4 Genetic-Based Optimization 31

2.4.1 Overview of Genetic Algorithm 31

2.4.2 Optimization via Genetic Algorithm 33

2.5 Simulation Results 35

2.5.1 Single Cell 36

2.5.1.1 Frequency Reuse over RS-MS Links 46

2.5.1.2 Shadowing Effects 50

2.5.1.3 Sectorization 52

2.5.2 Multiple Cells 54

2.6 Summary 56

Chapter 3 Uplink Performance and Optimization of Relay-assisted Cellular Networks 57

3.1 Background 58

3.2 System Setups 58

3.3 Problem Formulation 59

3.3.1 Measure 1—Minimization of Average MS's Transmit Power 60

3.3.2 Measure 2—Maximization of Uplink System SE 62

3.4 Genetic-Based Optimization 65

3.4.1 MAI Estimation Algorithm 67

3.5 Simulation Results 68

3.5.1 Measure 1—Minimization of Average MS's Transmit Power 68

3.5.2 Measure 2—Maximization of Uplink System SE 77

3.6 Summary 84

Chapter 4 Resource Scheduling with Directional Antennas for Multi-hop Relay Networks in a Manhattan-like Environment 85

4.1 Background 86

4.2 System Setups and Propagation Models 93

4.2.1 System Setup 93

4.2.2 Propagation Models and Antenna Pattern 96

4.3 Resource Scheduling Methods 98

4.3.1 Scheduling with Omni-Directional Antennas 98

4.3.2 Scheduling with Directional Antennas 100

4.3.2.1 Method-1 100

4.3.2.2 Method-2 105

4.4 Numerical Results 109

4.5 Summary 116

Chapter 5 Conclusions 117

References 120

Appendix 127

Vita 130

List of Figures

Figure 1. Examples of (a) contiguous carrier aggregation, and (b) non-contiguous carrier aggregation. 7

Figure 2. An example of CoMP joint processing. 8

Figure 3. The multi-cell architecture $(3,3,3)$ 19

Figure 4. (a) A detailed layout of a cell, and (b) the radio resource allocation. 20

Figure 5. A simplified shadowing model. 22

Figure 6. The general operation principle of GAs. 32

Figure 7. Optimal RSs' positions and throughput distribution for FBA-SE. 38

Figure 8. CDF of user throughput for FBA-SE. 39

Figure 9. Convergence behavior of the proposed GA for FBA-SE ($N = 6$) under different control parameters $(N_{pop}, \beta, P_{mut})$ 41

Figure 10. Complementary CDF of bandwidth consumption for FTA-SE. 44

Figure 11. System SE of four system configurations. 45

Figure 12. Throughput distribution (bps per unit area) of different frequency-reuse patterns for FBA-SE ($N=6$). 47

Figure 13. System SE of different frequency-reuse patterns ($N=6$). 48

Figure 14. Throughput distribution (bps per unit area) of FBA-SE under shadowing effects. 51

Figure 15. Optimal RSs' positions and bandwidth consumption (Hz per unit area) for FTA-SE in a three-sector cell. 53

Figure 16. RSs' positions and bandwidth consumption (Hz per unit area) with joint

optimization of B_1, B_2 and B_3 in Figure 3 for FTA-SE. 55
Figure 17. The operation of genetic algorithm. 66
Figure 18. Optimal RSs' positions and uplink transmit power distribution (in dBm). 71
Figure 19. Complement CDFs of uplink transmit power. 72
Figure 20. Transmit power distributions (in dBm) of different frequency-reuse patterns. 74
Figure 21. Optimal RSs' positions and uplink transmit power distribution (in dBm) in shadowed environment. 76
Figure 22. Optimal RSs' positions and uplink throughput distribution. 78
Figure 23. CDF of link SE for P_M=15 dBm. 79
Figure 24. Optimal RSs' positions and uplink SE distribution (bps/Hz) in shadowed environment. 82
Figure 25. Relay-assisted cell architecture in a Manhattan-like environment—Scenario 1. ... 88
Figure 26. Multi-cell setup of Scenario 1. 89
Figure 27. Transmission frame structure of Scenario 1. 90
Figure 28. Relay-assisted cell architectures in a Manhattan-like environment—Scenario 2... 91
Figure 29. Frequency reuse pattern in the multi-cell environment of Scenario 2. 92
Figure 30. The deployment of BS and four RSs and their serving areas. 94
Figure 31. The relevant distances from BS to determine the path loss and the probability of having LOS. 95
Figure 32. Resource scheduling with omni-directional antennas. 99
Figure 33. Two phases of transmissions in Method-1, (a) Phase 1 and (b) Phase 2. 101
Figure 34. Two phases of transmissions of the neighboring cells in Method-1, (a) Phase 1 and (b) Phase 2. 103
Figure 35. The frame structure of Method-1. 104

Figure 36. Two phases of transmissions in Method-2, (a) Phase 1 and (b) Phase 2. 106

Figure 37. Two phases of transmissions of the neighboring cells in Method-2, (a) Phase 1 and (b) Phase 2. 107

Figure 38. The frame structure of Method-2. 108

Figure 39. The CDF of SINR for different scheduling methods. 112

Figure 40. Comparisons of cell capacity between different scheduling methods. 114

List of Tables

Table 1. IMT-Advanced requirements 5

Table 2. Important parameters for four system setups. 40

Table 3. Important parameters for frequency reuse patterns (*N*=6). 49

Table 4. System parameters of Measure 1 for *N* = 0 to *N* = 10. 70

Table 5. System parameters for different frequency-reuse patterns of Scenario 1, *N = 6*. 75

Table 6. System parameters of Measure 2 for *N* = 0 to *N* = 10. 80

Table 7. System parameters for different frequency-reuse patterns of Measure 2, *N* = 6. 83

Table 8. The propagation loss model for the urban micro-cell environment. 97

Table 9. OFDMA parameters for system-level simulation. 110

Table 10. The used MCS. 111

Table 11. The analysis of the capacity gain. 115

Acronyms

3GPP	3rd Generation Partnership Project
AF	amplify-and-forward
AMPS	Advanced Mobile Phone System
AWGN	Additive White Gaussian Noise
BS	base station
CDF	cumulative distribution function
CDMA	code division multiple access
CoMP	coordinated multi-point transmissions and receptions
DF	decode-and-forward
DSP	digital signal processing
EDGE	Enhanced Data rates for GSM Evolution
ETACS	European-TACS
FBA	fixed bandwidth allocation
FCC	Federal Communications Commission
FDMA	frequency division multiple access
FTA	fixed throughput allocation

GA	genetic algorithm
GPRS	General Packet Radio Service
GSM	Global System for Mobile communications
IEEE	Institute of Electrical and Electronics Engineers
IMT-2000	International Mobile Telecommunications - 2000
ITU-R	International Telecommunication Union - Radio communication sector
ISI	inter-symbol interference
LOS	line of sight
LTE	Long Term Evolution
LTE-Advanced	Long Term Evolution- Advanced
MAI	multiple access interference
MCS	modulation and coding scheme
MIMO	multiple-input multiple-output
MS	mobile station
NLOS	non line of sight
OFDM	orthogonal frequency-division multiplexing
OFDMA	orthogonal frequency-division multiple access

PSD	power spectral density
QoE	quality of end-user experience
QoS	quality of service
RF	radio frequency
RS	relay station
SE	spectral efficiency
SINR	signal-to-noise-plus-interference ratio
SMS	short message service
TACS	Total Access Communication System
TDMA	time division multiple access
VLSI	very large scale integration
WCDMA	Wideband Code Division Multiple Access

Chapter 1
Introduction

Wireless communications and networks over the last decades have experienced rapid growth. Thanks to the advanced development in wireless access techniques, and the dramatic progress in digital signal processing (DSP) and very-large-scale integration (VLSI) circuits. To further fulfill the increasing demand for various wireless applications and to better provide ubiquitous services with good quality to users, the evolution trend is still ongoing and will continue in the future.

Among wireless communications, cellular systems are one of the most successful wireless applications in the world and have tremendously changed our daily lives. The cellular radio idea was first emerged by Bell Laboratories in 1940s [1], the cellular plan was submitted to FCC (Federal Communications Commission) in 1971 [2], and the first cellular system was commercialized in 1980s [3]. The essential features of cellular concept are summarized by frequency reuse and cell splitting [1]. A cellular system divides a service area into multiple cells, where each cell is covered and served by a base station (BS). Due to the physical phenomenon that radio signal attenuates by distance, the frequency spectrum

can be reused when the co-channel interference is not objectionable. In order to support the growth in traffic, a single cell can be further split into several smaller cells with lower power so as to reuse frequency more times, which is known as cell splitting. Cellular calls are transferred from one BS to another as a mobile station (MS) moves from cell to cell. These characteristics provide cellular networks with a number of advantages, such as spectrum efficiency improvement, system capacity increment, and BS transmission power reduction, over alternative solutions.

1.1 Evolution of Cellular Communication Systems

In 1980s, Advanced Mobile Phone System (AMPS) was developed by Bell Labs and launched in United States to afford wireless voice services by using analog signaling with frequency division multiple access (FDMA) [3]-[5]. Meanwhile, Total Access Communication System (TACS) and its extended version, European-TACS (ETACS), were used in some European and Asian countries. These are known as *the first generation mobile communication systems* (1G).

With more demands other than the voice services, the digital mobile communications were started in 1990s, known as *the second generation mobile communication systems* (2G), including Global System for Mobile Communications (GSM), IS-136, which are time division multiple access (TDMA) systems, and IS-95, which is a code division multiple access (CDMA) based system [4], [5]. 2G systems provided more efficient transmissions in terms of spectral utilization and power consumption by using digital signaling. Moreover, data services for mobile were also introduced in 2G, starting with short message service (SMS).

Evolved from 2G to 3G (*the third generation mobile communication systems*), several

systems were with enhanced functionality as compared to 2G, named 2.5G or 2G transitional, such as General Packet Radio Service (GPRS) and Enhanced Data rates for GSM Evolution (EDGE) for GSM.

In the late 1990s, *International Telecommunication Union - Radio communication Sector* (ITU-R) had defined *International Mobile Telecommunications - 2000 (IMT-2000)* as framework of the global standard 3G [6]. Evolved from narrowband to wideband, 3G wireless communication systems allow people access a wider range of advanced multimedia applications anytime and anywhere, such as video conferencing, Voice-over-IP (VoIP), faster web browsing, gaming, and audio/video streaming. Main trends of 3G systems are *Wideband Code Division Multiple Access* (WCDMA) and CDMA2000.

In fact, such evolution trend is not over yet. Next generation wireless communication, known as 4G (*the forth generation mobile communication systems*), is envisioned to provide high-data-rate multimedia services, ubiquitous network connectivity, and seamless services in a wide variety of environments, such as indoors, outdoors, low-mobility, and high-mobility, at an affordable cost [5]. ITU-R has specified the next generation 4G mobile systems with new capabilities of IMT which go beyond those of IMT-2000 as *IMT-Advanced* [7].

1.2 Requirements of IMT-Advanced Systems

The IMT-Advanced system is expected to afford access to telecommunication services with various applications in various ways. In [8], it is specified that IMT-Advanced systems support mobility applications from stationary (0 km/h) to high speed vehicular (120 to 350 km/h), and provide a wide range of data rates and service demands in multi-user environments. IMT-Advanced systems are with advanced packet-based services and have

capability to provide high-quality multimedia applications.

The key features of IMT-Advanced systems are summarized in Table 1. As can be seen, IMT-Advanced systems support peak data rates of up to approximately 100 Mbps for high mobility access and up to approximately 1 Gbps for stationary or low mobility wireless access, which makes multimedia applications, such as video on demand, much more capable. In addition to peak data rate, IMT-Advanced has also specified the targeted spectral efficiency in terms of peak, cell, and cell edge user perspectives for different test environments and antenna configurations. For example, the minimal requirements of average spectral efficiency in downlink should be 3 bps/Hz, 2.6 bps/Hz, 2.2 bps/Hz, and 1.1 bps/Hz for indoor, microcellular, base coverage urban, and high speed environments, respectively, on the antenna configurations of 4 at the transmitter side and 2 at receiver side. Scalable and wider bandwidth up to and including 40 MHz should be supported in IMT-Advanced systems to achieve peak data rate requirements.

Moreover, latency and handover requirements are also specified in IMT-Advanced. The control plane latency, which is measured as the transition time from different connection modes, e.g., from idle mode to active state, should be less than 100 ms, while the user plane latency, which is known as transport delay, should be less than 10 ms in unloaded conditions for small IP packets for both downlink and uplink. To support the smooth handover across sites/networks, the handover interruption time should be within 27.5 ms for intra-frequency handover, and be within 40 ms and 60 ms for inter-frequency handover in a spectrum band and between spectrum bands, respectively.

More detailed descriptions of requirements, configurations, and evaluation criteria for IMT-Advanced systems can be found in [8].

Table 1. IMT-Advanced requirements

Metrics	IMT-Advanced Requirements	
Peak data rate	1 Gbps for stationary or low mobility 100 Mbps for high mobility	
Bandwidth (MHz)	40	
User plane latency (ms)	10	
Control plane latency (ms)	100	
Handover interruption time (ms)	Intra-freq	27.5
	Inter-freq -within a spectrum band -between spectrum bands	 40 60
Peak spectral efficiency (bps/Hz) (Antenna configurations of DL 4 × 4, UL 2 × 4)	DL	15
	UL	6.75
Average spectral efficiency (bps/Hz) (Antenna configurations of DL 4 × 2, UL 2 × 4)	DL	Indoor: 3 Microcellular: 2.6 Base coverage urban: 2.2 High speed: 1.1
	UL	Indoor: 2.25 Microcellular: 1.8 Base coverage urban: 1.4 High speed: 0.7
Cell edge spectral efficiency (bps/Hz) (Antenna configurations of DL 4 × 2, UL 2 × 4)	DL	Indoor: 0.1 Microcellular: 0.075 Base coverage urban: 0.06 High speed: 0.04
	UL	Indoor: 0.07 Microcellular: 0.05 Base coverage urban: 0.03 High speed: 0.015

1.3 Key Technologies toward IMT-Advanced Systems

In order to meet the higher data rate requirements and to provide better quality of service (QoS) to users, technology advancements in transmissions, multiple accesses, advanced antenna systems, scalable bandwidth, and cellular architectures have been fully exploited in next generation mobile systems. Two standard proposals toward next generation mobile communization systems drawn mainly attentions are 802.16m standardized by the *Institute of Electrical and Electronics Engineers* (IEEE) [9], and Long Term Evolution- Advanced (LTE-Advanced) standardized by *the 3rd Generation Partnership Project* (3GPP) [10].

In September 2009, both 3GPP LTE-Advanced and IEEE 802.16m have been submitted to ITU-R as 4G candidates. The potential key technologies toward IMT-Advanced systems which are comprehensively investigated by these standard bodies are summarized as follows.

1.3.1 Transmission Technology and Multiple Access Scheme – OFDMA

Orthogonal frequency-division multiplexing (OFDM) is an effective modulation scheme to combat inter-symbol interference (ISI) in a high-rate environment. By using parallel orthogonal subcarriers along with cyclic-prefix, ISI can be removed completely as long as the cyclic-prefix is lager than the maximum delay spread of the channel [11]. OFDM can also be used as an effective multiple access scheme, known as orthogonal frequency-division multiple access (OFDMA). OFDMA, which has been widely considered as one of the promising multiple access schemes for the next-generation system, is adopted in both the 3GPP LTE-Advanced and IEEE 802.16m [9], [10].

1.3.2 Carrier Aggregation

One reasonable way to fulfill the targets of very high peak-data rate for IMT-Advanced is to increase the transmission bandwidth. Wide and scalable bandwidth up to and including 40 MHz, which may be carried by single or multiple RF (radio frequency) carriers, should be supported in IMT-Advance [8]. The carrier aggregation method is then investigated where several contiguous or non-contiguous component carriers are aggregated on the physical layer to provide the necessary bandwidth for higher data rate transmissions [9], [10]. In Figure 1 (a), an example of contiguous carrier aggregation is illustrated, where three contiguous component carriers with 20 MHz bandwidth of each is aggregated into a wide 60 MHz bandwidth; while in Figure 1 (b), two non-contiguous component carriers with 20 MHz are aggregated to provide 40 MHz bandwidth. With the carrier aggregation methods, the bandwidth and peak data rate requirements of IMT-Advanced system might be met.

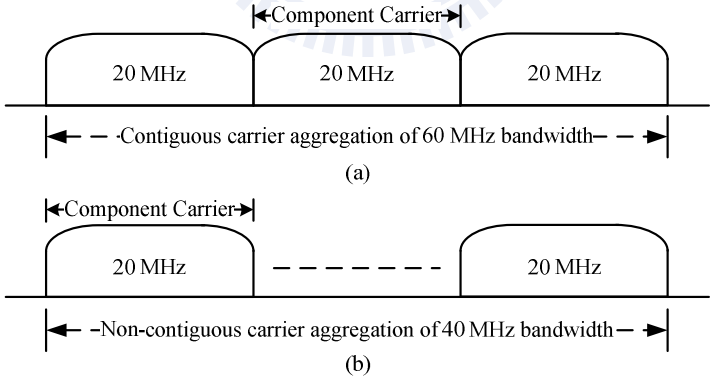

Figure 1. Examples of (a) contiguous carrier aggregation, and (b) non-contiguous carrier aggregation.

1.3.3 Multiple-Input Multiple-Output Antenna Technology

Multiple-input multiple-output (MIMO) antenna technology, which is to equip with

multiple antennas at communication devices in both transmitter and receiver sides, is used to substantially enhance the capacity of the transmission. It has been studied that the capacity of MIMO systems is linearly increased with the minimum number of transmit and receive antennas in a flat fading channel [12]. The higher order MIMO and advanced MIMO technologies, including beamforming and spatial multiplexing, will be well-integrated into next generation wireless communication system to achieve the higher spectral utilization.

1.3.4 Coordinated Multi-Point Transmissions and Receptions

One way to improve the link quality of cell-edge users is to coordinate and combine signal transmissions and receptions from/to multiple cell sites, which is known as coordinated multi-point transmissions and receptions (CoMP). The coordination can be as simple as inter-cell interference coordination, i.e., coordinated scheduling/beamforming, or can be more advanced as the same data transmission from multiple cell sites, i.e., joint processing [10]. Figure 2 shows an example of joint processing scheme. CoMP makes it possible for users who are scattered in the cell to enjoy more consistent performance and quality.

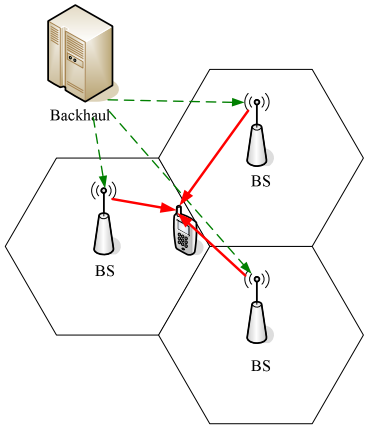

Figure 2. An example of CoMP joint processing.

1.3.5 Relaying Technology

Reduction the propagation loss between the transmitter and the receiver is also a way to increase the data rate. By setting relay stations (RSs) into the traditional cellular networks, the transmission between a BS and an MS can be divided into multiple hops. In each hop, the propagation loss then can be reduced, and higher order modulation coding scheme (MCS) can be applied so that the transmission rate can be enhanced. Relaying technology is introduced to improve the user throughput and to enhance the system capacity [9], [10], [13].

Each key technology mentioned above has drawn lots of research attention. However, it is noted that even though these technologies have been studied, it does not necessarily mean that all of them will be included in the specifications for the next generation mobile communication systems. The introduced complexity and the obtained gain of each technology will be detailed evaluated.

The comprehensive study of all key technologies is out of the scope of this dissertation. In this dissertation, we aim to investigate relaying technologies and relay-assisted cellular networks.

1.4 Overview of Relay-Assisted Cellular Networks

Deploying fixed RSs in traditional mobile cellular networks to relay information from a BS to an MS, and vice versa, which is known as relay-assisted cellular networks [13]. Relay-assisted cell architecture is expected to be an alternative of cost effective cell architecture for the wireless communication systems. Very recently, the first commercial relay-assisted network has been standardized by the IEEE 802.16j Task Group [13], aiming

to improve the performance of IEEE 802.16e wireless mobile broadband networks [14].

Relay-assisted cellular systems have been recognized with the following potential benefits compared to conventional cellular architectures. At the link level, by exploiting cooperative diversity, RSs can be used to enhance user throughput, to improve outage probability, and to reduce error rate [15]-[24]. At the system level of cellular systems, RSs can be deployed to improve system capacity, to extend cell coverage, to save transmit power (in the uplink), and to provide more uniform data rates to users who are scattered over a cell. In addition, since the transmit antennas of both ends of a relay link (BS ↔ RS) and/or an access link (BS, RS ↔ MS) are closer to each other, per user throughput can be improved as well. Furthermore, RSs have no direct backhaul connections to the network, so it is much simpler and easier to deploy than a BS. Such benefit allows flexible and fast network roll-out and is easy to adapt to traffic load [25]-[58].

With great application potential, the relay technology has also been adopted in IEEE 802.16m [9] and 3GPP LTE-Advanced [10] as one of the key technologies toward next generation mobile systems.

1.4.1 Classifications of Relay Stations

Relay-assisted networks can be classified into different categories depending on their characteristics. For example, a wireless relay-assisted network can be classified as homogeneous relaying or heterogeneous relaying [29]. Homogeneous relaying uses the same radio access technology for all of its connections including relay links (BS ↔ RS) and access links (BS, RS ↔ MS), while heterogeneous relaying uses different access technologies for these links.

Moreover, RSs are considered to wirelessly connect to the backhaul network via a BS.

The connection can be in-band connection (in-band relaying) or out-band connection (out-band relaying). If the BS-RS link shares the same band with direct BS to MS link, it is referred as in-band relaying; if the BS to RS link does not operate in the same band as direct BS to MS links, it is called out-band relaying scenario [10].

Another example of classification is that RSs can be categorized as either amplify-and-forward (AF) or decode-and-forward (DF) RSs according to the forwarding strategy [29]. An AF RS simply amplifies and retransmits the received analog signal to the destination, while a DF RS decodes the received signal and re-encodes before re-transmission. The AF RS has a simpler signal processing and a lower transmission delay but suffers from noise enhancement, as compared with the DF RS.

The RSs can also be distinguished as fixed, nomadic and mobile RSs depending on their mobility [9], [13]. RSs may be permanently installed in certain locations, i.e. attached to buildings, which are known as fixed RSs, or they may be mobile, i.e. traveling with transportation vehicles, which are mobile RSs. Besides, nomadic RSs are the RSs which may be temporarily deployed in certain locations for a period of time to assist data transmissions.

1.4.2 Relay Operation Modes

As mention to the operation modes of RSs, two general types of RSs have been classified: transparent RSs and non-transparent RSs, which are with respect to the knowledge in MSs. In the transparent mode, an MS is not aware of whether or not it communicates with the network via an RS; while in the non-transparent mode, an MS is aware of whether or not it is communicating via an RS. In IEEE 802.16j and 802.16m, they are simply referred as non-transparent RSs and transparent RSs [9], [13], while in 3GPP LTE-Advanced they are named as Type-I RSs and Type-II RSs, respectively [10].

- **Non-Transparent Relay (Type I Relay)**

A non-transparent RS operates like a BS, except that there is no backhaul connection to the core network. All control signaling and data transmissions between a BS and an MS are forwarded by RSs in the non-transparent mode [9], [10], [13]. The non-transparent RS controls its own cell, which appears to an MS as a separate cell, so that an MS can camp on the RS, just like camping on the BS. The non-transparent RS can operate in both centralized and distributed scheduling in the in-band or out-band of the BS operation. Besides the throughput enhancement, the non-transparent RS may be located at the cell edge to cover the area that is originally not covered by the BS, which is known as coverage extension.

- **Transparent Relay (Type II Relay)**

On the other hand, in the transparent relay mode, the control signaling from a BS can directly reach MSs and only data traffic is forwarded by an RS [9], [10], [13]. The transparent RS is usually located within the coverage of the BS and is under the BS's supervision so that only centralized scheduling is supported in the transparent mode. The MS should camp on the BS and it may not be aware of the existence of the RS. The main objective of the transparent relay is to enhance the user throughput and to increase the system capacity by achieving multipath diversity.

1.5 Problem and Motivation

The concept of relay-assisted cellular networks, the potential benefits, and the detailed relaying technologies are discussed in Section 1.4. With the basic knowledge, the crucial step in developing relay-assisted cellular networks is to fully evaluate their performance from both theoretical and practical points of view.

In relay-assisted cellular systems, the number of RSs, the locations of RSs, the

operations of RSs, the reuse pattern among RSs, and the scheduling method of data transmissions among BSs, RSs, and MSs are important design issues reflecting the system performance. How RSs effectively and efficiently assist cellular systems has been a topic of extensive research in both academia and industry.

From the previous literature, however, the performance evaluation of relay-assisted cellular networks has been mostly done for very specific system scenarios, such as fixed number of RSs and locations, fixed reuse pattern, or seeking optimal RSs' positions with a simplified one-dimensional model. Furthermore, although several works have been done to evaluate the system performance in some environments which are especially suitable for deploying RSs such as the Manhattan-like environment, previous research has mostly focused on the aspects of coverage extension and end-to-end user throughput enhancement.

In this dissertation, we aim to fully investigate a general relay-assisted network in a multi-cell environment both in the downlink and in the uplink from the information-theoretic point of view. By jointly considering RSs' locations, reuse patterns, path selections and resource allocation, in the downlink, two types of *quality of end-user experience* (QoE): *fixed bandwidth allocation* (FBA) and *fixed throughput allocation* (FTA), are investigated along with two path selection methods: *spectral efficiency* (SE) based and *signal-to-noise-plus-interference ratio* (SINR) based; in the uplink part, two performance measures: *average MS's power consumption* and *uplink system spectral efficiency*, are optimized.

In addition, from the practical point of view, we aim to evaluate the overall system capacity enhancement for the relay-assisted network in the Manhattan-like environment with new scheduling methods proposed for the system where directional antennas are equipped at the BSs and RSs.

Detailed literature review, problem formulation, and optimized solutions corresponding to each topic will be provided in the following sections.

1.6 Organization of the Dissertation

This dissertation consists of three themes. The first part is to investigate the downlink performance and optimization of relay-assisted cellular networks in multi-cell environments. The second part aims to look into the uplink performance and optimization of a relay-assisted cellular network. The third part studies resource scheduling with directional antennas for multi-hop relay networks in a Manhattan-like environment.

The rest of this dissertation is organized as follows. In Chapter 2, the adopted system setups, including multi-cell architecture, relaying technology, propagation models, antenna configurations, power setting criteria, path selection methods, and frequency reuse patterns for downlink performance evaluation, are addressed. The joint optimizations based on GA for maximizing system capacities of different system configurations are proposed. The numerical results and the summary are then provided and discussed. In Chapter 3, those of system settings for uplink evaluation are presented. Both the minimization of average MS's transmit power and the maximization of uplink system capacity are formulated and solved by the proposed GA-based algorithm and MAI estimation algorithm. Also, the numerical results of uplink optimization and the summary are indicated. In Chapter 4, we first show the system setups and the propagation models adopted for multi-hop relay networks in a Manhattan-like environment. We propose two efficient resource scheduling methods with directional antennas equipped in BSs and RSs to enhance the system capacity under these settings. The simulation results and the discussion are then provided. Finally, Chapter 5 draws conclusions for this dissertation.

Chapter 2
Downlink Performance and Optimization of Relay-Assisted Cellular Networks in Multi-cell Environments

In this chapter, we investigate the downlink performance limits of a general relay-assisted network with optimized system parameters in a multi-cell environment. A genetic algorithm (GA) based method is proposed for joint optimization of system parameters, including the number of RSs and their locations, frequency reuse pattern, path selection and resource allocation so as to maximize the system spectral efficiency. Two types of *quality of end-user experience (QoE)*, i.e., fixed bandwidth allocation (FBA) and fixed throughput allocation (FTA), are studied along with two path selection methods, i.e., spectral-efficiency (SE) based and signal-to-noise-plus-interference ratio (SINR) based. The background, system setups, the objective function, the proposed optimization algorithm and the numerical results are completely described in the following subsections.

2.1 Background

As mentioned in Section 1.5, one crucial step in developing a relay-assisted cellular network is to fully evaluate its performance from both theoretical and practical points of view. The setups and the performance of relay-assisted networks have been a topic of extensive research in both academia and industry [37]-[44].

In [37], a relay-assisted network was studied in a multi-cell environment with six RSs in a cell, where a frequency reuse scheme over the relaying links was proposed to improve the system spectral efficiency. In [38], the issues of RS positioning and spectrum partitioning were investigated with RSs located on the lines connecting BS and the six vertices of a hexagonal cell. Again, they considered the case of six RSs in a cell. The RSs' positions were optimized along the line to maximize the user throughput at cell boundary. In [39], the performance of a relay-assisted OFDMA network was evaluated for the specific setup of three RSs in a cell with and without intra-cell resource reuse; numerical results showed that the relay-assisted network significantly outperforms the conventional cellular network with respect to system capacity and coverage. Very recently, the IEEE 802.16j multi-hop relay networks were evaluated in [40]-[44]. In particular, the downlink capacity was simulated in [40] with one RS or three RSs in a sector for different modes of RS operations, including the transparent and non-transparent RSs with centralized or distributed scheduling. In [41] the deployment of RSs for coverage extension was investigated, and in [42], [43], the issue of placement of BSs and RSs was considered with [42] focusing on the coverage extension application and [43] on the downlink performance with different number of RSs and cell radii. Lastly, in [44], the optimal placement of RS and the time allocation were studied for the system employing one RS in a cell with uneven traffic distribution.

So far, as discussed above, the performance evaluation and optimization of the relay-assisted cellular networks has been limited to very specific system configurations: with a fixed number and location of RSs and/or using fixed reuse patterns.

In this chapter, our aim is to investigate the downlink optimization and performance limits of a general relay-assisted network in a multi-cell environment from an information-theoretic point of view. Two types of quality of QoE, FBA and FTA, are explored along with two path selection methods, SE based and SINR based. A GA-based method is proposed for joint optimization of the system parameters including RS's positions, reuse pattern, path selection, and resource allocation among different links to maximize the system spectral efficiency. The theoretical performance serves as a benchmark. For more practical relay-assisted cellular networks, where the effects of MCSs and signaling overhead that enables the RSs' operation need to be taken into consideration.

2.2 System Setups

This section describes the system setups and parameters we adopt in this work to evaluate the downlink performance in relay-assisted cellular systems.

2.2.1 Cell configuration

We study a multi-cell network that consists of BSs, fixed RSs, and MSs. Figure 3 is such an example, where RSs are deployed in the sectors of a sectorized network to improve the system performance. The cell architecture is described by a three-tuple, $(K_{\text{cluster}}, K_{\text{sector}}, K_{\text{band}})$, where K_{cluster}, K_{sector}, and K_{band} are the size of the cluster, the number of sectors in a cell, and the number of frequency bands used in the sectors of a cell, respectively. For example, the cell architecture in Figure 3 is described by $(3,3,3)$. An area of K co-channel cells will

be regarded as the design area in which RSs are deployed for performance enhancement. The BSs of these cells are designated as B_i, $i = 1, \cdots, K$.

Figure 4 (a) is a more detailed layout of a cell, for example, *i*-th cell, with no sectorization. The BS is located at the center of the cell, D is the cell radius, N_i RSs are deployed to improve the cell performance, $\vec{r}_{i,j}$ is the position vector of the *j*-th RS, denoted by $R_{i,j}$, and $\vec{m}$ is the MS's position vector. The MSs are assumed to be uniformly distributed over the cell region Ω_i. The number of RSs can be different from cell to cell in its most general case.

2.2.2 Relaying technology

In this dissertation, we assume the RSs operate in the in-band, homogeneous relaying, and DF mode which means the RSs decode the received signal first and then forward it to MS using the same radio technology as the BS in the same frequency band. An MS can communicate with the BS either through the direct path or the two-hop path (via an RS) that constitutes the BS-RS and RS-MS links. Two-hop relaying is considered as the most common scenario in practical applications because of the excessive delay incurred in more than two-hop relaying. Figure 4 (b) shows a practical downlink radio resource allocation scheme, where orthogonal radio resources are allocated to the direct and two-hop paths, respectively. The radio resource for the two-hop path is further divided into two parts: one for the BS-RS link and the other for the RS-MS link. With this type of resource allocation, RSs are not required to transmit and receive at the same time (half-duplex relaying).

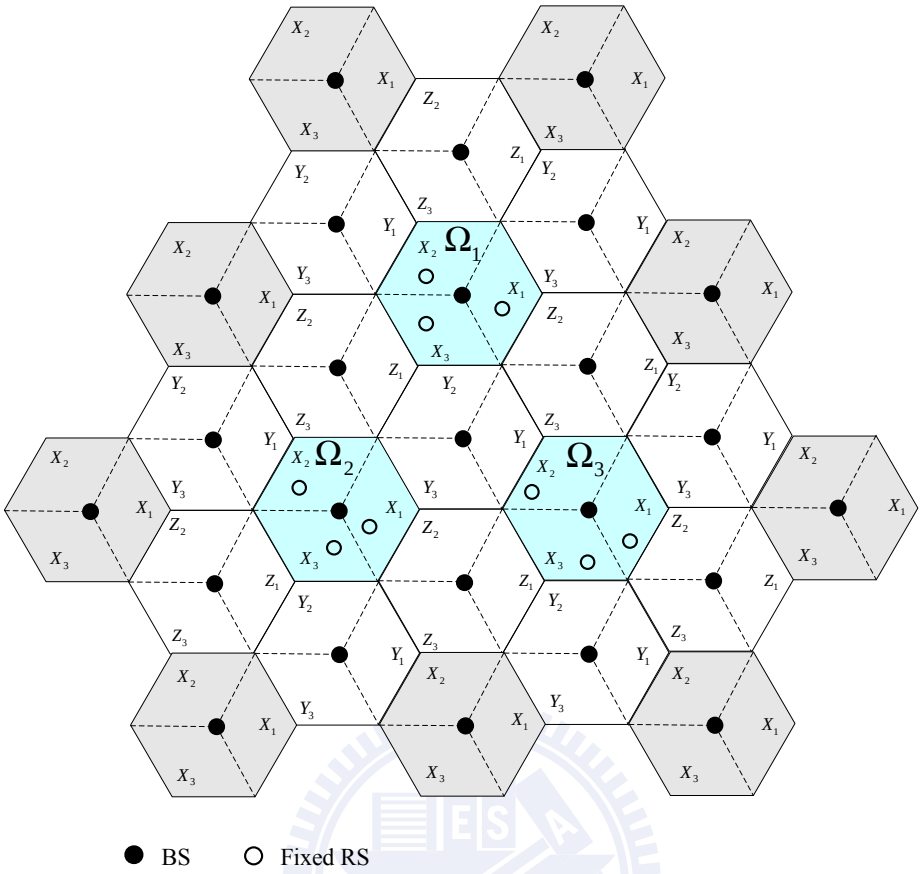

Sectors denoted by the same letter use the same frequency.

Figure 3. The multi-cell architecture $(3,3,3)$.

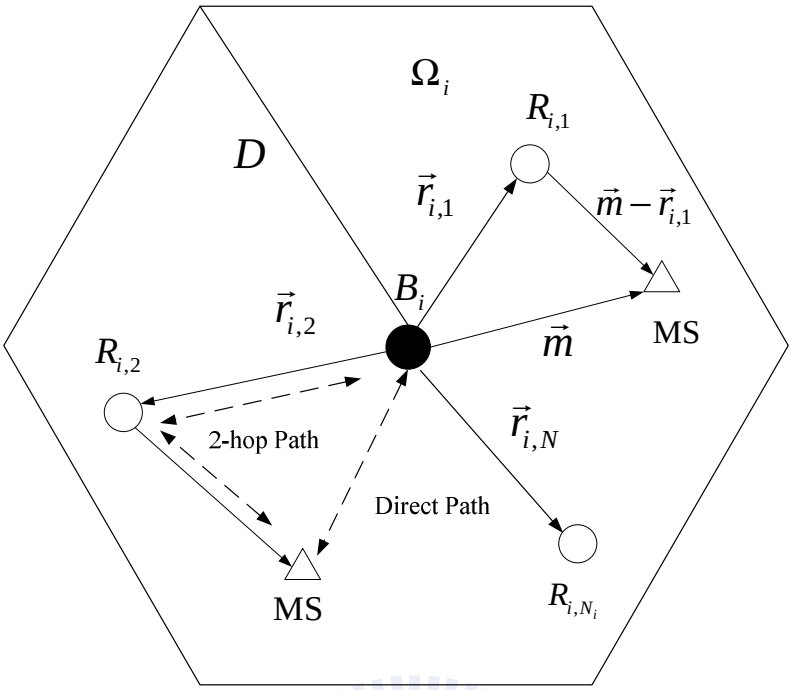

(a)

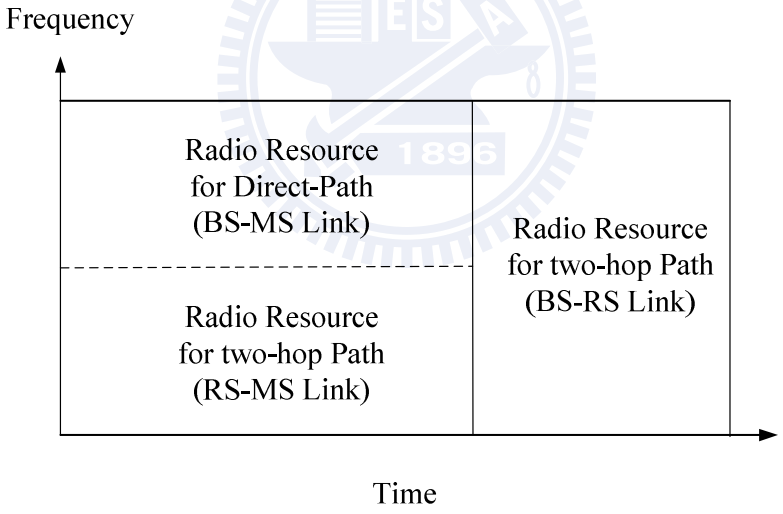

(b)

Figure 4. (a) A detailed layout of a cell, and (b) the radio resource allocation.

2.2.3 Propagation Models

The path and shadowing losses are treated separately from the small scale fading. For the path loss, the line-of-sight (LOS) and non-line-of-sight (NLOS) models for the suburban macro-cell environment in [29] are adopted; that is

$$L_{path}^{LOS}(d) = 23.8\log_{10}(d) + 41.9 \text{ dB} \tag{2.1}$$

and

$$L_{path}^{NLOS}(d) = 40.2\log_{10}(d) + 27.7 \text{ dB} \tag{2.2}$$

where d is the separation (in meters) between the transmitter and the receiver. The LOS model is used for the BS-RS link because RSs are often mounted over the rooftops, whereas the NLOS model is for the BS-MS and RS-MS links. Also, the NLOS model is used for the calculation of MAI.

For the shadowing loss, a simplified model given in (2.3) is adopted mainly for verifying the effectiveness of the proposed method in a shadowed environment. Some other shadowing models can be used as well.

$$L_{shadow}(\vec{m}) = \begin{cases} \delta \text{ dB, if } \vec{m} \text{ is in a shadowed area} \\ 0 \text{ dB, otherwise} \end{cases} \tag{2.3}$$

In particular, the shadowed environment in Figure 5, which consists of 4 obstacles, will be used in Section 2.5.1.2 for numerical results. In this setup, an MS is said to be in a shadowed area if the LOS between the BS (RS) and the MS is blocked by an obstacle. No shadowing loss is imposed on the BS-RS link.

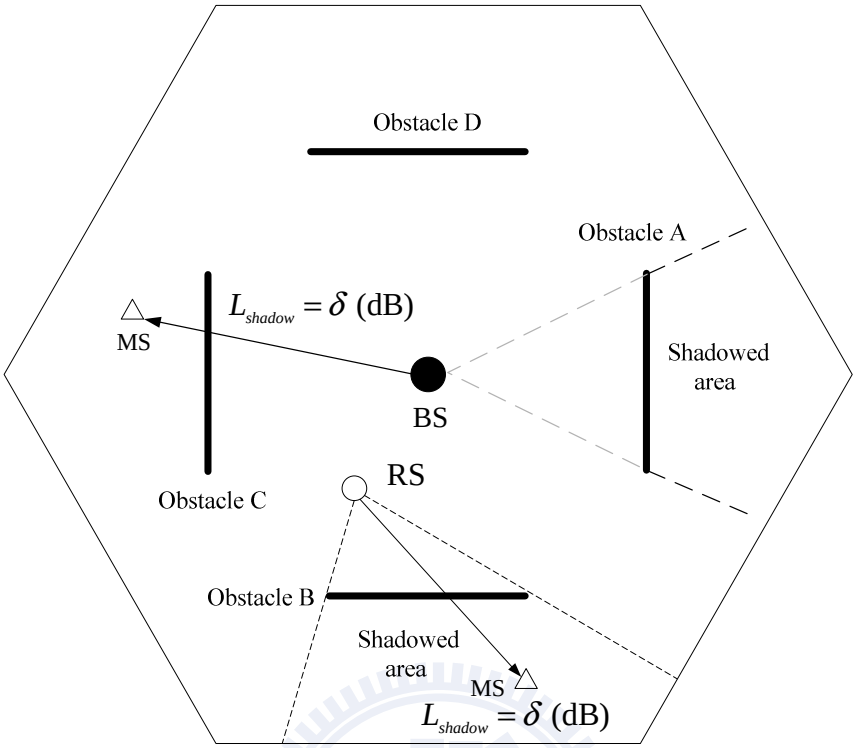

Figure 5. A simplified shadowing model.

2.2.4 Antenna Configurations

RS and MS are equipped with one omni-directional antenna, respectively, whereas both omni-directional and sectored antenna configurations are investigated for BSs. For the sectored antenna, the antenna pattern proposed in [59] is adopted, which is

$$A(\theta) = -\min\left[12\left(\frac{\theta}{\theta_{3dB}}\right)^2, A_m\right] \text{ dB}, \tag{2.4}$$

where $-180° \le \theta \le 180°$ is the angle between the direction of interest and the bearing direction of the antenna, $\theta_{3dB} = 70°$ is the 3-dB beamwidth, and $A_m = 20$ is the maximum attenuation.

2.2.5 Power Setting of BS and RS

A pre-specified spectral efficiency (SE) for users at the cell boundary is used for setting up the transmitted power of a BS and its subordinate RSs. Let $S = f(\text{SINR})$ (in bits per second per hertz, bps/Hz) denote the link SE as a function of average SINR which is defined by

$$\text{SINR} = \frac{p_t \cdot g_t \cdot L_{all}^{-1}(d) \cdot g_r \cdot \text{E}[|h|^2]}{N_0 + I_0}, \tag{2.5}$$

where p_t is the transmit power spectral density (PSD), g_t and g_r are the transmit and receive antenna gains, respectively, $L_{all}(d) \doteq L_{path}(d) \cdot L_{shadow}$ is the composite effect of the path and shadowing losses in linear scale, h is a complex channel gain due to the small-scale fading, $\text{E}[\bullet]$ denotes the expectation operation, and N_0 and I_0 are the PSDs

of additive white Gaussian noise (AWGN) and MAI, respectively.

For AWGN channels,

$$f\left(\text{SINR}\right)=\log_2\left(1+\text{SINR}\right), \tag{2.6}$$

where h is a constant in (2.5). For fading channels, on the other hand, $f\left(\text{SINR}\right)$ may not assume a close form as in (2.6) and needs to be evaluated numerically, depending on the considered fading characteristics and whether the channel state information is available at transmitter [60]. In any case, for a specific SE S, the required SINR can be found by $\text{SINR}=f^{-1}\left(S\right)$.

Let S_{edge} be the targeted SE for an MS at the cell boundary, the transmit PSD of the BS is then set as

$$p_{B_i}=\frac{\text{SINR}_{\text{edge}}\cdot\left(N_0+I_0\right)}{g_t\cdot L_{all}^{-1}(D)\cdot g_r\cdot\text{E}\left[\left|h_{B_i\to M}\right|^2\right]}\ \text{watts/Hz}, \tag{2.7}$$

where $\text{SINR}_{\text{edge}}=f^{-1}\left(S_{\text{edge}}\right)$. Likewise, the transmit PSD of $R_{i,j}$ is set as

$$p_{R_{i,j}}=\frac{\text{SINR}_{\text{edge}}\cdot\left(N_0+I_0\right)}{g_t\cdot L_{all}^{-1}\left(D-\left\|\vec{r}_{i,j}\right\|\right)\cdot g_r\cdot\text{E}\left[\left|h_{R_{i,j}\to M}\right|^2\right]}\ \text{watts/Hz}, \tag{2.8}$$

where $\left\|\vec{r}_{i,j}\right\|$ denotes the Euclidean distance of the position vector $\vec{r}_{i,j}$. Note that with the power settings in (2.7) and (2.8), the coverage of RSs is entirely within that of the BS. In this setup, RSs are mainly used to improve system capacity, user throughput and to remove coverage holes due to shadowing effect within the cell.

2.2.6 Path Selection

Path selection is a procedure to determine whether the direct path or the two-hop path is to be chosen by a BS to communicate with an MS. Two types of path selection will be investigated: SINR based and SE based. For the SINR-based path selection, the direct path is selected if $\mathrm{SINR}_{B_i \to M}(\vec{m}) \geq \max_{R_{i,j}} \left\{ \mathrm{SINR}_{R_{i,j} \to M}(\vec{m}) \right\}$; otherwise, the two-hop path through $R_{i,k}$ is selected, where $\mathrm{SINR}_{B_i \to M}(\vec{m})$ and $\mathrm{SINR}_{R_{i,j} \to M}(\vec{m})$ are the received SINR over the B_i-MS and $R_{i,j}$-MS links, respectively, and $R_{i,k} = \arg\left\{ \max_{R_{i,j}} \left\{ \mathrm{SINR}_{R_{i,j} \to M}(\vec{m}) \right\} \right\}$.

Let $S_{B_i \to M}(\vec{m})$, $S_{B_i \to R_{i,j}}(\vec{m})$ and $S_{R_{i,j} \to M}(\vec{m})$ be the SEs of the B_i-MS, B_i-$R_{i,j}$, and $R_{i,j}$-MS links, respectively. For the SE-based path selection, the direct-path is selected if $S_{B_i \to M}(\vec{m}) \geq \max_{R_{i,j}} \left\{ S_{B_i \to R_{i,j} \to M}(\vec{m}) \right\}$; otherwise the two-hop path through $R_{i,k}$ is selected, where

$$S_{B_i \to R_{i,j} \to M}(\vec{m}) = \frac{1}{\frac{1}{S_{B_i \to R_{i,j}}(\vec{m})} + \frac{1}{S_{R_{i,j} \to M}(\vec{m})}} = \frac{S_{B_i \to R_{i,j}}(\vec{m}) \cdot S_{R_{i,j} \to M}(\vec{m})}{S_{B_i \to R_{i,j}}(\vec{m}) + S_{R_{i,j} \to M}(\vec{m})} \tag{2.9}$$

is the effective SE of the B_i - $R_{i,j}$-MS link [61], and $R_{i,k} = \arg\left\{ \max_{R_{i,j}} \left\{ S_{B \to R_{i,j} \to M}(\vec{m}) \right\} \right\}$.

2.2.7 Frequency Reuse over RS-MS Links

In addition to frequency reuse in the co-channel cells, the frequency band for the RS-MS links in a cell can be reused as well, thanks to the spatial separation between RSs. To exploit this advantage, RSs in a cell are divided into L reuse groups, where $L \leq N_i$, $i = 1, \cdots, K$, and each group shares the same radio resource. In addition, the reuse

pattern can be specified by the set $\mathrm{G}_i \doteq \{\mathrm{G}_{i,l}\}_{l=1}^{L}\ \forall i$, where $\mathrm{G}_{i,l} = \{R_{i,k_l}\}$ is the set of RSs in the l-th group of cell i. Obviously, $N_i = \sum_{l=1}^{L} |\mathrm{G}_{i,l}|$, where $|\mathrm{G}_{i,l}|$ is the cardinality of the set $\mathrm{G}_{i,l}$. The number of reuse groups is the same for all co-channel cells in this study. In its most general case, some reuse groups in a particular cell may be empty; that is, it contains no RSs.

2.3 Optimization of System Parameters

In this section, the RSs' positions and the frequency reuse pattern are jointly optimized over the design area $\Omega \doteq \bigcup_{i=1}^{K} \Omega_i$ to maximize the system SE, under different QoE criteria and path selection methods.

2.3.1 Objective Function

Let T_Ω and W_Ω be the aggregate throughput and the total allocated bandwidth over the design area Ω, respectively. The system SE S_Ω is then defined by

$$S_\Omega \doteq \frac{T_\Omega}{W_\Omega}. \tag{2.10}$$

Our objective is to search for the optimal set of RSs' positions $\Upsilon \doteq \{\vec{r}_{i,j}\}$ and the reuse pattern $\mathrm{G} \doteq \{\mathrm{G}_i\}$ so that the SE S_Ω is maximized.

Two types of QoE criteria will be investigated along with two path selection methods (given in Subsection 2.2.6). One is the FBA, where a fixed amount of bandwidth is allocated to MSs in the cell, and the other is the FTA, where a fixed throughput (data rate) is supported no matter where the MS is located (uniform data rate coverage). FBA and FTA

represent two extremes of QoE criteria, and real systems may lie between these two.

2.3.1.1 Fixed Bandwidth Allocation

In FBA, a fixed downlink bandwidth per unit area w_d (in Hz per unit area) is allocated to an MS. Therefore, $w_d = w_{B_i \to M}(\vec{m}) = w_{B_i \to R_{i,j}}(\vec{m}) + w_{R_{i,j} \to M}(\vec{m})$ for an MS located at $\vec{m}$, where $w_{B_i \to M}(\vec{m})$ is the bandwidth allocated to the $B_i \to \text{MS}$ link, $w_{B_i \to R_{i,j}}(\vec{m})$ to the $B_i \to R_{i,j}$ link, and $w_{R_{i,j} \to M}(\vec{m})$ to the $R_{i,j} \to \text{MS}$ link, respectively. Furthermore, the total allocated bandwidth over Ω is calculated by

$$W_\Omega = W_{B \to M} + W_{B \to R} + W_{R \to M}, \tag{2.11}$$

where

$$W_{B \to M} = \max_i \left\{ W_{B_i \to M} \right\}, \tag{2.12}$$

$$W_{B \to R} = \max_i \left\{ \sum_{j=1}^{N_i} W_{B_i \to R_{i,j}} \right\} \tag{2.13}$$

and

$$W_{R \to M} = \sum_{l=1}^{L} \max_i \left\{ W_{\mathrm{G}_{i,l} \to M} \right\}, \quad i = 1, \cdots, K \tag{2.14}$$

are the aggregated downlink bandwidth allocated to the $B \to \text{MS}$, $B \to R$, and $R \to \text{MS}$ links, respectively. In (2.12)-(2.14),

$$W_{B_i \to M} = \int_{\vec{m} \in \Omega_{B_i}} w_{B_i \to M}(\vec{m})\, dA, \tag{2.15}$$

$$W_{B_i \to R_{i,j}} = \int_{\vec{m} \in \Omega_{R_{i,j}}} w_{B_i \to R_{i,j}}(\vec{m})\, dA, \tag{2.16}$$

and

$$W_{G_{i,l}\to M} = \max_{R_{i,j}\in G_{i,l}} \int_{\vec{m}\in\Omega_{R_{i,j}}} w_{R_{i,j}\to M}(\vec{m})\, dA\,, \tag{2.17}$$

where Ω_{B_i} and $\Omega_{R_{i,j}}$ are the coverage areas of B_i and $R_{i,j}$, respectively. Note that given Υ and the path selection method, the coverage areas of the Ω_{B_i} and $\Omega_{R_{i,j}}$ are determined under the power settings in (2.7) and (2.8). In addition, in (2.11), we have used the fact that the co-channel regions are allocated with the same bandwidth, and thus, the maximum bandwidth required among the co-channel regions is used in the calculation of the total bandwidth.

Recall that $S_{B_i\to M}(\vec{m})$, $S_{B_i\to R_{i,j}}(\vec{m})$ and $S_{R_{i,j}\to M}(\vec{m})$ are the SEs of the $B_i \to \text{MS}$, $B_i \to R_{i,j}$, and $R_{i,j} \to \text{MS}$ links, respectively. Using these notations, the throughputs per unit area supported for those links are given by

$$t_{B_i\to M}(\vec{m}) = w_{B_i\to M}(\vec{m})\cdot S_{B_i\to M}(\vec{m}), \tag{2.18}$$

$$t_{B_i\to R_{i,j}}(\vec{m}) = w_{B_i\to R_{i,j}}(\vec{m})\cdot S_{B_i\to R_{i,j}}(\vec{m}) \tag{2.19}$$

and

$$t_{R_{i,j}\to M}(\vec{m}) = w_{R_{i,j}\to M}(\vec{m})\cdot S_{R_{i,j}\to M}(\vec{m}). \tag{2.20}$$

In addition, the effective throughput $t_{B_i\to R_{i,j}\to M}(\vec{m})$ for the two-hop path (via $R_{i,j}$) is obtained by $t_{B_i\to R_{i,j}\to M}(\vec{m}) = \min\left\{t_{B_i\to R_{i,j}}(\vec{m}),\ t_{R_{i,j}\to M}(\vec{m})\right\}$. It is shown in Lemma 1 of the Appendix that $t_{B_i\to R_{i,j}}(\vec{m}) = t_{R_{i,j}\to M}(\vec{m})$ provides the highest spectrum efficiency. Thus, we get

$$w_{B_i \to R_{i,j}}(\vec{m}) = \frac{S_{R_{i,j} \to M}(\vec{m})}{S_{B_i \to R_{i,j}}(\vec{m}) + S_{R_{i,j} \to M}(\vec{m})} \cdot w_d \,, \tag{2.21}$$

$$w_{R_{i,j} \to M}(\vec{m}) = \frac{S_{B_i \to R_{i,j}}(\vec{m})}{S_{B_i \to R_{i,j}}(\vec{m}) + S_{R_{i,j} \to M}(\vec{m})} \cdot w_d \tag{2.22}$$

and

$$t_{B_i \to R_{i,j} \to M}(\vec{m}) = \frac{S_{B_i \to R_{i,j}}(\vec{m}) \cdot S_{R_{i,j} \to M}(\vec{m})}{S_{B_i \to R_{i,j}}(\vec{m}) + S_{R_{i,j} \to M}(\vec{m})} \cdot w_d \,. \tag{2.23}$$

Using (2.18) to (2.23), the aggregate throughput (in bps) can be calculated as follows.

$$T_\Omega = \sum_{i=1}^{K} \left(T_{B_i} + \sum_{l=1}^{L} T_{G_{i,l}} \right), \tag{2.24}$$

where

$$T_{B_i} = \int_{\vec{m} \in \Omega_{B_i}} t_{B_i \to M}(\vec{m}) \, dA \tag{2.25}$$

and

$$T_{G_{i,l}} = \sum_{R_{i,j} \in G_{i,l}} \int_{\vec{m} \in \Omega_{R_{i,j}}} t_{B_i \to R_{i,j} \to M}(\vec{m}) \, dA \,. \tag{2.26}$$

2.3.1.2 Fixed Throughput Allocation

In FTA, a targeted downlink throughput per unit area t_d (in bps per unit area) is supported for an MS, no matter where it is located. To achieve this, the bandwidth allocation for the direct path is

$$w_{B_i \to M}(\vec{m}) = \frac{t_d}{S_{B_i \to M}(\vec{m})}. \tag{2.27}$$

For the two-hop path via $R_{i,j}$, from Lemma 2 in the Appendix, the best bandwidth allocation is to make $t_{B_i \to R_{i,j}}(\vec{m}) = t_{R_{i,j} \to M}(\vec{m}) = t_d$. As a result, we get

$$w_{B_i \to R_{i,j}}(\vec{m}) = \frac{t_d}{S_{B_i \to R_{i,j}}(\vec{m})} \tag{2.28}$$

and

$$w_{R_{i,j} \to M}(\vec{m}) = \frac{t_d}{S_{R_{i,j} \to M}(\vec{m})}. \tag{2.29}$$

By substituting (2.27) – (2.29) into (2.15) – (2.17), respectively, the aggregate bandwidth can be calculated as in (2.11). Furthermore, in this case,

$$T_\Omega = \sum_{i=1}^{K} \int_{\vec{m} \in \Omega_i} t_d \, dA \tag{2.30}$$

Note that $W_{B \to M}$, $W_{B \to R}$ and $W_{R \to M}$ in (2.12) – (2.14) are derived under the assumption of a fully-loaded system, that is, there is one user per unit area. In practice, a radio resource allocation, as illustrated in Figure 4 (b), can subsequently be done depending on how many users are to be supported in a cell. Let W_{req} be the bandwidth required to support a total of N_{user} users in a cell. For FBA, $W_{req} = N_{user} \cdot W_d$, where W_d (Hz) is the downlink bandwidth allocated an MS, whereas for FTA, $W_{req} = N_{user} \cdot T_d / S_\Omega$, where T_d (bps) is the target downlink throughput for an MS. Then, the bandwidth for the $B \to \text{MS}$, $B \to R$, an $R \to \text{MS}$ links can be allocated as $\frac{W_{B \to M}}{W_{B \to M} + W_{B \to R} + W_{R \to M}} \cdot W_{req}$,

$\frac{W_{B\to R}}{W_{B\to M}+W_{B\to R}+W_{R\to M}}\cdot W_{req}$, and $\frac{W_{R\to M}}{W_{B\to M}+W_{B\to R}+W_{R\to M}}\cdot W_{req}$, respectively.

2.4 Genetic-Based Optimization

It is easy to see, from (2.10), that S_Ω is a highly nonlinear function of Υ and G given a QoE criterion and a path selection method, and generally, an analytic close-form solution is not available. In this section, a GA-based optimization algorithm is devised to solve the optimization problem.

2.4.1 Overview of Genetic Algorithm

GA is an evolutionary algorithm invented by John Holland in the 1970s, apparently inspired by Darwin's theory of natural evolution, and has widely been recognized as a powerful technique to find exact or approximate solutions to a wide range of optimization and search problems. The general operation of GAs is illustrated in Figure 6. Assume that the parameters of the targeted objective function can be encoded as genes, and that the set of genes consists of a chromosome which is a candidate solution to the objective function. Initially, GA is started with a random generation of a set of chromosomes, called population. Each chromosome will be evaluated against objective function. Then a survivor selection criterion is applied to select better-fitness chromosomes for evolution if the best one so far is considered not satisfying. The evolution operations include mate selection, crossover and mutation. Mate selection picks chromosome mates (parents) from the survivors. Crossover (recombination) is then carried out over the selected mates to reproduce new offspring who inherits partial genes from its parents. Mutation is an operation performed to produce a few offspring where some genes may be altered. The evolution process repeats from one generation to another until some condition (for example, number of iterations or

improvement of the best solution) is met.

GA has been successfully applied to a wide range of optimization problems that involve a large number of variables [62]-[65]. In our problem, the GA-based approach is particularly useful when the total number of RSs is large where optimization based on an exhaustive search is quite inefficient.

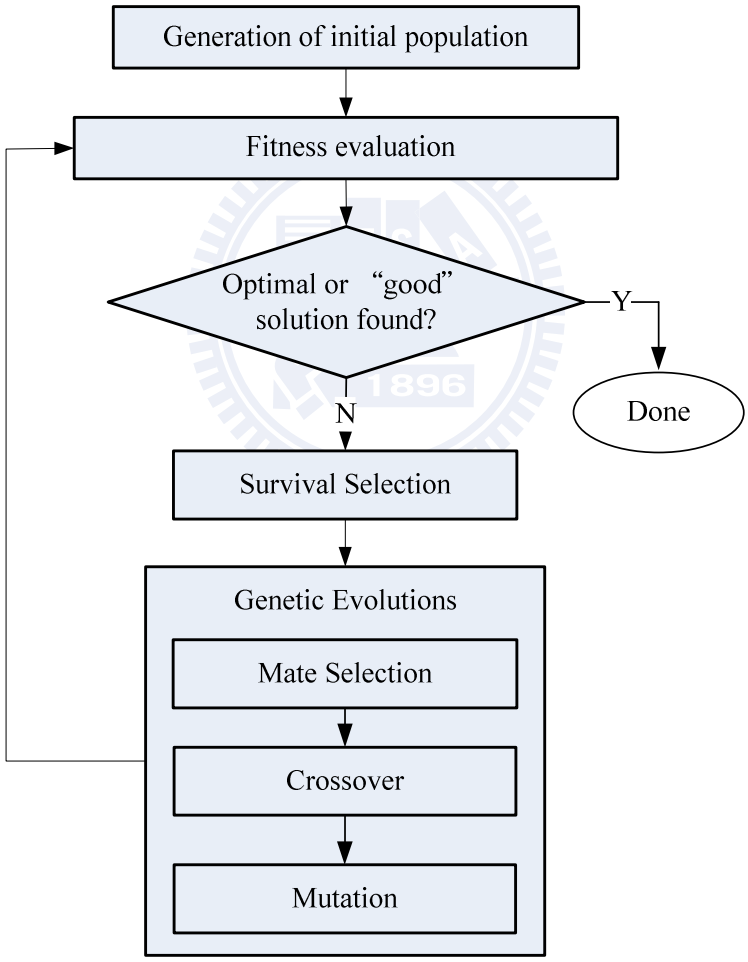

Figure 6. The general operation principle of GAs.

2.4.2 Optimization via Genetic Algorithm

In this subsection, a more detailed description on the proposed GA is provided.

- **Chromosome Representation**: The Cartesian coordinate and the reuse group of $R_{i,j}$, $(\vec{r}_{i,j}, \mathrm{G}_{i,l})$, is encoded as a gene, and the set of RSs' positions and the corresponding reuse pattern (Υ, G) is a chromosome. In our formulation, the cell region is discretized into grids with $\vec{r}_{i,j}$ located at the grid intersection points.

- **Initial Population**: At the beginning, N_{pop} chromosomes are randomly generated and used as the population size involving in evolution at each generation. Each randomly generated coordinate is rounded off to the nearest grid intersection point.

- **Fitness Evaluation**: Each chromosome is evaluated against the objective function in (2.10) under different QoE criteria, path selection methods and reuse patterns.

- **Survivor Selection**: Chromosomes with better fitness survive and will be involved in the evolution in the next generation, whereas those with less fitness are discarded. The selection rate to survive is denoted as β so that only the best $N_{sur} = \beta \cdot N_{pop}$ chromosomes survive after evaluation, and the rest ones are discarded to make room for the new offspring.

- **Mate Selection**: Two mates (chromosomes) are selected from the mating pool of N_{sur} chromosomes to produce two new offspring. We apply the most commonly used mate selection scheme in GA applications: **Roulette wheel selection** [63], where the survival chromosome is chosen to be one of the parents with the probability

$$P(\Upsilon_k, \mathrm{G}_k) = \frac{S_\Omega(\Upsilon_k, \mathrm{G}_k)}{\sum_{\Upsilon_i} S_\Omega(\Upsilon_i, \mathrm{G}_i)} \quad , \tag{2.31}$$

where $S_\Omega(\Upsilon_k, \mathrm{G}_k)$ is the fitness value for the particular chromosome Υ_k. Roulette wheel selection emulates the survival of the fittest mechanism in nature, where the fitter chromosome (to have good genes to survive) will have higher chance to be selected to create offspring. The offspring inherits good genes from parents may have higher probability of survival in the subsequent generation.

- **Crossover**: After two distinct chromosomes (mates) are selected, a crossover is performed to produce two new offspring. The **uniform crossover** is adopted in this work, where each gene in offspring is randomly decided whether to interchange information between the two mates [63], [64]. In addition, in a real-valued encoding scheme a small zero-mean random perturbation is suggested to add to each gene of the offspring [64] in order to prevent the evolutions being dominated by few genes. In our method, the Gaussian variable with variance equal to a grid length is used as the perturbation. Sufficient offspring are produced until the total number of the survivors and the offspring equals to N_{pop}. The new population is then involved in the next step evolution.

- **Mutation**: Besides the crossover, mutation is another way to force GA to explore other areas of the solution space so as to avoid overly fast converging into a local optimum. A mutation probability P_{mut} is set to determine whether a gene is mutated or not. For the case of no intra-cell frequency reuse, the coordinate of the RS (the gene) is regenerated randomly for each mutation. For the case of intra-cell frequency reuse, on the other hand, the mutation is done with half a chance to regenerate the RS's coordinate and with the

other half to swap the coordinate with one randomly chosen from other reuse groups in the cell. This design maintains the genetic diversity and usually leads a faster convergence to the optimum result.

In the proposed GA-based optimization, the computational complexity is dominated by the complexity in evaluating the objective function in (2.10) which has to be evaluated N_{pop} times in each iteration. Furthermore, the computational complexity of (2.10) is of $O\left((N+1)\cdot N_{grid}\cdot K\right)$, where N_{grid} is the number of partitioned grids in a cell, because the radio link information (spectrum efficiency, consumed bandwidth, received SINR, etc.) has to be calculated between an RS (BS) and an MS which is located at one of the grids in the cell. Therefore, the total complexity of the proposed method is $O\left(N_{ite}\cdot N_{pop}\cdot(N+1)\cdot N_{grid}\cdot K\right)$, where N_{ite} is the number of iterations in GA.

2.5 Simulation Results

In our numerical results, the cell radius is set to be 1400 m, the cell is divided into grids with each side equal to 20 m, and all stations (BS, RSs, and MS) are located at the grid intersection points. Four system configurations will be considered, including FBA with SE-based path selection (FBA-SE), FBA with SINR-based path selection (FBA-SINR), FTA with SE-based path selection (FTA-SE), and FTA with SINR-based path selection (FTA-SINR). All results are obtained for AWGN channels with $w_d = 1$ Hz per unit area for FBA, and $t_d = 1$ bps per unit area for FTA. In addition, $S_{edge} = 0.5$ (bps/Hz) for all results unless specified otherwise, and $N_i = N, \forall i$.

In a GA, clearly, the control parameters, such as initial population, survivor selection

scheme, mutation probability, crossover mechanism, affect the convergence of GA. To the best of our knowledge, the conditions for GAs to converge have been proved only for the binary encoding type of GAs with infinite iteration number, by using Markov chain models [66], [67]. For the case of finite iteration number and/or integer or real encoding, the convergence of the algorithm is still an open problem. In this work, instead of using an analytical approach, extensive simulations are employed to look at the convergence issue. As to be shown Section 2.5.1, the convergence of the proposed GA is quite insensitive to the control parameters $(N_{pop}, \beta, P_{mut})$ if they are selected to within a proper range of values. In all our simulations, N_{pop} = 200, β = 0.5 and P_{mut} = 0.05. In addition, the number of iterations of GA depends on the number of RSs involved; more generations are needed for a larger number of RSs.

2.5.1 Single Cell

Figure 7 illustrates how RSs are placed in an optimal way, and how they can improve the SE and user throughput for FBA-SE. The BS is equipped with an omni-directional antenna and no frequency reuse and shadowing are considered. Figure 7 (a) shows the case of no RS ($N = 0$), where the maximum throughput is 23.37 bps (per unit area) at the locations close to the BS, and the minimum throughput is 0.5 bps at the cell vertices (as planned at the power setting of BS). Clearly, the achievable throughput rapidly decreases from the cell center to the edge due to path loss. Figure 7 (b) shows the case of two RSs, where the RSs are placed (after optimization) on the lines connecting the cell center and two vertices of the hexagonal cell at distance of 680 m from BS. As can be seen, user throughput is significantly improved at the close proximity of RSs. Note that the optimal placement of RSs is not unique in this case; as long as RSs are placed on the lines connecting the cell center and any two of vertices at the same distance from BS, the system performance is the same. Figure 7 (c) illustrates the case

of six RSs. Again, RSs are placed on the lines connecting the cell center and vertices, and all of them locate on the ring with distance about 680 m from BS. As the number of RS increases, however, the optimal RS locations can split into more than one ring, as one might expect. Figure 7 (d) is such an example with fourteen RSs (*N = 14*).

Table 2 (a) summarizes the important system parameters for FBA-SE, including service area ratio of BS and RSs, bandwidth allocation ratio for the BS-MS link, the BS-RS link and the RS-MS link, and the system SE. As shown, the system SE is significantly improved with the deployment of RSs, which is around 4.23% for each addition of RS when $N \le 6$. The improvement becomes smaller, however, as the number of RSs is larger than 6, where RSs begin to compete to each other for serving MS rather than to compete with BS. Figure 8 is the cumulative distribution function (CDF) of the user throughput for different *N*. Clearly, the percentage of user with low throughput decreases as *N* increases. In other words, the achievable data rate is distributed more uniformly over the cell. In addition, it is observed that the improvement becomes smaller when $N \ge 10$.

Figure 9 shows simulation results to illustrate the convergence behavior of the proposed GA for FBA-SE with $N = 6$. As can be seen, the convergence of the proposed GA algorithm is quite insensitive to the control parameters $(N_{pop}, \beta, P_{mut})$ if they are selected to be within a proper range of values. In addition, we investigate the convergence behavior for the fixed set of control parameters $\left(N_{pop} = 200, \beta = 0.5, P_{mut} = 0.05\right)$ under different initial populations (seeds). For example, for FBA-SE $(N = 6)$ our result shows that with a total number of 50 runs, the empirical mean and standard deviation of the reached values is 3.432926 and $3.9e^{-5}$, respectively. This means that the proposed GA algorithm converges very well in this case. Similar convergence behaviors are observed for different system setups.

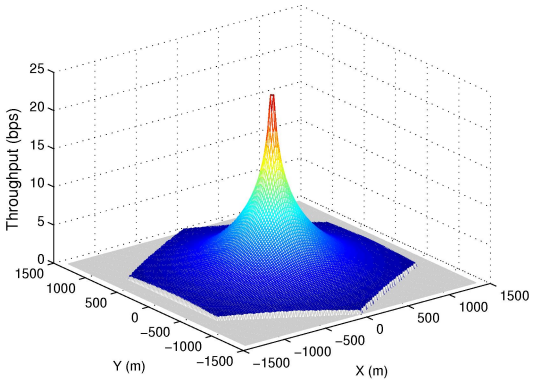

(a) $N = 0$

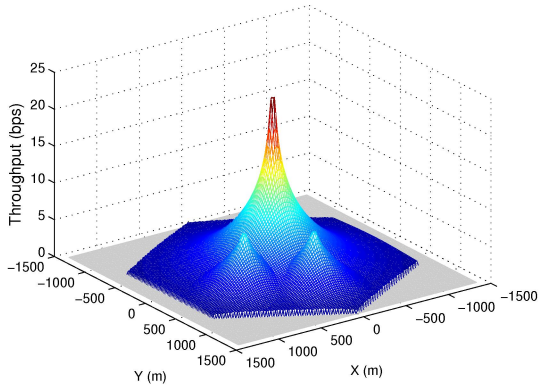

(b) $N = 2$

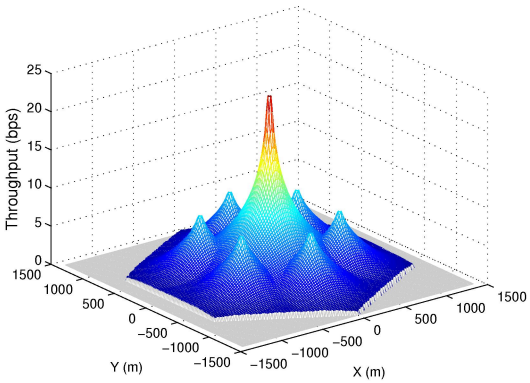

(c) $N = 6$

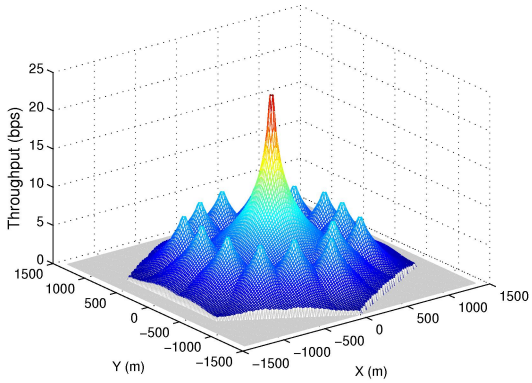

(d) $N = 14$

Figure 7. Optimal RSs' positions and throughput distribution for FBA-SE.

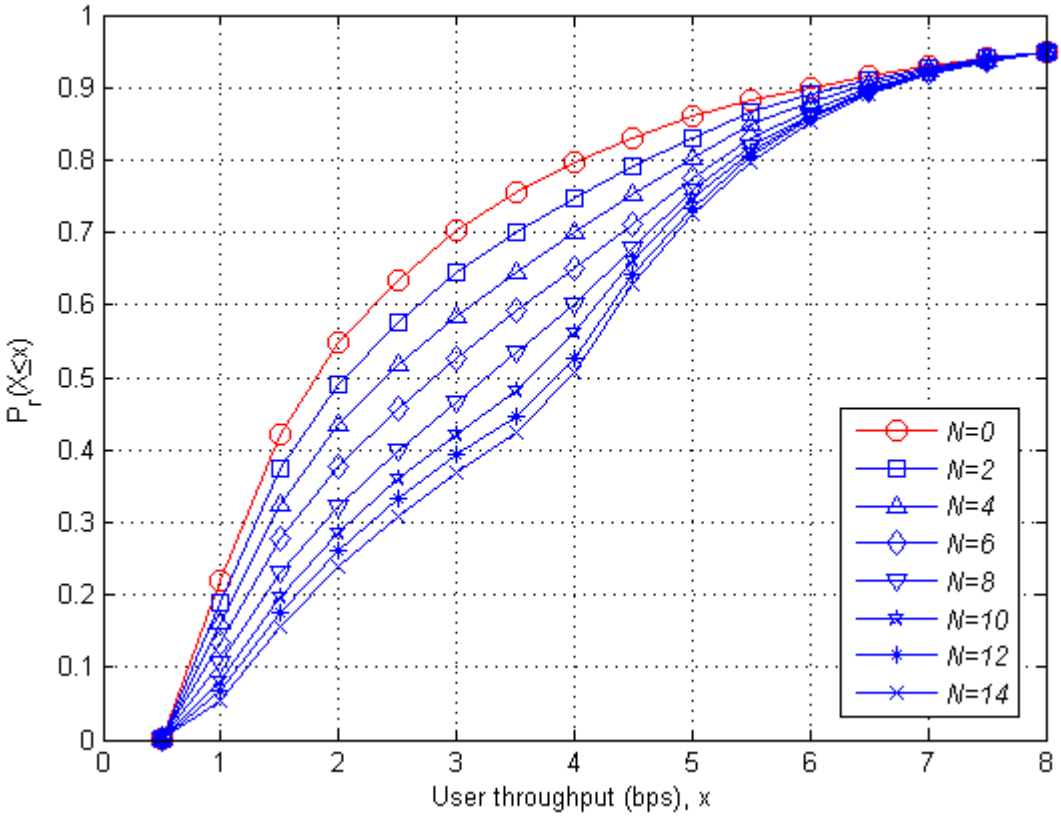

Figure 8. CDF of user throughput for FBA-SE.

Table 2. Important parameters for four system setups.

	N	0	2	4	6	8	10	12	14	16
(a) FBA-SE	Ω_B:Ω_R (%)	100:0	76:24	53:47	29:71	23:77	22:78	21:79	20:80	18:82
	$w_{B\to M}$: $w_{B\to R}$:$w_{R\to M}$ (%)	100:0:0	76:5:19	53:9:38	29:14:57	23:16:61	22:17:61	21:18:61	20:19:61	18:20:62
	S_{cell} (bps/Hz)	2.7372	2.9793	3.2214	3.4634	3.6786	3.8414	3.9606	4.0524	4.1386
(b) FBA-SINR	Ω_B:Ω_R (%)	100:0	75:25	50:50	25:75	18:82	18:82	19:81	19:81	17:83
	$w_{B\to M}$: $w_{B\to R}$:$w_{R\to M}$(%)	100:0:0	75:5:20	50:10:40	25:15:60	18:17:65	18:18:64	19:19:62	19:19:62	17:21:62
	S_{cell} (bps/Hz)	2.7372	2.9705	3.2033	3.4369	3.6563	3.8224	3.9436	4.0356	4.1160
(c) FTA-SE	Ω_B:Ω_R (%)	100:0	82:18	64:36	46:54	37:63	30:70	30:70	32:68	32:68
	$w_{B\to M}$: $w_{B\to R}$:$w_{R\to M}$ (%)	100:0:0	84:2:14	65:5:30	41:8:51	31:10:59	21:12:67	17:14:69	20:14:66	20:15:65
	$\overline{W}$ (Hz)	0.6428	0.5903	0.5379	0.4854	0.4475	0.4106	0.3789	0.3613	0.3460
	S_{cell} (bps/Hz)	1.5557	1.6939	1.8591	2.0601	2.2347	2.4356	2.6390	2.7678	2.8900
(d) FTA-SINR	Ω_B:Ω_R (%)	100:0	81:19	62:38	42:58	33:67	27:73	28:72	29:71	30:70
	$w_{B\to M}$: $w_{B\to R}$:$w_{R\to M}$(%)	100:0:0	83:2:15	62:5:33	37:8:55	25:11:64	16:13:71	15:14:71	17:14:69	19:15:66
	$\overline{W}$ (Hz)	0.6428	0.5909	0.5391	0.4872	0.4491	0.4119	0.3800	0.3626	0.3470
	S_{cell} (bps/Hz)	1.5557	1.6923	1.8550	2.0524	2.2265	2.4276	2.6315	2.7580	2.8815

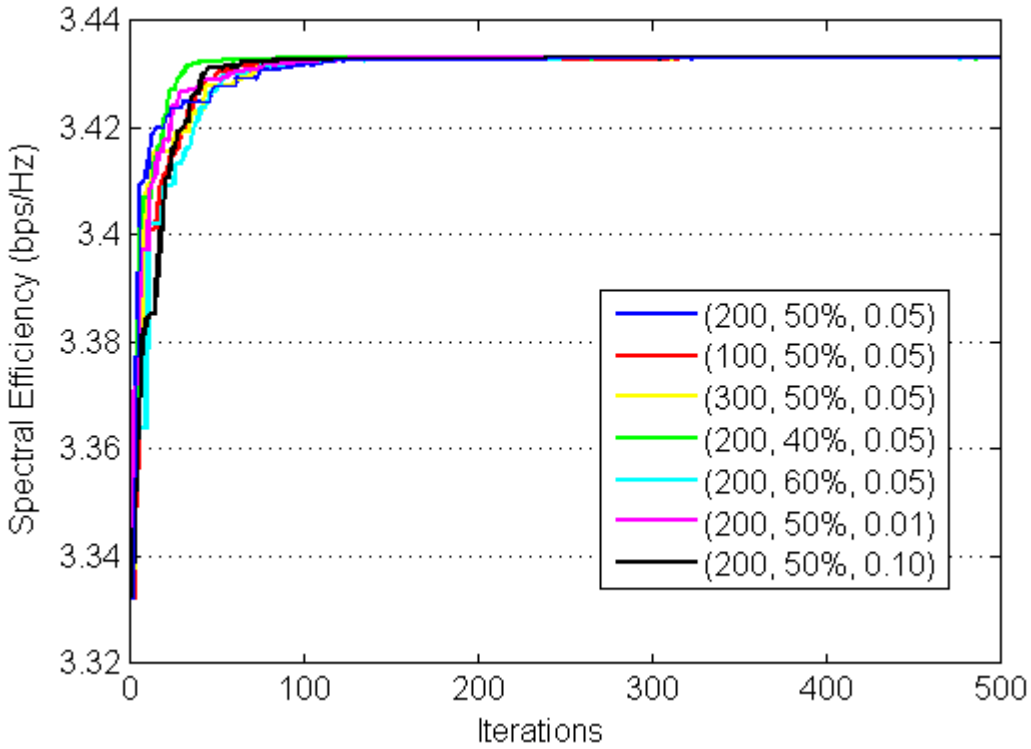

Figure 9. Convergence behavior of the proposed GA for FBA-SE ($N = 6$) under different control parameters $(N_{pop}, \beta, P_{mut})$.

As for FBA-SINR, the optimal RSs are placed in a way similar to FBA-SE except that the RSs are generally a bit farther from BS than that of FBA-SE. Table 2 (b) shows a summary of important system parameters. Somewhat surprising, FBA-SINR performs very closely to that of FBA-SE with respect to system SE after optimization with GA. The reason is that for a large proportion of the two-hop users, the BS-RS link is much better than the RS-MS links due to the LOS condition in the BS-RS link, and when $S_{B_i \to R_{i,j}}(\vec{m})$ is much greater than $S_{R_{i,j} \to M}(\vec{m})$, the SE-based path selection degenerates to the SINR-based path selection, as can be seen in (2.9). Note that the SINR-based path selection is much simpler to implement than the SE-based path selection.

Figure 10 shows the complementary CDF of bandwidth consumption for FTA-SE. As can be seen, the percentage of high bandwidth consumption is reduced as the number of RSs increases. Table 2 (c) and (d) summarizes the important parameters for FTA-SE and FTA-SINR, respectively, where $\bar{w}$ is the average bandwidth consumption. Again, FTA-SINR performs close to FTA-SE.

Figure 11 compares the system SE of the four system configurations. As can be seen, the system SE of FTA is much less than that of FBA in all cases. To explain this, consider a system with m users who have the link SE of $s_1, s_2, ..., s_m$, $\forall s_i \geq 0$, respectively. For FBA, the system SE is given by the arithmetic mean $\frac{1}{m}\sum_{i=1}^{m} s_i$, whereas for FTA, it is given by the harmonic mean $1 \Big/ \frac{1}{m}\sum_{i=1}^{m} 1/s_i$. Clearly,

$$\frac{1}{m}\sum_{i=1}^{m} s_i \geq \frac{1}{\frac{1}{m}\sum_{i=1}^{m} 1/s_i} \tag{2.32}$$

The equality holds if and only if $s_1 = s_2 = \ldots = s_m$; a condition doesn't hold in our cases. Note that the harmonic mean is dominated by the smallest s_i. In other words, the system capacity may significantly be lowered if a fixed throughput is to be maintained for those users in bad channel conditions; that is uniform data rate coverage comes at a large expense on system capacity.

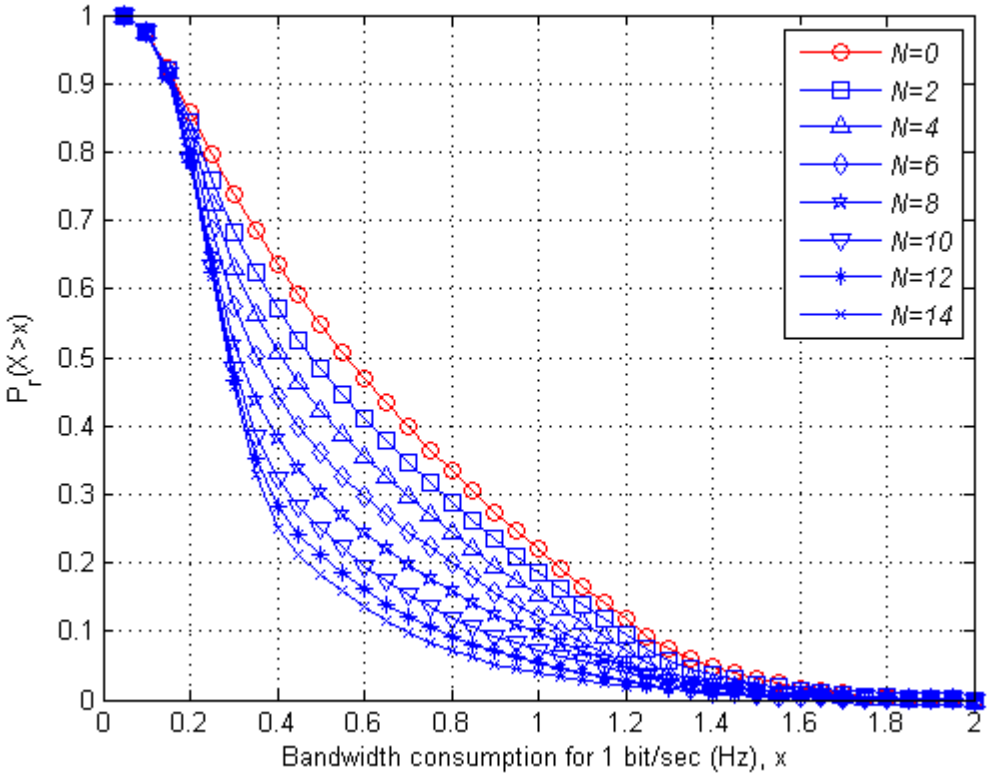

Figure 10. Complementary CDF of bandwidth consumption for FTA-SE.

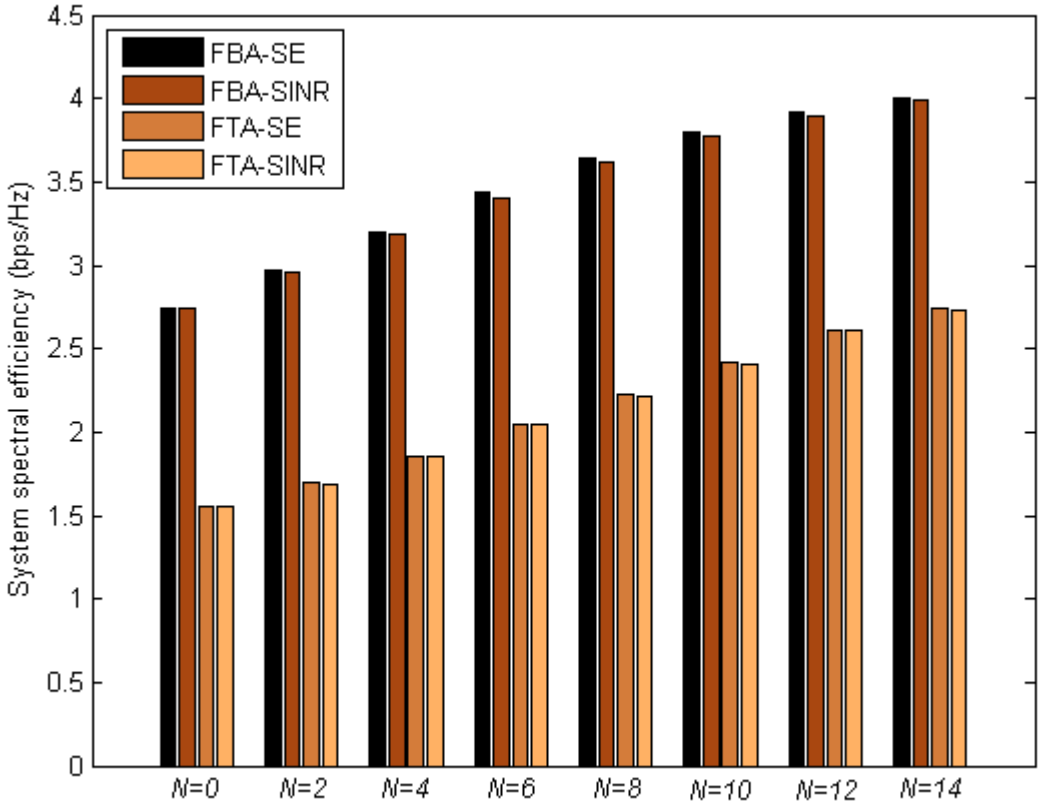

Figure 11. System SE of four system configurations.

2.5.1.1 Frequency Reuse over RS-MS Links

To better utilize the radio resource, frequency reuse over the RS-MS links is explored here. The case of six RSs is taken as an example with the following reuse patterns, $G=\{G_1,G_2,G_3,G_4,G_5,G_6\}$, $G=\{G_1,G_2,G_3\}$, $G=\{G_1,G_2\}$, and $G=\{G_1\}$ where each reuse group has equal number of RSs. Figure 12 depicts the throughput distribution of FBA-SE. Circles with the same letter indicate the service area of RSs in the same reuse groups. Again, RSs are placed on the line connecting cell center to six vertexes of the cell, with RSs in the same reuse group being pulled away as far as possible. In the full reuse case, as shown in Figure 12 (d), severe interference leads to a shrinking of the service area of RSs. With respect to system SE, the reuse cases always outperform the no-reuse cases, as shown in Figure 13, where the reuse pattern $G=\{G_1,G_2\}$ gives the highest SE. Also, it is very interesting to see that SINR-based path selection has a higher SE than the SE-based path selection for both FBA and FTA in the frequency-reuse cases. This can be attributed to that RSs always have larger service area with the SINR-based path selection, which leads to a larger bandwidth saving in the frequency-reuse case. Table 3 summarizes the important system parameters for four different system configurations. Note that in this example, the reuse pattern $G=\{G_1,G_2,G_3\}$ gives the largest service area of RS, whereas $G=\{G_1,G_2\}$ gives the highest system SE; that is, there is a tradeoff between MAI and frequency reuse.

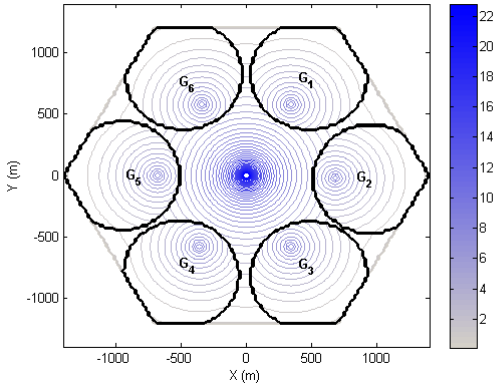

(a) G={G_1, G_2, G_3, G_4, G_5, G_6}

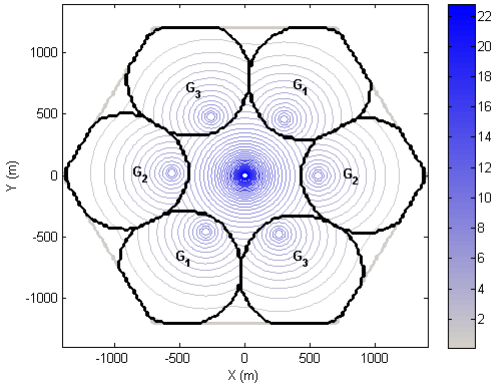

(b) G={G_1, G_2, G_3}

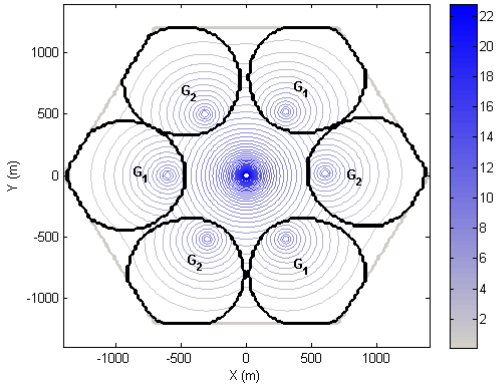

(c) G={G_1, G_2}

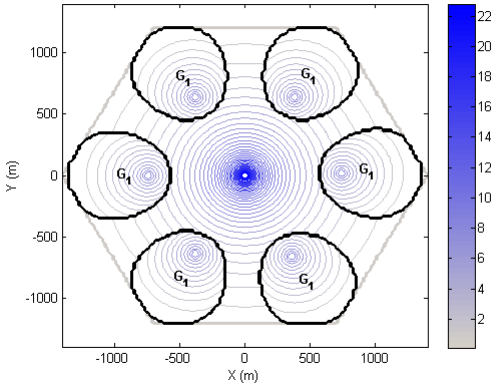

(d) G={G_1}

Figure 12. Throughput distribution (bps per unit area) of different frequency-reuse patterns for FBA-SE (*N*=*6*).

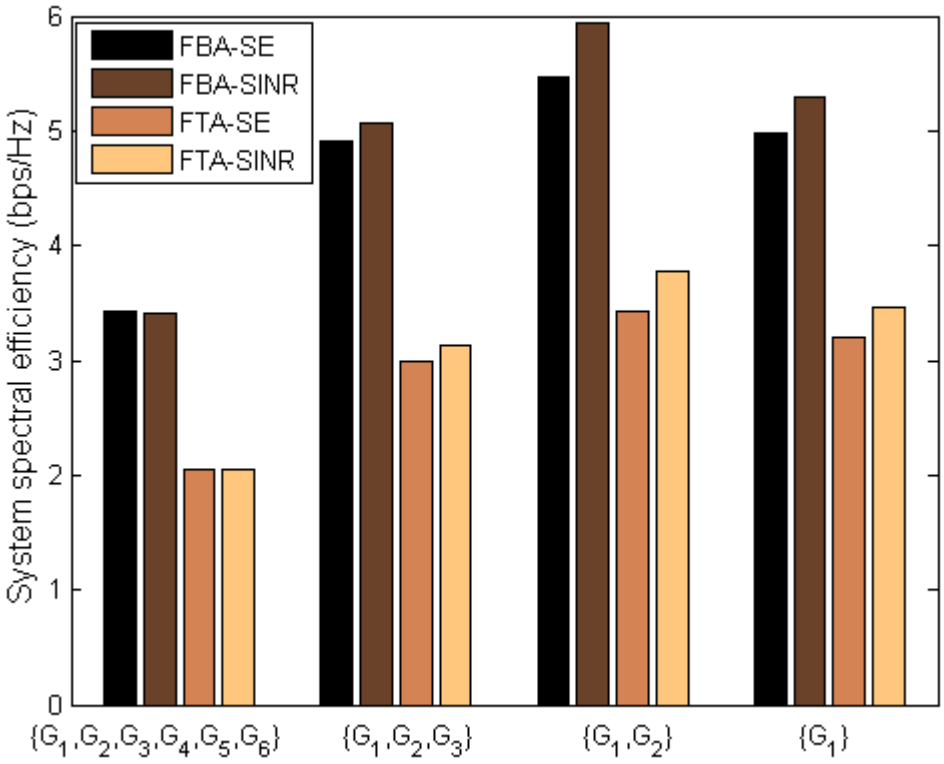

Figure 13. System SE of different frequency-reuse patterns (*N=6*).

Table 3. Important parameters for frequency reuse patterns (N=6).

	G	$\{G_1, G_2, G_3, G_4, G_5, G_6\}$	$\{G_1, G_2, G_3\}$	$\{G_1, G_2\}$	$\{G_1\}$
(a) FBA-SE	Ω_B:Ω_R (%)	31:69	21:79	28:72	49:51
	$w_{B\to M}$: $w_{B\to R}$:$w_{R\to M}$ (%)	31:14:55	31:22:47	45:23:32	74:16:10
	S_Ω (bps/Hz)	3.4329	4.9120	5.4713	4.9848
(b) FBA-SINR	Ω_B:Ω_R (%)	27:73	14:86	16:84	43:57
	$w_{B\to M}$: $w_{B\to R}$:$w_{R\to M}$(%)	27:15:58	21:26:53	29:29:42	69:18:13
	S_Ω (bps/Hz)	3.4043	5.0586	5.9428	5.2868
(c) FTA-SE	Ω_B:Ω_R (%)	47:53	25:75	30:70	50:50
	$w_{B\to M}$: $w_{B\to R}$:$w_{R\to M}$ (%)	43:8:49	31:16:53	44:17:39	75:12:13
	S_Ω (bps/Hz)	2.0516	2.9570	3.4322	3.2042
(d) FTA-SINR	Ω_B:Ω_R (%)	44:56	16:84	18:82	43:57
	$w_{B\to M}$: $w_{B\to R}$:$w_{R\to M}$(%)	39:9:52	19:19:62	28:22:50	69:15:16
	S_Ω (bps/Hz)	2.0429	3.1383	3.7729	3.4575

2.5.1.2 Shadowing Effects

In this subsection, an example is given to verify the effectiveness of the proposed method in a shadowed environment. First, we show how the shadowing effect degrades the system performance under the same power setup criteria in Section 2.5.1. The simplified shadow model in Figure 5 is adopted with four obstacles (of length 800 m) centered at (0, ±750) and (±750, 0). Two sets of shadowing loss δ =10 dB and δ =20 dB are considered [see (2.3)]. In Figure 14 (a) and (c), the achievable throughput in the shadowed area is relatively low, as one might expect. Then, four RSs are deployed into the cell. FBA-SE is considered in this case. The optimization algorithm suggests that RSs should be placed at (0, ±760) and (±760, 0) which are right behind the four obstacles. The throughput enhancement is shown in Figure 14 (b) and (d) for δ =10 dB and δ =20 dB, respectively. In Figure 14 (b), in addition to serving the severely shadowed area, RSs also provide service to small fractions of the area across the obstacle, where the throughput provided by RSs is higher than that by BS. In Figure 14 (d), we can see that this area is reduced as the shadowing loss increases. As can be seen, in a relay assisted cellular system, the shadowing effects can largely be removed by deploying RSs.

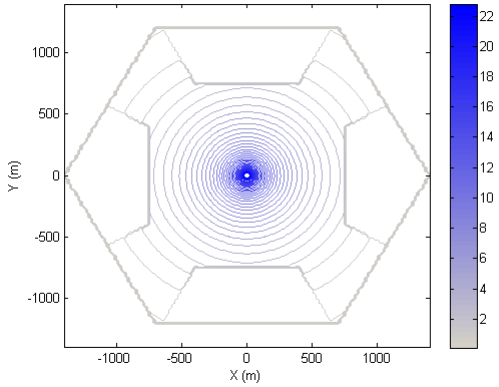

(a) $N = 0$, $\delta = 10$ dB

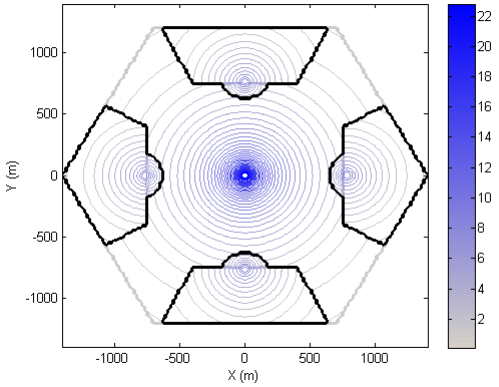

(a) $N = 4$, $\delta = 10$ dB

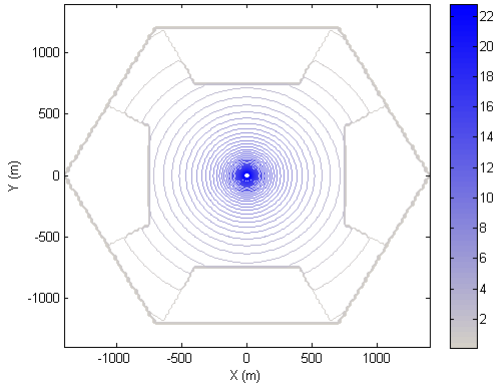

(a) $N = 0$, $\delta = 20$ dB

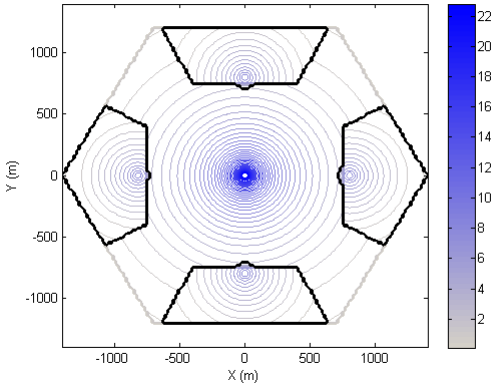

(a) $N = 4$, $\delta = 20$ dB

Figure 14. Throughput distribution (bps per unit area) of FBA-SE under shadowing effects.

2.5.1.3 Sectorization

In this subsection, we investigate how RSs are placed and how they can improve the system performance when the BS is equipped with a sectored antenna. A three-sector antenna is employed with the antenna pattern given in (2.4). FTA-SE is taken as an example. In the sectorized cell, the power of BS is set to achieve the targeted SE $S_{edge} = 0.5$ bps/Hz for the users at the worst locations, which are the cell vertices on the sector boundary. Notice that with this power setting, the users at the cell vertices in the antenna-bearing direction can enjoy higher SE. Figure 15 (a) shows the distribution of bandwidth consumption for achieving $t_d = 1$ bps (per unit area) with no RS in the cell. As can be seen, users at the cell vertices on the sector boundary need 2 Hz to support the targeted throughput, whereas users at the cell vertices in the antenna-bearing direction only need 0.5 Hz. The system SE S_Ω in this case is 2.92 bps/Hz. Figure 15 (b) – (d) show the results for using three RSs. No frequency reuse over the RS-MS links is considered. Figure 15 (b) gives the optimal RSs positions and the distribution of bandwidth consumption for S_{edge} = 0.5 bps/Hz for RSs. As expected, RSs tend to assist the areas with relatively low link SE. That is, RSs are placed on the sector boundaries to reduce the overall bandwidth consumption. From our numerical results, RSs serve about 13% of total area, and S_Ω is 3.32 bps/Hz, which is 14% improvement as compared with the case in Figure 15 (a). Figure 15 (c) and (d) show the results for S_{edge} = 1.0 bps/Hz and S_{edge} = 1.5 bps/Hz for RSs, respectively. Again, RSs are placed on the sector boundaries to enhance the system SE. In these cases, RSs provide 22% and 30% of the service area, and S_Ω are increased to 3.61 bps/Hz and 3.83 bps/Hz, respectively.

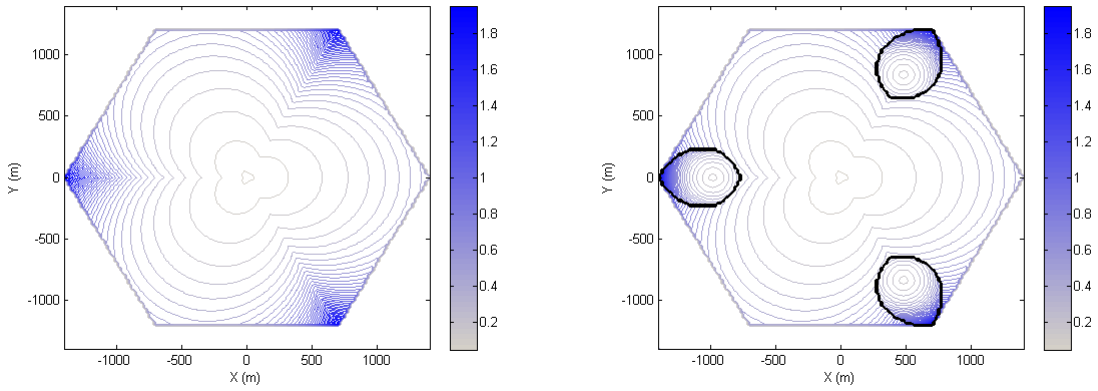

(a) $N = 0$ (b) $N = 3$, $S_{edge} = 0.5$ bps/Hz for RSs

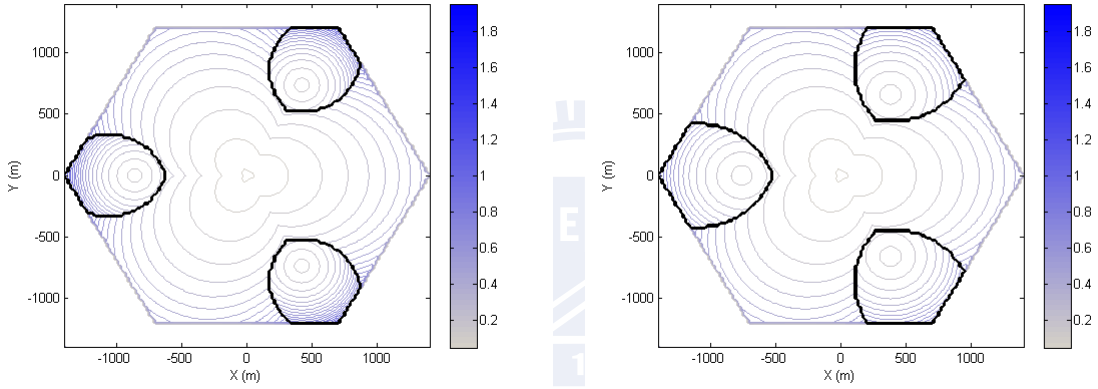

(c) $N = 3$, $S_{edge} = 1.0$ bps/Hz for RSs (d) $N = 3$, $S_{edge} = 1.5$ bps/Hz for RSs

Figure 15. Optimal RSs' positions and bandwidth consumption (Hz per unit area) for FTA-SE in a three-sector cell.

2.5.2 Multiple Cells

In this part, we use an example to illustrate how the joint optimization is done over multiple cells. We consider the cell structure of $(3,3,3)$ (see Figure 3), where a total of nine RSs are deployed in the cells Ω_1, Ω_2 and Ω_3 with three RSs for each cell. For BSs, the power is set to achieve $S_{\text{edge}} = 0.5$ bps/Hz for the users located at the cell vertices on the sector boundary, and for RSs, the setting is to achieve $S_{\text{edge}} = 1.0$ bps/Hz. The co-channel interference from the first-tier co-channel cells is taken into consideration. Figure 16 (a) – (c) show the optimal placement of RSs and the distribution of bandwidth consumption in Ω_1, Ω_2 and Ω_3, respectively, for FTA-SE. As expected, RSs are placed on the sector boundaries to best improve the SE, and the cells have a similar layout, where RSs in the same reuse group are placed as far apart as possible in order to reduce the co-channel interference. In addition, our numerical results show that S_Ω is 2.94 bps/Hz in the case of no RS, and S_Ω is improved to 3.60 bps/Hz with three RSs deployed, where RSs serve about 20% of the total area of each cell.

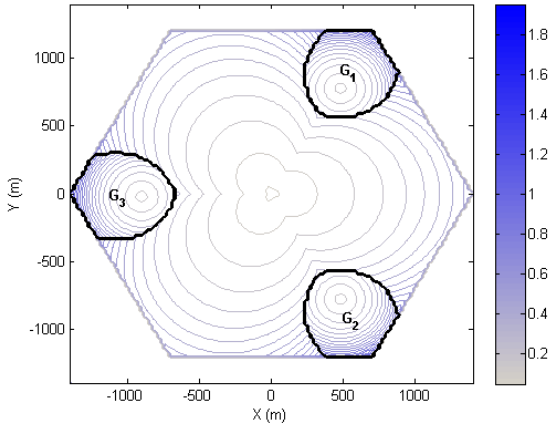

(a) Ω_1

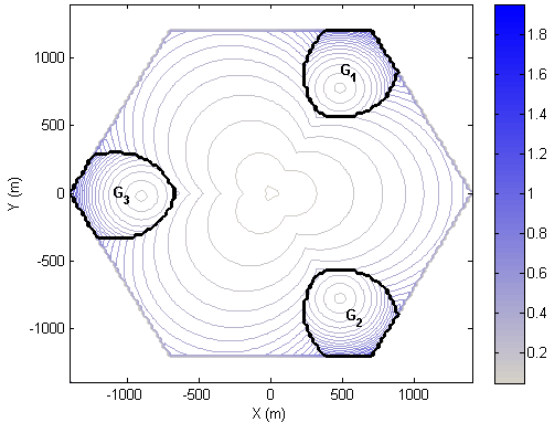

(b) Ω_2

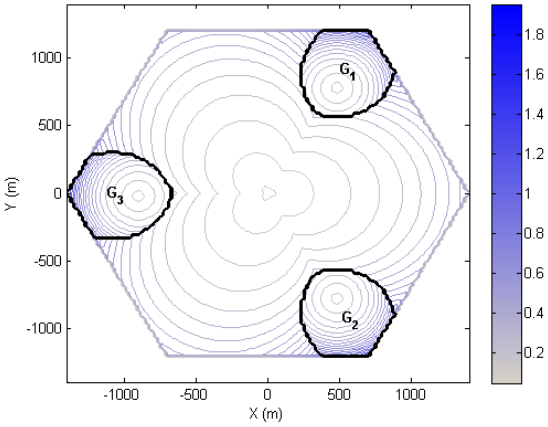

(c) Ω_3

Figure 16. RSs' positions and bandwidth consumption (Hz per unit area) with joint optimization of B_1, B_2 and B_3 in Figure 3 for FTA-SE.

2.6 Summary

In Chapter 2, the optimization and theoretical performance of relay-assisted cellular networks have been investigated in the multi-cell environment. A GA is proposed for joint multi-cell optimization of system parameters, including RS's positions, path selection, frequency reuse pattern, and resource allocation, to maximize system SE. Four different system configurations are considered, including FBA-SE (fixed-bandwidth allocation with SE-based path selection), FBA-SINR (fixed-bandwidth allocation with SINR-based path selection), FTA-SE (fixed-throughput allocation with SE-based path selection) and FTA-SINR (fixed throughput allocation with SINR-based path selection). Numerical results show that (i) RSs provide significant improvement with respect to system SE and user throughput over the traditional cellular networks. (ii) The uniformity of user data rate comes at the expense of a large loss in system SE when FTA is employed. (iii) Somewhat surprising, the low-complexity SINR-based path selection performs nearly as well as the SE-based one for the no-reuse case, while it is slightly better in the frequency reuse case.

Chapter 3
Uplink Performance and Optimization of Relay-assisted Cellular Networks

In this chapter, we aim to investigate the uplink performance of a general relay-assisted cellular system with optimal system parameters. Two performance measures, average power consumption of MSs and uplink system spectral efficiency (SE), are optimized by jointly considering the system parameters of RSs' locations, reuse patterns, path selections and resource allocation. The optimization is done based on a genetic algorithm (GA) and a method for multiple access interference (MAI) estimation. Numerical results show that the average MS's transmit power is significantly reduced and the uplink system SE is largely enhanced as RSs are deployed and used in the optimal way. The background, the system setups, the objective functions, the proposed optimization algorithm, and the numerical results are presented in the following subsections.

3.1 Background

There have been few studies on the uplink performance of the relay-assisted cellular systems [25], [38], [68]. In [25], the issues of capacity, cell coverage, and MS transmit power were considered in a relay-assisted CDMA network with six RSs under different frequency allocation methods. In [38], the issues of RS positioning and spectrum partitioning were studied by searching optimal RSs locations along the lines connecting BS and the six vertices of a hexagonal cell to maximize the mean user data rate. In [68], the uplink capacity of an 802.16j system was discussed, where a simplified one-dimensional model is analyzed for the maximal capacity gains, and fixed number of RSs with uniform placement is also simulated.

These studies, however, have been done for very limited system scenarios: fixed number RSs and locations, fixed reuse pattern, or seeking optimal RSs' positions with a simplified one-dimensional model.

In this dissertation, two important uplink performance measures, average MS's power consumption and uplink system SE, have been optimized for a general relay-assisted cellular system.

3.2 System Setups

For the uplink performance evaluation, the system parameters and setups are mostly similar to those in Section 2.2. Slight differences are highlighted as follows. For the cell configuration, the system parameters are adopted as described in Section 2.2.1, except that the single cell structure in the uplink evaluation is taken into consideration. In the uplink, MS communicates with BS either through a direct path (the MS-BS link) or a two-hop path (via an RS) which forms the MS-RS link and the RS-BS link. Here we assume that all stations (BS,

RSs and MSs) are equipped with an omni-directional antenna and one RF transceiver. For the PSD setting of an RS, the same setting as (2.8) is applied and we assume that RSs use the same power level (PSD) to communicate with BS in the reverse link. For the relaying technology, the propagation models, and the frequency reuse adopted in this chapter, please refer to Section 2.2.2, 2.2.3, 2.2.5, 2.2.7, respectively. With regard to the uplink path selection, different criteria will be mentioned in Section 3.3 in terms of different objectives.

3.3 Problem Formulation

In the uplink, in addition to the system SE, MSs' power consumption is also an important performance measure due to the limited battery life. In this section, given a fixed amount of bandwidth for each MS, two system performance measures are investigated: one is to minimize the average MS's transmit power for a specified throughput; the other is to maximize the uplink SE by given a fixed MS's transmit power, by jointly searching optimal RSs' positions, reuse pattern, path selection and bandwidth allocation.

Let w_u (Hz per unit area) be the uplink bandwidth allocated to an MS at location $\vec{m}$. Then, $w_u = w_{M\to B}(\vec{m}) = w_{M\to R_j}(\vec{m}) + w_{R_j\to B}(\vec{m})$, where $w_{M\to B}(\vec{m})$ is the bandwidth allocated to the $\text{MS}\to\text{BS}$ link, $w_{R_j\to B}(\vec{m})$ to the $R_j\to\text{BS}$ link, and $w_{M\to R_j}(\vec{m})$ to the $\text{MS}\to R_j$ link, respectively. Let $S_{M\to B}(\vec{m})$, $S_{M\to R_j}(\vec{m})$, and $S_{R_j\to B}(\vec{m})$ denote the SE for the $\text{MS}\to\text{BS}$ link, the $\text{MS}\to R_j$ link, and the $R_j\to\text{BS}$ link, respectively.

In the AWGN channel,

$$S_{M\to B}(\vec{m}) = \log_2\left(1+\frac{P_{M\to B}(\vec{m})\cdot L_{NLOS}^{-1}(\|\vec{m}\|)}{(N_0+I_{M\to B})\cdot w_u}\right), \tag{3.1}$$

$$S_{M\to R_j}(\vec{m}) = \log_2\left(1+\frac{P_{M\to R_j}(\vec{m})\cdot L_{NLOS}^{-1}(\left\|\vec{r}_j-\vec{m}\right\|)}{(N_0+I_{M\to R_j})\cdot w_{M\to R_j}(\vec{m})}\right), \tag{3.2}$$

and

$$S_{R_j\to B}(\vec{m}) = \log_2\left(1+\frac{P_{R_j\to B}(\vec{m})\cdot L_{LOS}^{-1}(\left\|\vec{r}_j\right\|)}{(N_0+I_{R_j\to B})\cdot w_{R_j\to B}(\vec{r}_j)}\right), \tag{3.3}$$

where $P_{M\to B}(\vec{m})$ and $P_{M\to R_j}(\vec{m})$ are the MS's transmit power of the $\text{MS}\to\text{BS}$ link and the $\text{MS}\to R_j$ link, $P_{R_j\to B}(\vec{m})$ is the transmit power of R_j, and $I_{M\to B}$, $I_{M\to R_j}$ and $I_{R_j\to B}$ are the PSDs of average MAI appearing over the $\text{MS}\to\text{BS}$ link, the $\text{MS}\to R_j$ link, and the $R_j\to\text{BS}$ link, respectively. Note that we assume RSs apply the same PSD settings to communicate with their BS as that shows in (2.8). With this assumption, $S_{R_j\to B}(\vec{m})$ can be solved.

The throughput for the $\text{MS}\to\text{BS}$ link, the $\text{MS}\to R_j$ link, and the $R_j\to\text{BS}$ link are then expressed by

$$t_{M\to B}(\vec{m}) = w_u\cdot S_{M\to B}(\vec{m}), \tag{3.4}$$

$$t_{M\to R_j}(\vec{m}) = w_{M\to R_j}(\vec{m})\cdot S_{M\to R_j}(\vec{m}), \tag{3.5}$$

and

$$t_{R_j\to B}(\vec{m}) = w_{R_j\to B}(\vec{m})\cdot S_{R_j\to B}(\vec{m}). \tag{3.6}$$

3.3.1 Measure 1—Minimization of Average MS's Transmit Power

In this subsection, the average uplink transmit power of MS will be minimized to achieve

a targeted throughput T_u.

Derived by (3.1) and (3.4), the MS's transmit power for a direct path is given by

$$P_{M\to B}(\vec{m}) = (2^{\frac{T_u}{w_u}} - 1)\cdot L_{NLOS}(\|\vec{m}\|)\cdot(N_0 + I_{M\to B})\cdot w_u. \tag{3.7}$$

For a two-hop path, since $t_{M\to R_j\to B}(\vec{m}) = \min\left\{t_{M\to R_j}(\vec{m}),\ t_{R_j\to B}(\vec{m})\right\}$, where $t_{M\to R_j\to B}(\vec{m})$ is the effective throughput of a two-hop link, the most efficient situation is to achieve $T_u = t_{M\to R_j}(\vec{m}) = t_{R_j\to B}(\vec{m})$. As a result, the bandwidth allocation for each hop is given by

$$w_{R_j\to B}(\vec{m}) = \frac{T_u}{S_{R_j\to B}(\vec{m})}, \tag{3.8}$$

and

$$w_{M\to R_j}(\vec{m}) = w_u - w_{R_j\to B}(\vec{m}). \tag{3.9}$$

Since the optimal case for $t_{M\to R_j}(\vec{m})$ is equal to T_u, by (3.2) and (3.5), the MS's transmit power to RS can be expressed as

$$P_{M\to R_j}(\vec{m}) = (2^{\frac{T_u}{w_{M\to R_j}(\vec{m})}} - 1)\cdot L_{NLOS}(\|\vec{r}_j - \vec{m}\|)\cdot(N_0 + I_{M\to R_j})\cdot w_{M\to R_j}(\vec{m}). \tag{3.10}$$

Given $S_{R_j\to B}(\vec{m})$ solved in the previous section, both (3.8) and (3.9) can be calculated so that (3.10) can be obtained.

The optimal path selection is then to select the direct path if $P_{M\to B}(\vec{m}) \le P_{M\to R_j}(\vec{m})$, where $P_{M\to R_j}(\vec{m}) = \min_{R_i}\{P_{M\to R_i}(\vec{m})\}$; otherwise the two-hop path via R_j is selected, where $R_j = \arg\min_{R_i}\{P_{M\to R_i}(\vec{m})\}$. Finally, the objective function is given

$$\min \ P_{M,avg} \tag{3.11}$$

with

$$P_{M,avg} = \frac{1}{\Omega_B}\int_{\vec{m}\in\Omega_B} P_{M\to B}(\vec{m})\, dA + \sum_{j=1}^{N}\frac{1}{\Omega_{R_j}}\int_{\vec{m}\in\Omega_{R_j}} P_{M\to R_j}(\vec{m})\, dA, \tag{3.12}$$

where Ω_B and Ω_{R_j} are the service area of BS and R_j, respectively. It is clear that $\Omega = \Omega_B \bigcup \Omega_R$ with $\Omega_R = \bigcup_{j=1}^{N}\Omega_{R_j}$.

3.3.2 Measure 2—Maximization of Uplink System SE

In this subsection, given a fixed among of uplink bandwidth w_u and a fixed transmit power P_M of each MS, the system SE will be maximized.

For a direct-path, the throughput is

$$t_{M\to B}(\vec{m}) = w_u \cdot \log_2\left(1+\frac{P_M \cdot L_{NLOS}^{-1}(\|\vec{m}\|)}{(N_0 + I_{M\to B})\cdot w_u}\right). \tag{3.13}$$

For a two-hop path, again, $t_{M\to R_j}(\vec{m}) = t_{R_j\to B}(\vec{m})$ gives the highest SE. Therefore, when

$$w_{R_j\to B}(\vec{m}) = \frac{s_{M\to R_j}(\vec{m})}{s_{R_j\to B}(\vec{m}) + s_{M\to R_j}(\vec{m})}\cdot w_u, \tag{3.14}$$

and

$$w_{M\to R_j}(\vec{m}) = \frac{s_{R_j\to B}(\vec{m})}{s_{R_j\to B}(\vec{m}) + s_{M\to R_j}(\vec{m})}\cdot w_u, \tag{3.15}$$

the maximum attainable throughput is

$$t_{M\to R_j\to B}(\vec{m}) = t_{M\to R_j}(\vec{m}) = t_{R_j\to B}(\vec{m}) = \frac{s_{R_j\to B}(\vec{m})\cdot s_{M\to R_j}(\vec{m})}{s_{R_j\to B}(\vec{m}) + s_{M\to R_j}(\vec{m})}\cdot w_u \,. \tag{3.16}$$

Notice that from (3.2) together with (3.15), we need to solve the following nonlinear equation for the optimal $S_{M\to R_j}(\vec{m})$,

$$S_{M\to R_j}(\vec{m}) = \log_2\left(aS_{M\to R_j}(\vec{m}) + b\right), \tag{3.17}$$

where

$$a = \frac{P_M \cdot L_{NLOS}^{-1}(\left\|\vec{r}_j - \vec{m}\right\|)}{(N_0 + I_{M\to R_j})\cdot S_{R_j\to B}(\vec{r}_j)\cdot w_u}, \tag{3.18}$$

and

$$b = \frac{P_M \cdot L_{NLOS}^{-1}(\left\|\vec{r}_j - \vec{m}\right\|)}{(N_0 + I_{M\to R_j})\cdot w_u} + 1, \tag{3.19}$$

The optimal path selection is then to select the direct path if $t_{M\to B}(\vec{m}) \geq t_{M\to R_j\to B}(\vec{m})$, where $t_{M\to R_j\to B}(\vec{m}) = \max_{R_i}\left\{t_{M\to R_i\to B}(\vec{m})\right\}$; otherwise, the two-hop path via R_j is selected, where $R_j = \arg\max_{R_i}\left\{t_{M\to R_i\to B}(\vec{m})\right\}$.

Let S_{Ω_u}, T_{Ω_u}, and W_{Ω_u} denote the uplink SE, uplink system throughput, and uplink system bandwidth consumption, respectively. The objective function is then expressed by

$$\max\ S_{\Omega_u} \doteq \frac{T_{\Omega_u}}{W_{\Omega_u}}\ \text{(bps/Hz)}, \tag{3.20}$$

where

$$T_{\Omega_u} = T_{\Omega_B} + \sum_{j=1}^{N} T_{\Omega_{R_j}}, \tag{3.21}$$

with

$$T_{\Omega_B} = \int_{\vec{m}\in\Omega_B} t_{M\to B}(\vec{m})\, dA, \tag{3.22}$$

$$T_{\Omega_{R_j}} = \int_{\vec{m}\in\Omega_{R_j}} t_{M\to R_j\to B}(\vec{m})\, dA, \tag{3.23}$$

and

$$W_{\Omega_u} = W_{\Omega_B} + W_{\Omega_R}, \tag{3.24}$$

where

$$W_{\Omega_B} = \int_{\vec{m}\in\Omega_B} w_u\, dA, \tag{3.25}$$

and

$$W_{\Omega_R} = \sum_{j=1}^{N} W_{R_j\to B} + \sum_{l=1}^{L} W_{M\to R,l}, \tag{3.26}$$

with

$$W_{R_j\to B} = \int_{\vec{m}\in\Omega_{R_j}} w_{R_j\to B}(\vec{m})\, dA, \tag{3.27}$$

$$W_{M\to R,l} = \max_{R_j\in G_l}\{W_{M\to R_j}\}, \tag{3.28}$$

and

$$W_{M\to R_j} = \int_{\vec{m}\in\Omega_{R_j}} w_{M\to R_j}(\vec{m})\, dA. \tag{3.29}$$

3.4 Genetic-Based Optimization

It is observed that (3.11) and (3.20) are highly nonlinear functions for RSs' positions and the reuse pattern G so that the analytic solutions are not available in general. To solve these problems, a particular design of GA based optimization and an MAI estimation method for uplink are proposed. For the GA operation, the detailed concept is described in Section 2.4.1. For the manipulation for uplink optimization, similar ideas from downlink optimization are adopted and please refer to Section 2.4.2. Besides, in the uplink, when applying intra-cell frequency reuse among the MS to RS links, MAI estimation is important since the exact locations of interferer are usually unknown to the MS. The design of MAI estimation algorithm is detailed in Section 3.4.1. The overall flowchart of GA operation and the MAI estimation is illustrated in Figure 17.

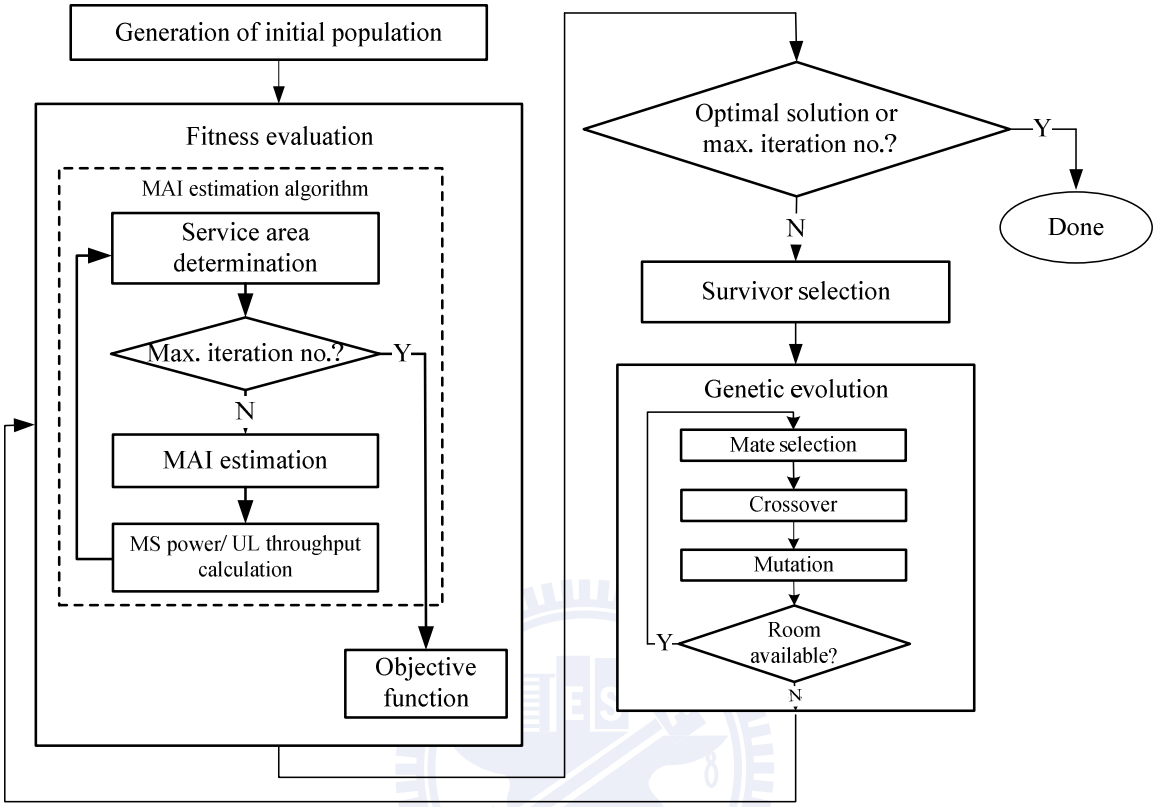

Figure 17. The operation of genetic algorithm.

3.4.1 MAI Estimation Algorithm

An MAI estimation algorithm, shown in Figure 17, is proposed to determine the MAI level when the frequency is reused over the MS-RS links.

First, MS chooses the nearest BS or RS as its serving station so that the Ω_B and Ω_{R_j} are predetermined. Given an MS served by the *k*-th RS in the reuse group l, i.e., $\vec{m} \in \Omega_{R_{k_l}}$, the MAI for this MS is caused by the co-channel user in G_l. We calculate the MAI level for the MS by averaging over the potential interfering area, which is expressed by

$$I_{M_I \to R_k} = \sum_{\substack{R_i \in G_l \\ i \neq k}} \int_{\vec{m}_I \in \Omega_{R_i}} \frac{1}{\Omega_{R_i}} \cdot P_{M_I \to R_i}(\vec{m}_I) \cdot L_{NLOS}(\|\vec{m}_I - \vec{r}_k\|) dA, \tag{3.30}$$

where M_I is the interferer with position vector $\vec{m}_I$ and R_i is its serving station.

In Measure 1, we assume $I_0 = N_0$ for the initial power setup of the interfering source, which is

$$P_{M_I \to R_i}(\vec{m}_I) = (2^{\frac{T_u}{w_{M_I \to R_i}}} - 1) \cdot L_{NLOS}(\|\vec{r}_i - \vec{m}_I\|) \cdot 2N_0 \cdot w_{M_I \to R_i}. \tag{3.31}$$

Substituting (3.2) into (3.1), the average MAI level for the MS is obtained. Then, the transmit power of $\vec{m}$ for a two-hop path can be determined by

$$P_{M \to R_k}(\vec{m}) = (2^{\frac{T_u}{w_{M \to R_k}}} - 1) \cdot L_{NLOS}(\|\vec{r}_k - \vec{m}\|) \cdot (N_0 + I_{M_I \to R_k}) \cdot w_{M \to R_k}. \tag{3.32}$$

MS can decide its new serving station by choosing minimal transmit power among direct path and two-hop path. Then, Ω_B and Ω_R are re-determined.

In Measure 2, $P_{M_I \to R_i}(\vec{m}_I) = P_M$, and the throughput for two-hop path can be determined

by following the process (3.21) to (3.29). Again, MS can decide its new serving station by choosing maximization throughput among the direct path and the two-hop path so that Ω_B and Ω_R can be are re-decided.

The procedure is repeated until the service area is converged or the maximum iteration number is reached.

3.5 Simulation Results

In our numerical results, the cell radius is set as 1400 m, the cell region is divided into grids with each side equal to 20 m, and the locations of all stations (BS, RSs, and MS) are rounded off to the nearest grid vertices. Let S_{edge} be 0.5 bps/Hz for PSD setup of RSs. In the GA operation, N_{pop} = 200, β = 0.5 and P_{mut} = 0.05 are adopted. The Gaussian variable with variance equal to a grid length is used as the perturbation when performing crossover operations. Through the work, w_u = 28.5 KHz per unit area is allocated to MS. Newton's method is adopted to solve the nonlinear equation mentioned in (3.17) to (3.19). Besides, the inter-cell interference is assumed to be constant and embedded into the thermal noise, while the effect of intra-cell interference caused by frequency reuse over MS-RS links is evaluated in our simulations. Note that the number of generations (iterations) in GA depends on the number of RSs involved; more generations are needed for a larger number of RSs.

3.5.1 Measure 1—Minimization of Average MS's Transmit Power

In this subsection, we will see how RSs are placed to reduce the average transmit power of MS. $T_u = 14.25$ Kbps per unit area is set in this section. Assume that there is no

frequency reuse among MS-RS links. Figure 18 shows the optimal RSs placement and the distribution of transmit power consumption (in dBm). Figure 18 (a) is the case for no RS ($N=0$). Clearly, more transmit power is needed for a more distant MS. The average transmit power is 14.54 dBm, which is summarized in Table 4. Figure 18 (b) is for the case of $N=2$. The optimal RSs positions are in $(\pm 660, 0)$. The service area of BS and RSs is indicated by the black lines, where BS serves 31% of total area while two RSs serve the other 69%. The average transmit power is 10.75 dBm in this case, which is 3.79 dB lower than that of no RS case. Figure 18 (c) shows the case of four RSs, where the area served by RSs is 86% and the average transmit power is 3.18 dBm; gains of 11.36 dB and 7.57 dB as compared to $N=0$ and $N=2$, respectively. Figure 18 (d) is the case of 6 RSs. As can be seen, the optimal RSs positions are on the lines connecting the cell center and six vertices of the hexagonal cell with distance 900m from the BS, and the whole area is almost evenly partitioned by the BS and six RSs, where each station serves about 14% of total area. The average transmit power is -2.05 dBm, which is reduced 16.59 dB as compared to $N=0$. It is clear that if the RS-BS link was perfect in the two-hop path, the service area border of the BS and RSs would be in the perpendicular bisection of the line segment connecting the BS and RSs. Table 4 summarizes the service area ratio of the BS and RSs, bandwidth allocation ratio for MS-BS links, MS-RS links, and RS-BS links, and the average uplink transmit power for $N=0$ to $N=10$. Figure 19 depicts the complementary cumulative distribution functions (CDFs) of MS's power consumptions. As can be seen, the percentage of large power consumption area is significantly reduced with the help from RSs.

Table 4. System parameters of Measure 1 for N = 0 to N = 10.

N	$\Omega_B : \Omega_R$ (%)	$w_{M\to B} : w_{M\to R} : w_{R\to B}$ (%)	$P_{M,avg}$ (dBm)
0	100:0	100:0:0	14.54
2	31:69	31:65:4	10.75
4	14:86	14:80:6	3.18
6	14:86	14:80:6	-2.05
8	14:86	14:79:7	-3.75
10	11:89	11:82:7	-5.07

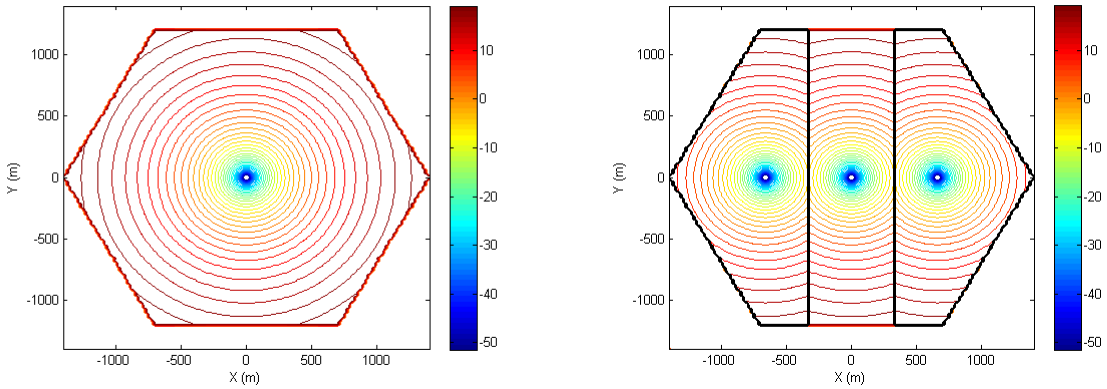

(a) $N = 0$ (b) $N = 2$

(c) $N = 4$ (d) $N = 6$

Figure 18. Optimal RSs' positions and uplink transmit power distribution (in dBm).

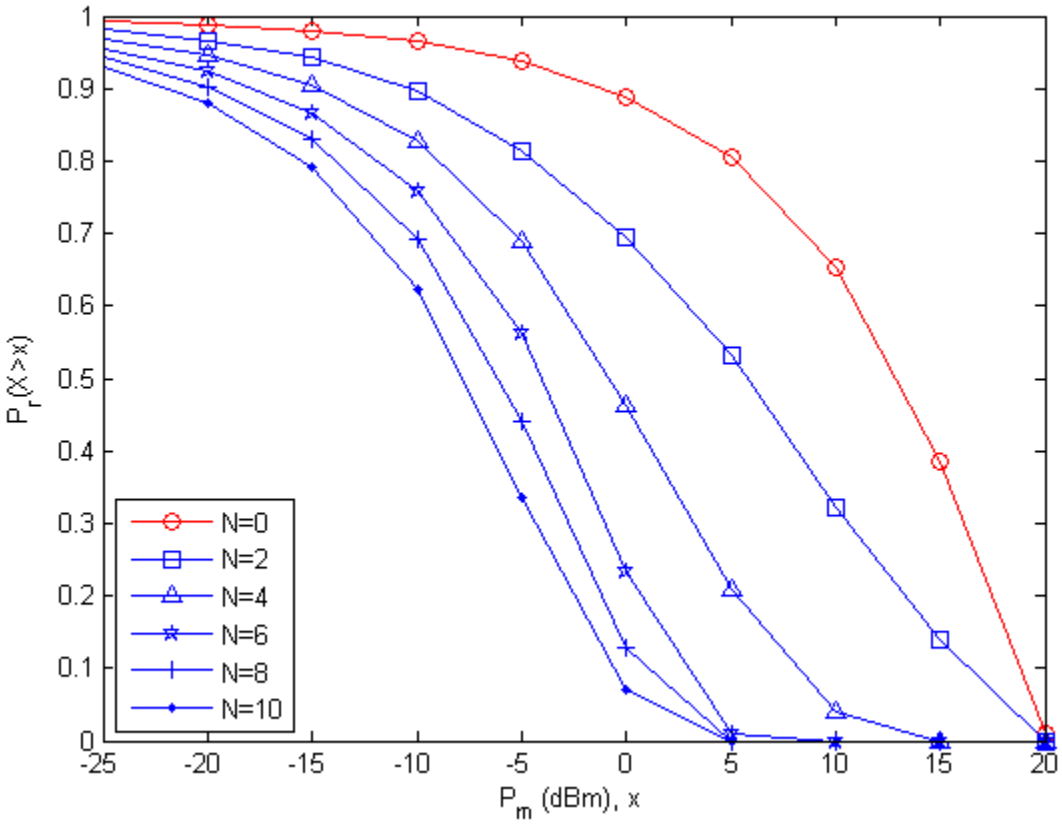

Figure 19. Complement CDFs of uplink transmit power.

In this subsection, frequency reuse over the MS-RS links is explored to further utilize the radio resource. The case of $N = 6$ is taken as an example. Figure 20 (a) to (d) depicts the optimal RSs' locations and the distribution of power consumptions for the following reuse patterns, $G=\{G_1, G_2, G_3, G_4, G_5, G_6\}$, $G=\{G_1, G_2, G_3\}$, $G=\{G_1, G_2\}$ and $G=\{G_1\}$, respectively. Note that each reuse group has equal number of RSs. As can be seen, RSs are placed on the line connecting the cell center to six vertices of the cell in each case with RSs in the same reuse group being pulled as far apart as possible. Table 5 provides more detailed parameters of all cases. The uplink system SE is getting better when the frequency is more aggressively reused (i.e., $G=\{G_1\}$); however, it costs more transmit power to achieve the same targeted throughput due to larger MAI.

A simplified shadowing model is also given to verify the effectiveness of the deployment of RSs. Two obstacles of length 800 m are centered at (690, 0) and (-690, 0). The shadow loss $\delta = 10$ dB is adopted if the line of sight of MS and BS is blocked by any obstacle. In Figure 21 (a), MS in the shadowed area needs very high transmit power level to achieve the targeted throughput $T_u = 14.25$ Kbps, as one might expect. The average MS's transmit power is 20.47 dBm in this case. Figure 21 (b) shows the case with two RSs deployed into the cell. The optimization algorithm suggests that the RSs should be placed at (700, -420) and (-700, 420) to reduce the percentage of blocked line of sight between an MS and its serving station (BS or RS). Black lines circle the service area of each RS. As can be seen, the ratio of MSs in the shadowed area is significantly decreased, except the case that a few MSs which are close to RS still have smaller propagation loss to RS than that to BS even if they suffer from shadowing loss to connect to RS. The average MS's transmit power is reduced to 10.89 dBm, which saves 9.58 dB in average as compared to Figure 21 (a). From this example, the shadowing effects can be largely removed by deploying RSs.

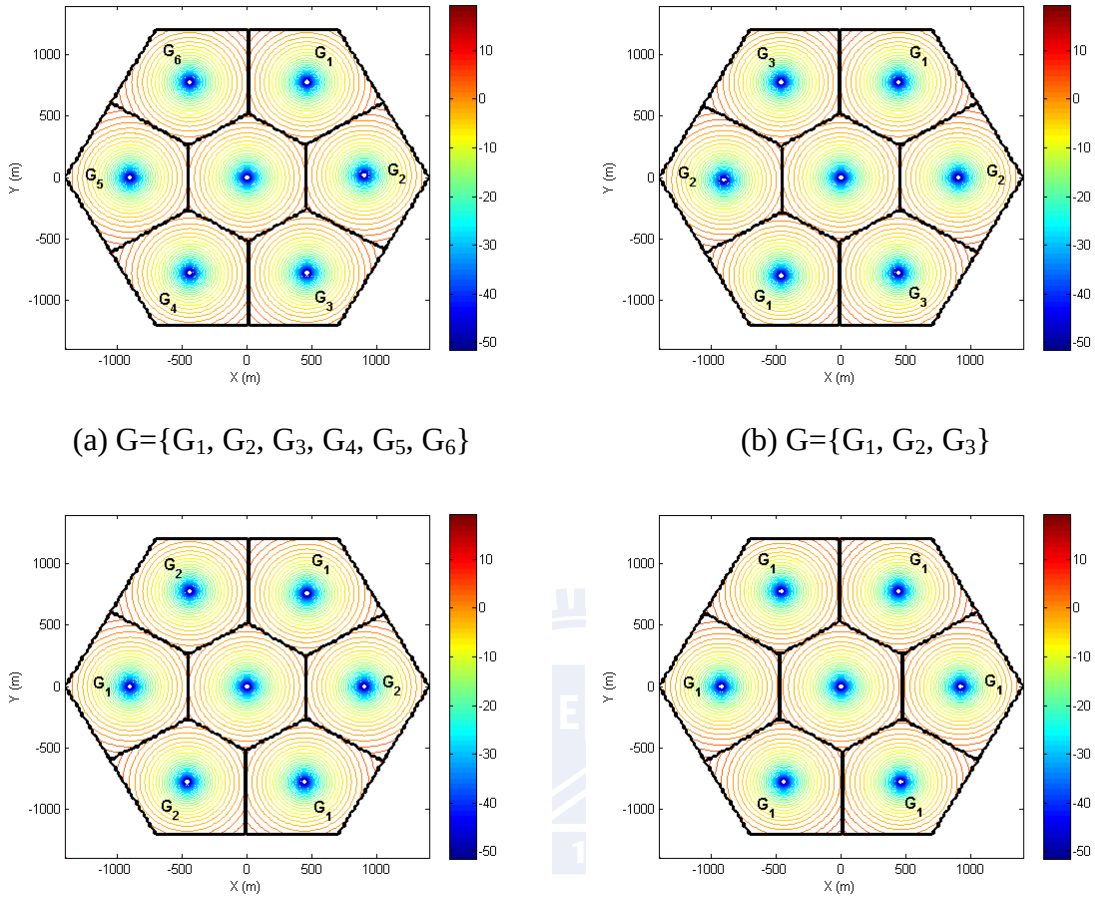

(a) G={G_1, G_2, G_3, G_4, G_5, G_6}

(b) G={G_1, G_2, G_3}

(c) G={G_1, G_2}

(d) G={G_1}

Figure 20. Transmit power distributions (in dBm) of different frequency-reuse patterns.

Table 5. System parameters for different frequency-reuse patterns of Scenario 1, $N = 6$.

G	$\Omega_B : \Omega_R$ (%)	$w_{M\to B} : w_{M\to R} : w_{R\to B}$ (%)	Avg. P_M (dBm)	S_Ω (bps/Hz)
$\{G_1, G_2, G_3, G_4, G_5, G_6\}$	14:86	14:80:6	-2.05	0.5
$\{G_1, G_2, G_3\}$	14:86	23:66:11	-2.03	0.83
$\{G_1, G_2\}$	14:86	29:57:14	-2.02	1.07
$\{G_1\}$	15:85	42:39:19	-1.57	1.46

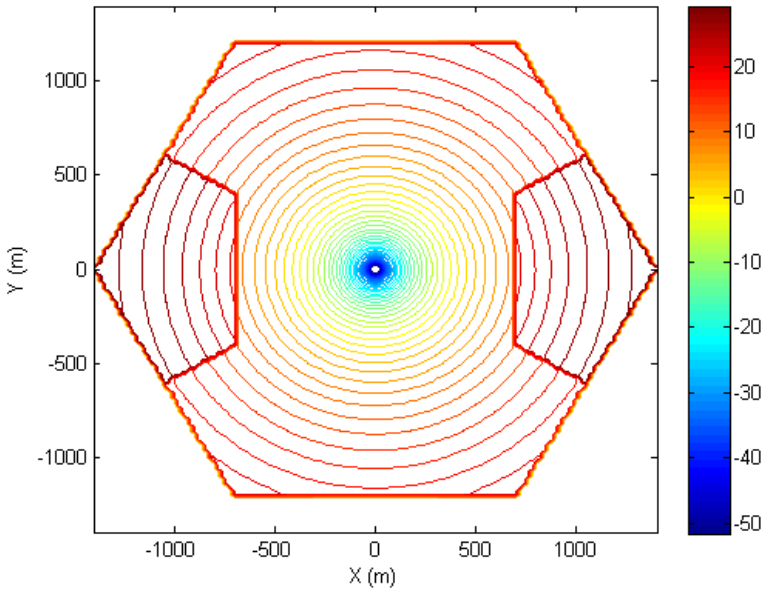

(a)

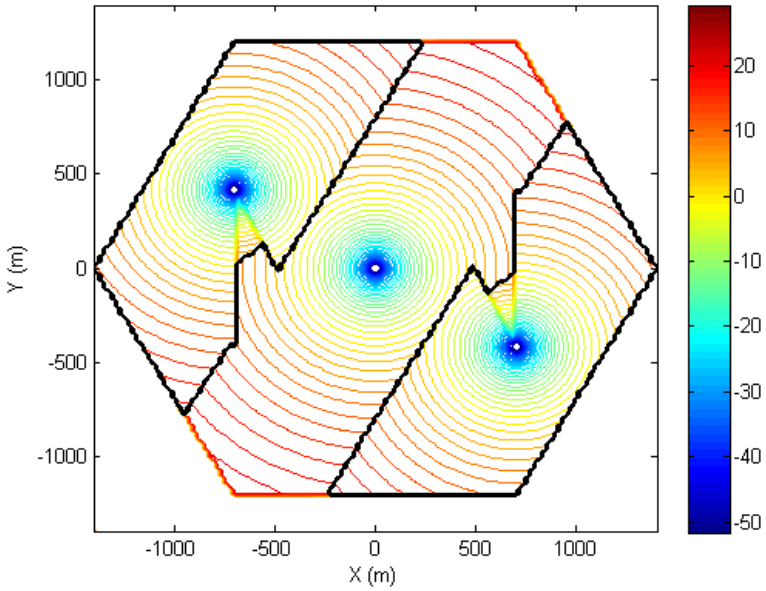

(b)

Figure 21. Optimal RSs' positions and uplink transmit power distribution (in dBm) in shadowed environment.

3.5.2 Measure 2—Maximization of Uplink System SE

In this section, given a fixed MS uplink transmit power, the system SE improvement offered by RSs is studied. Recall that the allocated uplink bandwidth to MS w_u is set as 28.5 kHz/m^2. There is no frequency reuse among MS-RS links.

First, we look at the case of $P_M = 15$ dBm. Figure 22 describes the ideas of optimal RSs positions and the uplink throughput distribution of each location. Figure 22 (a) is for $N = 0$, where the link SE decreases as the MS to BS distance increases. The system SE is 1.58 bps/Hz. Figure 22 (b) is the case of $N = 2$. The optimal RS positions are at $(\pm 700, 0)$. With the help of the RSs, the system SE is improved to be 2.54 bps/Hz, which is 60% improvement as compared to the case of $N = 0$. Figure 22 (c) shows the case of $N = 4$. The RSs provide service for 86% of total area and the system SE is 3.37 bps/Hz. Figure 22 (d) is for $N = 6$, where the optimal RSs positions are on the line connecting the cell center to the six vertices of the cell with distance 740m from BS. Notice that since the RS-BS link is not perfect, the maximum throughput for two-hop links is limited by the RS-BS link throughput no matter how close the MS and the RS is. Table 6 summarizes the service area ratio, bandwidth partition ratio and the system SE of each case. As the number of the RSs increases, the system SE is enhanced and the service area ratio of the RSs is also raised. However, since the average service area of each RS is reduced as the increment of deployed RS number, the system efficiency improvement of each additional RS is also narrowed. Figure 23 shows the CDF of link SE. The low SE area is significantly improved by the RSs. All lines merge together to the maximum SE 21.41 bps/Hz when the SE is greater than 10.

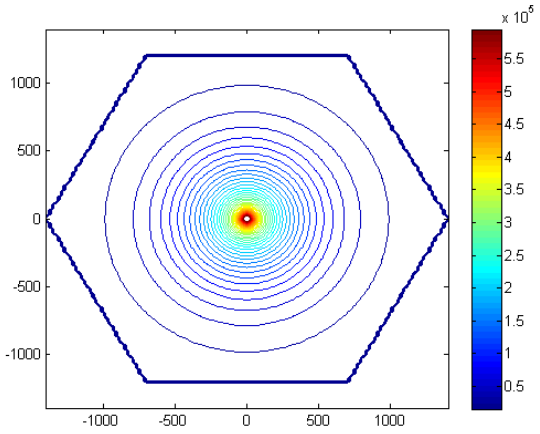

(a) $N = 0$

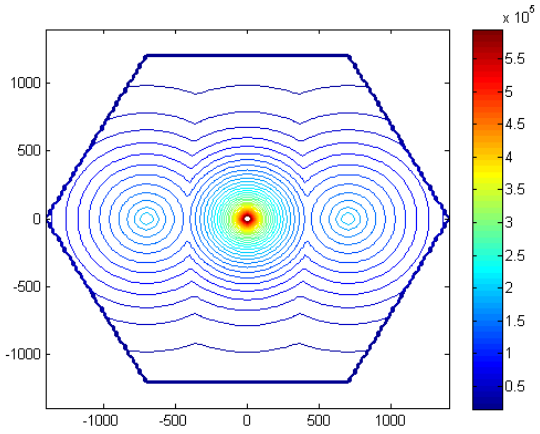

(a) $N = 2$

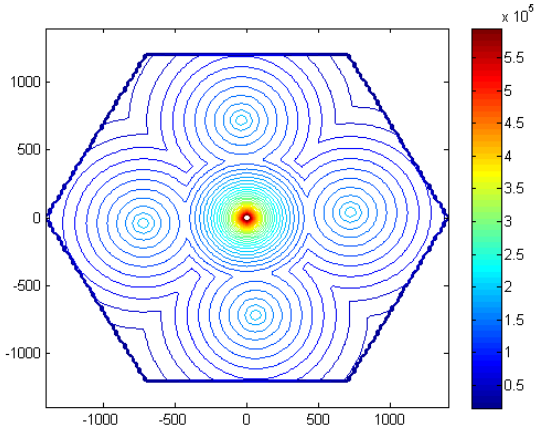

(a) $N = 4$

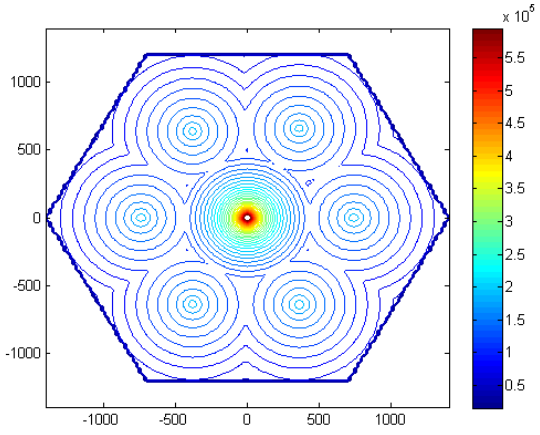

(a) $N = 6$

Figure 22. Optimal RSs' positions and uplink throughput distribution.

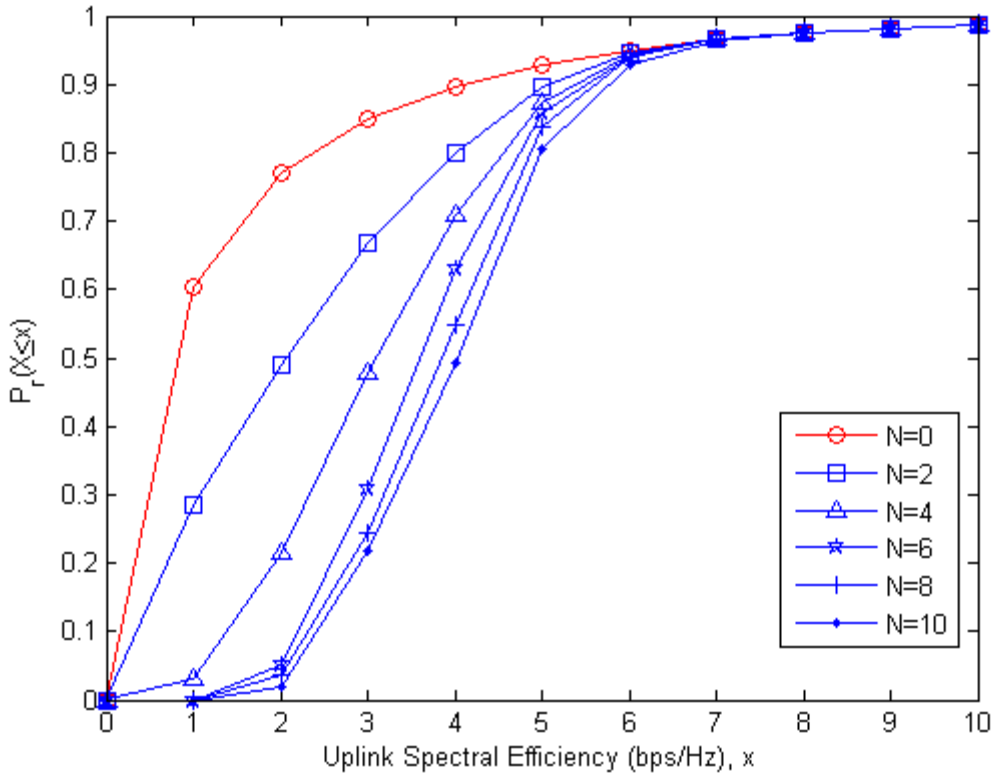

Figure 23. CDF of link SE for P_M=15 dBm.

Table 6. System parameters of Measure 2 for N = 0 to N = 10.

N	$\Omega_B : \Omega_R$ (%)	$w_{M\to B} : w_{M\to R} : w_{R\to B}$ (%)	S_Ω (bps/Hz)
0	100:0	100:0:0	1.58
2	36:64	36:49:15	2.54
4	14:86	14:59:27	3.37
6	13:87	13:53:34	3.83
8	12:88	12:51:37	4.02
10	11:89	11:50:39	4.16

Figure 24 summarizes the results of different reuse patterns for $N = 6$ with equal number of RSs in each reuse group. The system SE is getting better if the frequency is more aggressively reused (i.e., $G=\{G_1\}$). With respect to the service area ratio, Ω_R tends to be larger in $G=\{G_1, G_2, G_3\}$ and $G=\{G_1, G_2\}$ cases. However, in the case of $G=\{G_1\}$, Ω_R is shrunk due to large MAI.

The simplified shadowing model mentioned in Section 3.5.1 is investigated in this subsection. The shadow loss δ = 10 dB is adopted. MS's transmit power P_M is set as 20 dBm. As can be seen in Figure 24 (a), the throughput (link SE) of the MSs in the shadowed area is relatively low when only served by the BS. On the other hand, with two RSs' help, as shown in Figure 24 (b), the link SE is significantly improved. The optimal RSs' positions are at (700, -420) and (-700, 420), where the MSs may have higher probability to avoid blocking by any obstacle to its serving station. Similarly, the link SE of any two-hop link is restricted by the minimal throughput of the MS-RS link and the RS-BS link. Note that the optimal RSs' locations may highly depend on the topography and other constraints. The example we demonstrate here is to show the feasibility of the proposed method in the shadowed environment.

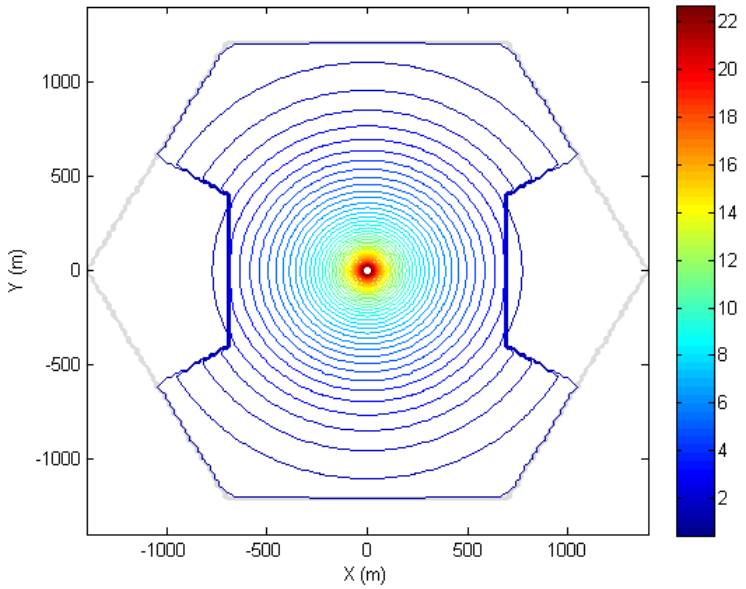

(a)

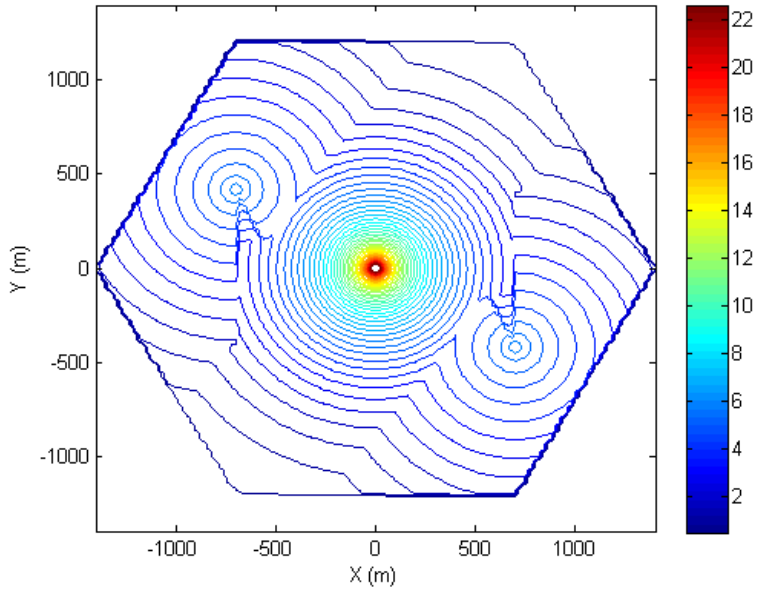

(b)

Figure 24. Optimal RSs' positions and uplink SE distribution (bps/Hz) in shadowed environment.

Table 7. System parameters for different frequency-reuse patterns of Measure 2, N = 6.

G	$\Omega_B : \Omega_R$ (%)	$w_{M\to B} : w_{M\to R} : w_{R\to B}$ (%)	S_Ω (bps/Hz)
$\{G_1, G_2, G_3, G_4, G_5, G_6\}$	13:87	13:53:34	3.83
$\{G_1, G_2, G_3\}$	10:90	14:44:42	5.31
$\{G_1, G_2\}$	9:91	16:39:45	6.08
$\{G_1\}$	13:87	31:27:42	6.23

3.6 Summary

In this work, the uplink performance of relay-assisted cellular networks is investigated with optimized system parameters. The optimal RSs' positions, reuse pattern, path selection and bandwidth allocation are searched to achieve two goals: one is to minimize the MS's average transmit power to achieve a specified throughput, and the other is to maximize the uplink system SE by given a fixed MS transmit power. The advance formulation of each objective function is contributed. The GA approach along with a multiple access interference estimation method designed for uplink performance evaluations are adopted to resolve the issues. The numerical results conclude that given a fixed allocated bandwidth to each MS, the average MS's transmit power is significantly reduced for a targeted throughput, and the user throughput as well as the system SE are largely enhanced for a fixed uplink transmit power with the assistance of RSs as compared to the conventional cellular system.

Chapter 4
Resource Scheduling with Directional Antennas for Multi-hop Relay Networks in a Manhattan-like Environment

Multi-hop relay (MR) networks have been proposed for user throughput improvement, coverage extension and/or system capacity enhancement to the traditional mobile cellular networks. In particular, an MR network has been adopted by the IEEE 802.16j Task Group as an amendment to the IEEE 802.16e standard. This chapter investigates the issue of resource scheduling for the IEEE 802.16j MR networks in the Manhattan-like environment. New scheduling methods are proposed for the MR networks with directional antennas equipped at both BSs and RSs. Simulation results show that the system throughput can be dramatically increased by the proposed methods as compared to the system with omni-directional antennas.

4.1 Background

In recent years, more and more research has been devoted to the design of relay-assisted network. In [69], a relay-assisted network was adopted as an amendment to the IEEE 802.16e standard [14], [70] for cell coverage extension, user throughput improvement and/or system capacity enhancement. In [26], [71], [72], a scenario of relay-assisted networks, named Scenario 1, was proposed for the Manhattan-like environment, where four RSs are deployed outside of the BS's coverage in a cell in order to extend the cell coverage, which is illustrated in Figure 25. In order to achieve frequency reuse factor of 1, the multi-cell setup and the transmission frame structure as illustrated in Figure 26 and Figure 27 are proposed in [72]. Through proper coordination between adjacent cells, when BSs in cell group A serve RSs and MSs in the phase 1, BSs in cell group B keep silence and RSs serve their MSs. Similarly, the BSs in cell group B and the RSs in cell group A become active in phase 2. In addition, by utilizing the spatial isolation which is inherent in the Manhattan-like environment, two relay stations (e.g., RS_1 and RS_2, or RS_3 and RS_4) within the same cell can be scheduled to be active simultaneously. However, as shown in Figure 27, since there are always some inactive BSs in every transmission phase, the radio resource is not fully utilized in this design.

Another relay-assisted network, Scenario 2, was proposed in [27], where RSs are deployed within the service range of the BS for the purpose of user throughput enhancement, which is illustrated in Figure 28. In this design, both the BS and RSs employ omni-directional antennas to serve users and to communicate with each other. Consequently, the frequency reuse factor has to be at least 2 in order to avoid severe co-channel interference, which is shown in Figure 29, and this reduces the system capacity.

The previous research works have been mostly focused on the aspects of coverage extension and end-to-end user-throughput enhancement of a relay-assisted network [26], [27], [71], [72]. In this chapter, we consider the overall system capacity enhancement issue for the relay-assisted network in the Manhattan-like environment. New scheduling methods are proposed for the system with directional antennas equipped at both the base station and relay stations. Simulation results show that the system throughput can be dramatically increased by the proposed methods, as compared to the system with omni-directional antennas.

The rest of this chapter is organized as follows. The system setups and the radio propagation models are described in Section 4.2. The proposed scheduling methods are detailed in Section 4.3. Simulation results are presented in Section 4.4, and finally, conclusions are given in Section 4.5.

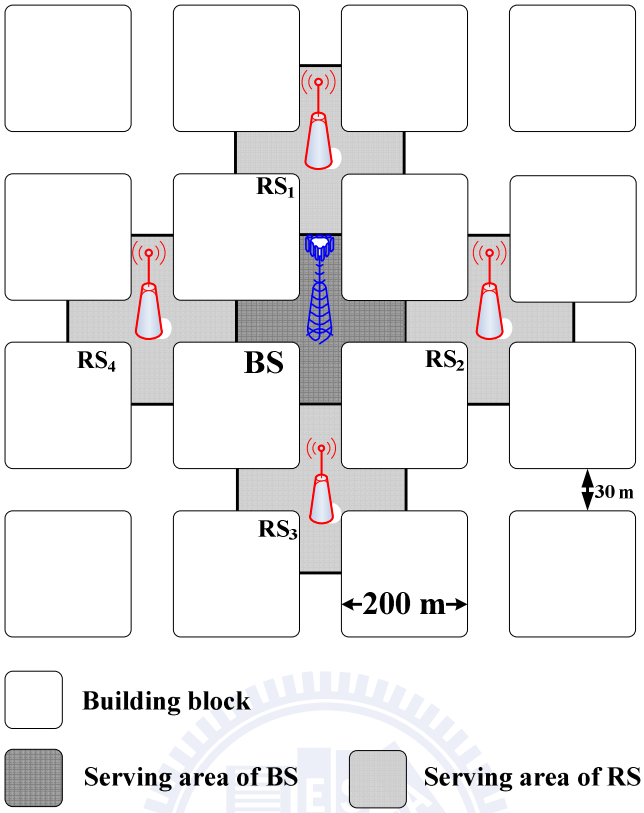

Figure 25. Relay-assisted cell architecture in a Manhattan-like environment—Scenario 1.

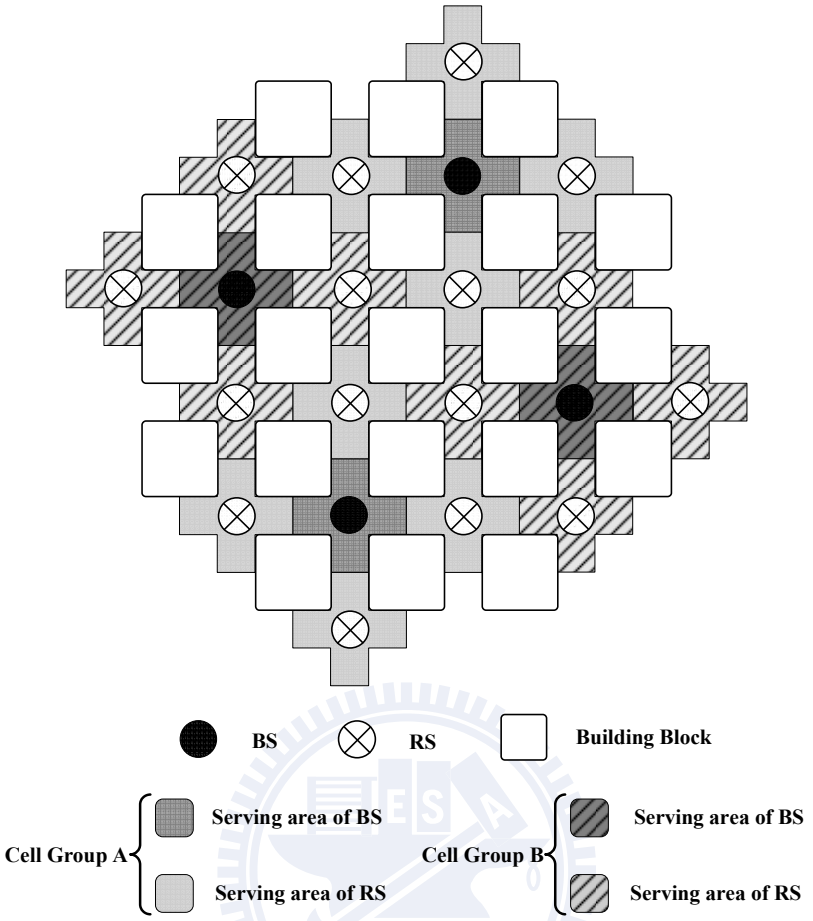

Figure 26. Multi-cell setup of Scenario 1.

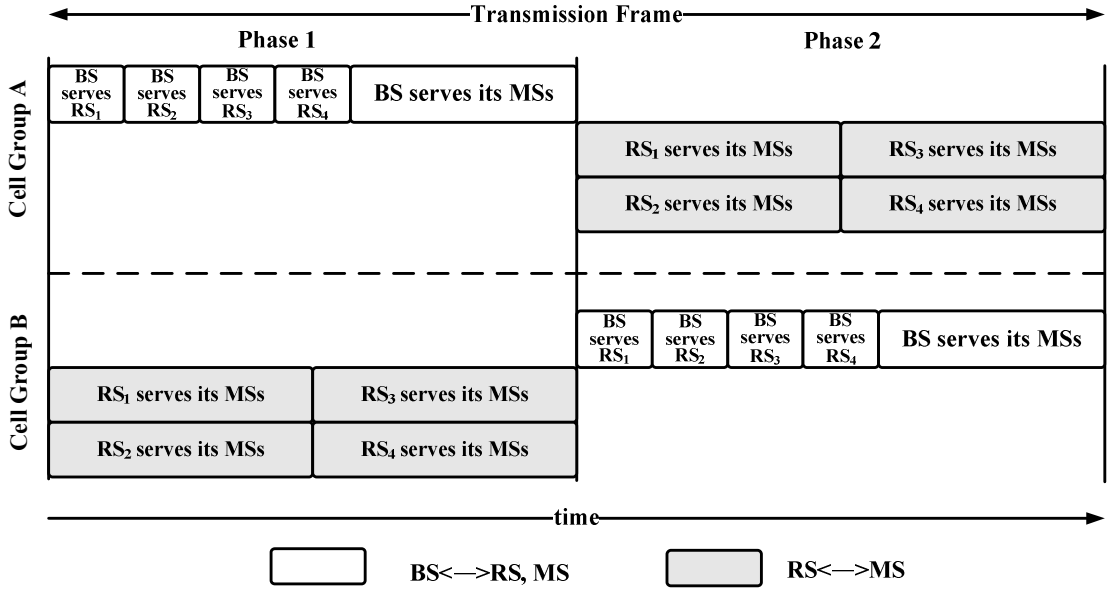

Figure 27. Transmission frame structure of Scenario 1.

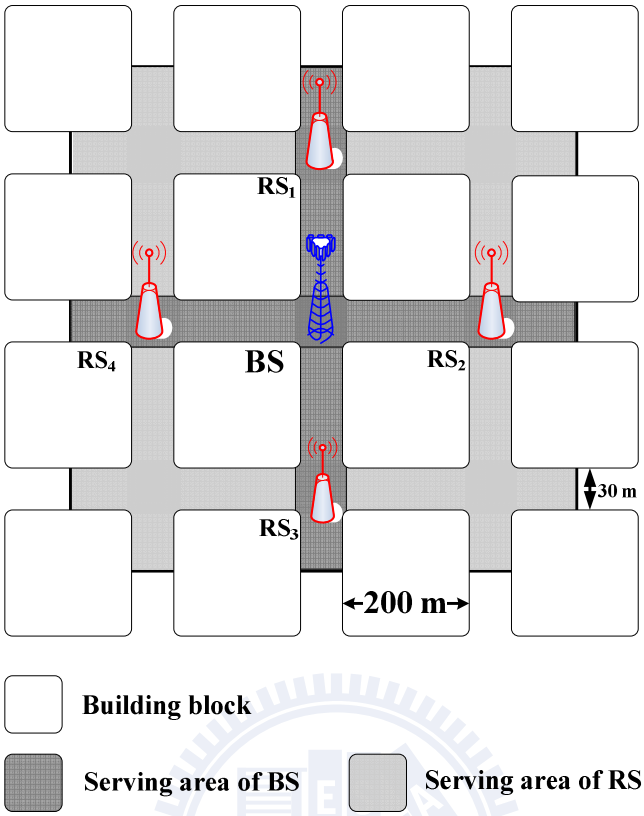

Figure 28. Relay-assisted cell architectures in a Manhattan-like environment—Scenario 2.

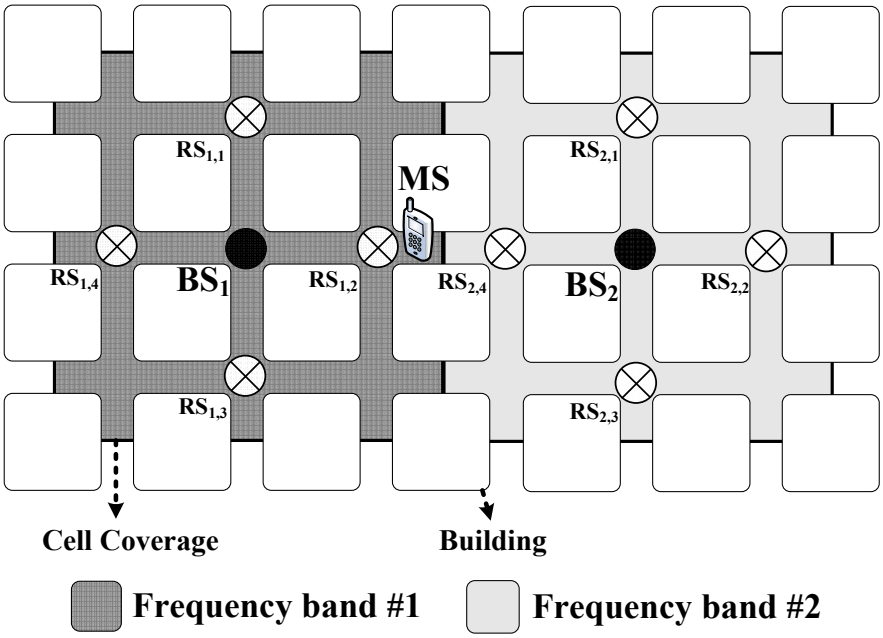

Figure 29. Frequency reuse pattern in the multi-cell environment of Scenario 2.

4.2 System Setups and Propagation Models

The system setups and the propagation models for multi-hop relay networks in the Manhattan-like environment are detailed in this section.

4.2.1 System Setup

A relay-assisted network with a relay-assisted cell structure consisting of one BS and four RSs in the Manhattan-like environment is considered in this section. As shown in Figure 30, the BS is located at the main street-crossing with four RSs deployed at the four street corners. The side-length of a street block and the street width are set to be 200 m and 30 m, respectively.

One relay-assisted cell covers nine blocks and thus the coverage of each cell is about 690x690 square meters. According to the technical requirements set forth by IEEE 802.16j baseline document [69], there is no backhaul network connection to RSs, and BS and RSs are assumed to use the same air interference to communicate with each other and MSs (homogeneous relaying). In addition, RSs decode the signal from the source and re-encodes it before forwarding to the destination (decode-and-forward mode).

To improve the system performance, the BS and RSs are equipped with directional antennas to communicate with users and/or each other. The service area of each station is also shown in Figure 30, where the BS serves RSs and MSs (e.g., MS_1) in its LOS area with single-hop connections, while RSs serve MSs (e.g., MS_2) in the BS's NLOS area through two-hop connections.

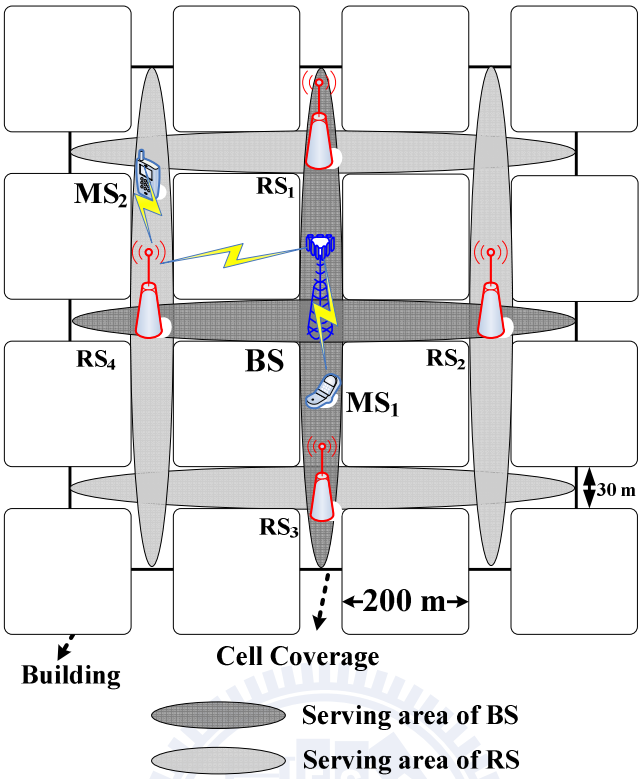

Figure 30. The deployment of BS and four RSs and their serving areas.

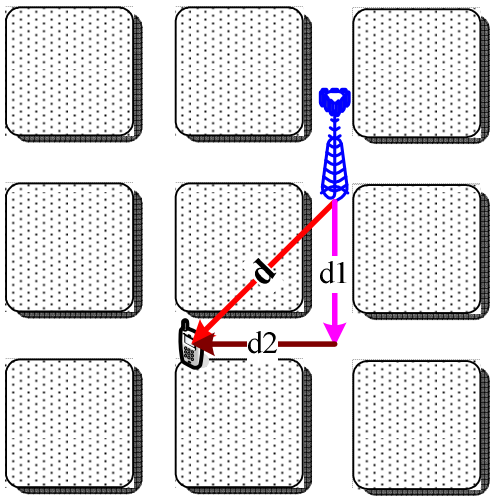

Figure 31. The relevant distances from BS to determine the path loss and the probability of having LOS.

4.2.2 Propagation Models and Antenna Pattern

In this section, the propagation loss model proposed in [74] is considered, where the path-loss and shadow fading models for the urban micro-cell environment are adopted. Table 8 summarizes the model parameters for both the LOS and NLOS cases, where f_c is the carrier frequency, and d, d_1, and d_2 are the distances as indicated in Figure 31. Note that the probability of having LOS depends on the distance value d. The antenna pattern mentioned in (2.4) is adopted for the BSs and the RSs.

Table 8. The propagation loss model for the urban micro-cell environment.

Path loss model	
LOS	$PL(d, f_c) = 41 + 22.7\log_{10}(d) + 20\log_{10}(f_c / 5.3)$
NLOS	$PL(d_1, d_2, f_c) = 0.096d_1 + 65 + (28 - 0.024d_1)\log_{10}(d_2) + 20\log_{10}(f_c / 5.3)$
Standard Deviation of log-normal shadow model	
LOS	2.3 dB
NLOS	3.1 dB
Probability of LOS	
$P_{LOS}(d) = \begin{cases} 1 & , d \le 15m \\ 1-(1-(1.56-0.48\log_{10}(d))^3)^{1/3} & , d > 15m \end{cases}$ where $d = \sqrt{d_1^2 + d_2^2}$	
Note: f_c *is in GHz,* d, d_1, d_2 *are in meters*	

4.3 Resource Scheduling Methods

In this section, resource scheduling methods for relay-assisted network in the Manhattan-like environment are presented. The scheduling with omni-directional antennas will be discussed first in Subsection 4.3.1 and it is used as a baseline for comparison. Then proposed scheduling methods with directional antennas will be discussed in Subsection 4.3.2. In these methods, we assume that RSs are multiplexed in the time domain. In other words, time domain relaying is considered here.

4.3.1 Scheduling with Omni-Directional Antennas

Since the BS and RSs use the omni-directional antennas, at least six phases of transmissions are needed to complete the two-hop connections between the BS and MSs, as shown in Figure 32. Each phase includes both downlink and uplink transmissions. Here we assume that all the transmission phases are completed in a frame. The BS takes turns to serve RSs and MSs in its LOS area in the first four phases. To take advantage of the shadowing effect in the environment, RS_1 and RS_3 serve MSs in their service areas simultaneously in Phase 5, and RS_2 and RS_4 do the same in Phase 6.

Now consider the multi-cell structure. Because of the use of omni-directional antennas, the reuse factor of at least 2 is required to avoid the severe inter-cell interference as clearly shown in Figure 29, and that decreases the overall system capacity.

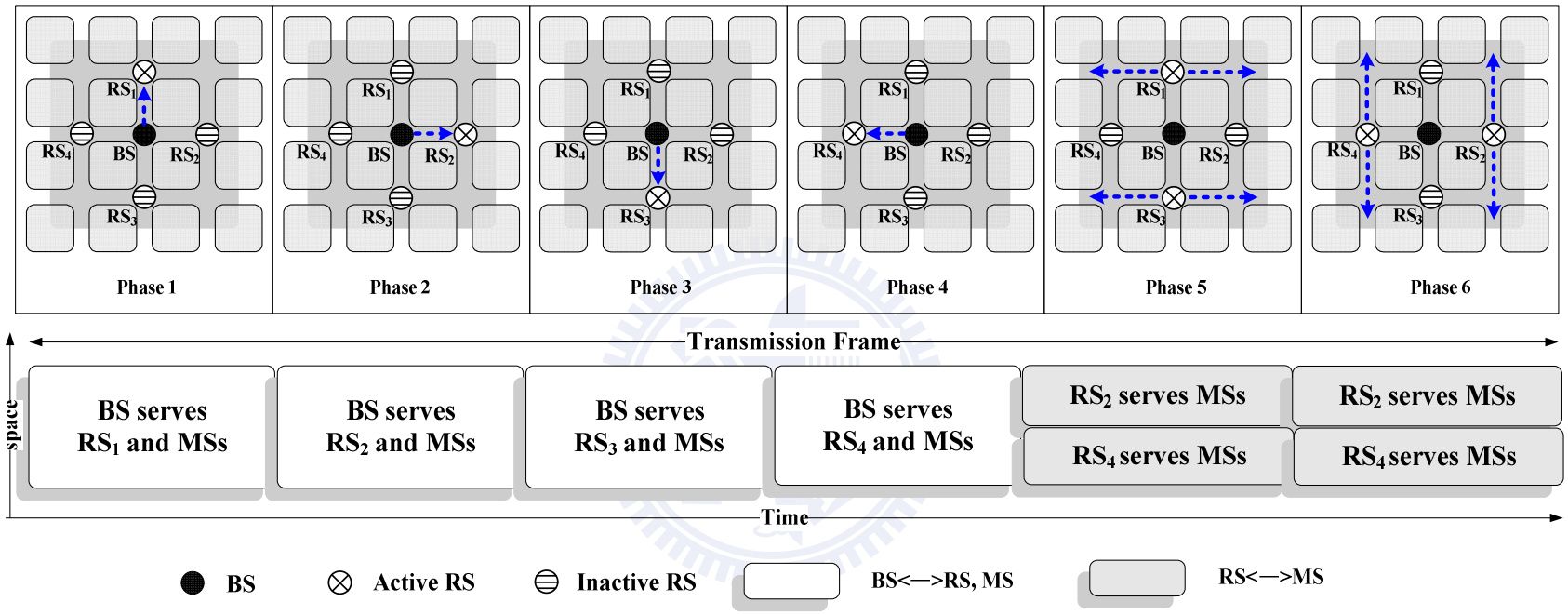

Figure 32. Resource scheduling with omni-directional antennas.

4.3.2 Scheduling with Directional Antennas

To improve the system performance as mentioned in Section 4.3.1, resource scheduling methods with directional antennas are proposed. In this scenario, the BS and RSs are equipped with directional antennas to further exploit the advantage of shadowing effect in a Manhattan-like environment. As shown in Figure 33, the BS and RSs are equipped with four directional antennas pointed to different directions, respectively. In different antenna directions, the radio resource can be reused completely. Accordingly, the RSs are divided into groups according to their mutual interference levels, and those in the same group are scheduled to transmit in the same transmission phase. In Figure 33, RS_1 and RS_3 are grouped as Group-A, and RS_2 and RS_4 as Group-B. Since there are two groups in a cell, two transmission phases are needed to complete the two-hop transmissions. Again, each phase comprises both downlink and uplink transmissions.

4.3.2.1 Method-1

In this design, as shown in Figure 33 (a), the BS serves the Group-A RSs (RS_1 and RS_3) and the MSs in its corresponding LOS area in Phase 1 (both up- and down-link). At the same time, the Group-B RSs (RS_2 and RS_4) serve the MSs in their service areas. Alternatively, in Phase 2, as illustrated in Figure 33 (b), the BS turns to serve the Group-B RSs and MSs in its corresponding LOS service areas, while the Group-A RSs serve the MSs in their service areas.

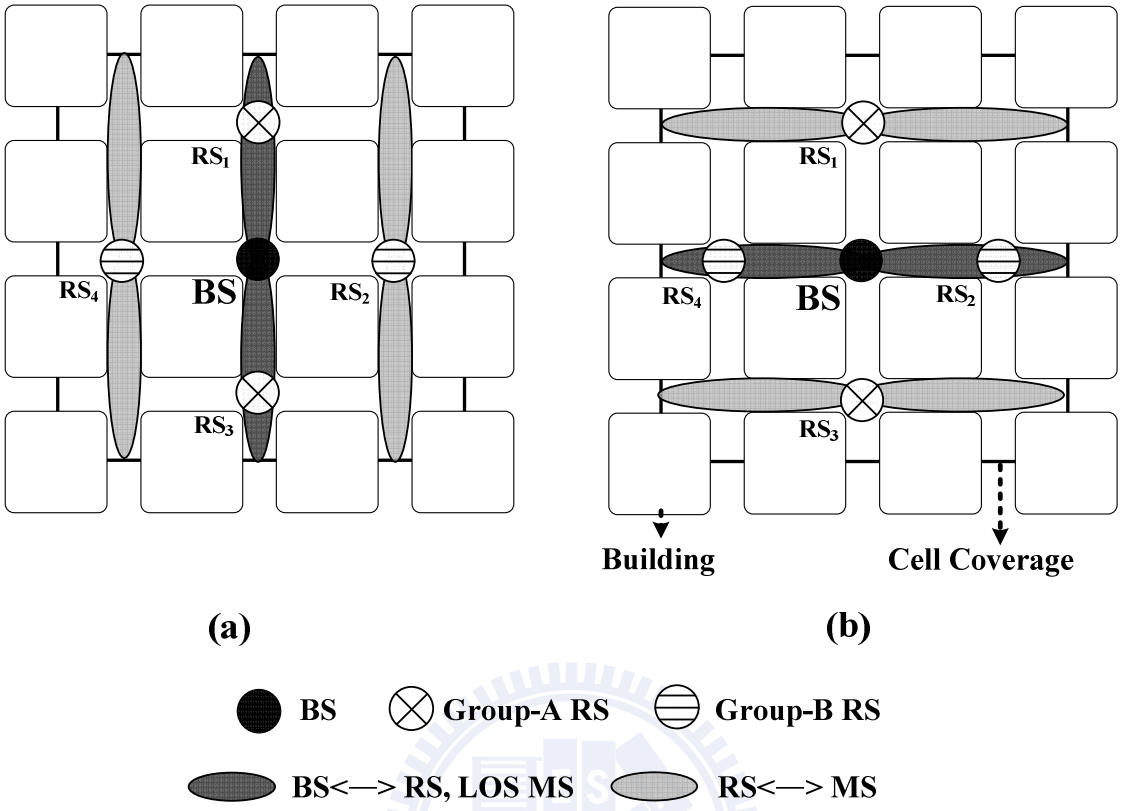

Figure 33. Two phases of transmissions in Method-1, (a) Phase 1 and (b) Phase 2.

When considering the multi-cell setup, the frequency reuse factor of 1 (universal frequency reuse) can be easily achieved as follows. As represented in Figure 34 (a), in Phase 1, when BS_1 serves the Group-A RSs and MSs in the respective directions, BS_2 in the neighboring cell serves the Group-B RSs and MSs in the indicated directions. Of course, at the same time, the Group-B RSs in the cell 1, and the Group-A RSs in the cell 2 provide services to the MSs in their service areas. In Phase 2, shown in Figure 34 (b), the operation is the same by changing the role of Group-A and Group-B in each cell. As clearly seen, with directional antennas indicated in the proposed scheduling scheme, the universal frequency reuse can be achieved very easily. The corresponding frame structure for Method-1 is shown in Figure 35.

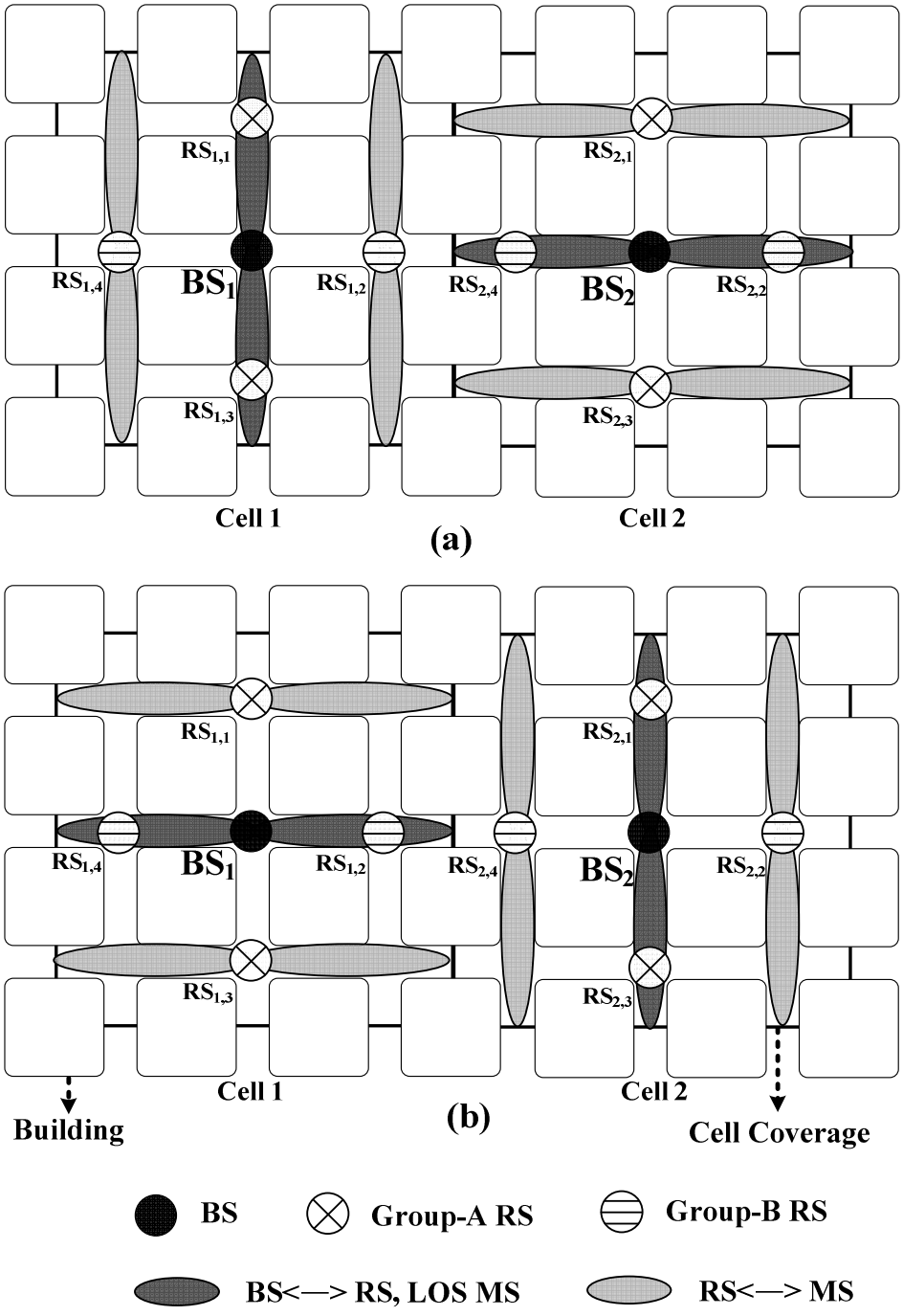

Figure 34. Two phases of transmissions of the neighboring cells in Method-1, (a) Phase 1 and (b) Phase 2.

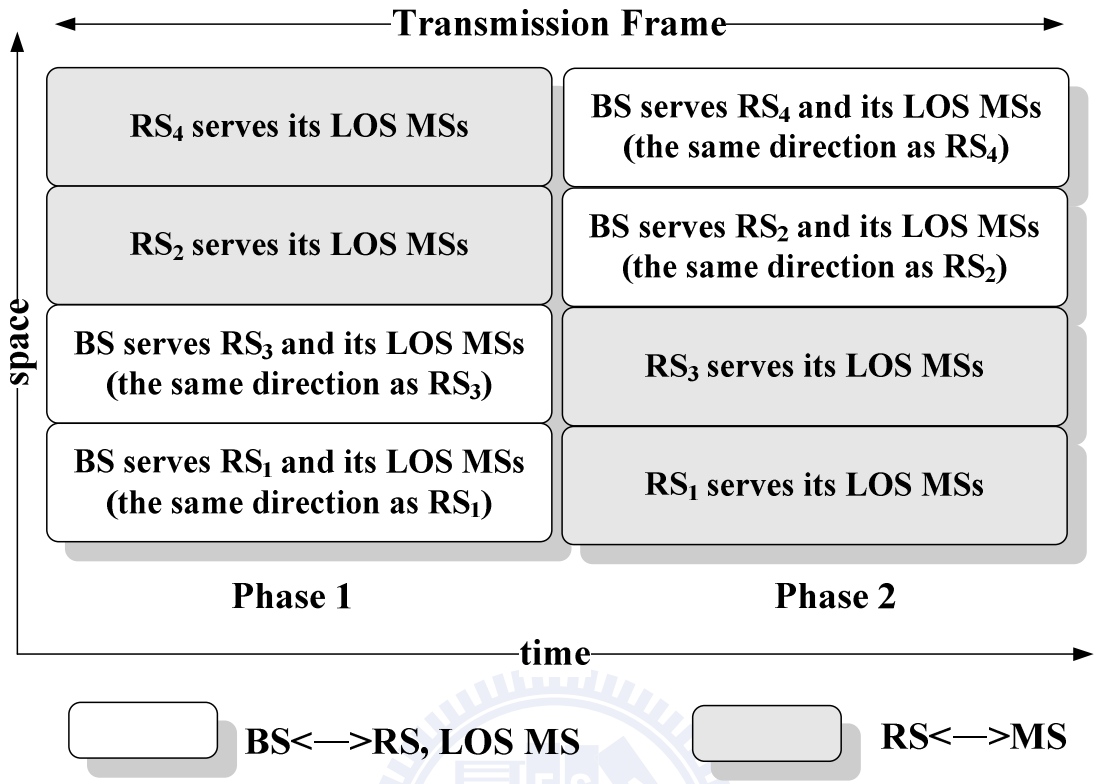

Figure 35. The frame structure of Method-1.

4.3.2.2 Method-2

In Method-1, only two antennas at the base station are activated in each transmission phase. Obviously, the other two idle antennas can also be activated to use the radio resource more efficiently. However, the transmit power of these two antennas needs to be properly controlled so that they will not cause too much interference to ongoing transmissions. Except for this added feature, Method-2 is the same as Method-1. Each phase of transmissions in a cell is shown in Figure 36, and the scheduling for the multi-cell setup to achieve frequency reuse factor of 1 is shown in Figure 37.

The frame structure of Method-2 is shown in Figure 38. We can see that since four directional antennas of the base station are active simultaneously, the number of BS's transmissions in each phase is four. The spectrum efficiency of Method-2 is twice of Method-1 ideally. Note that the data from/to the BS constitutes the effective throughput of the relay-assisted-cell; The RSs only relay data between the BS and MSs.

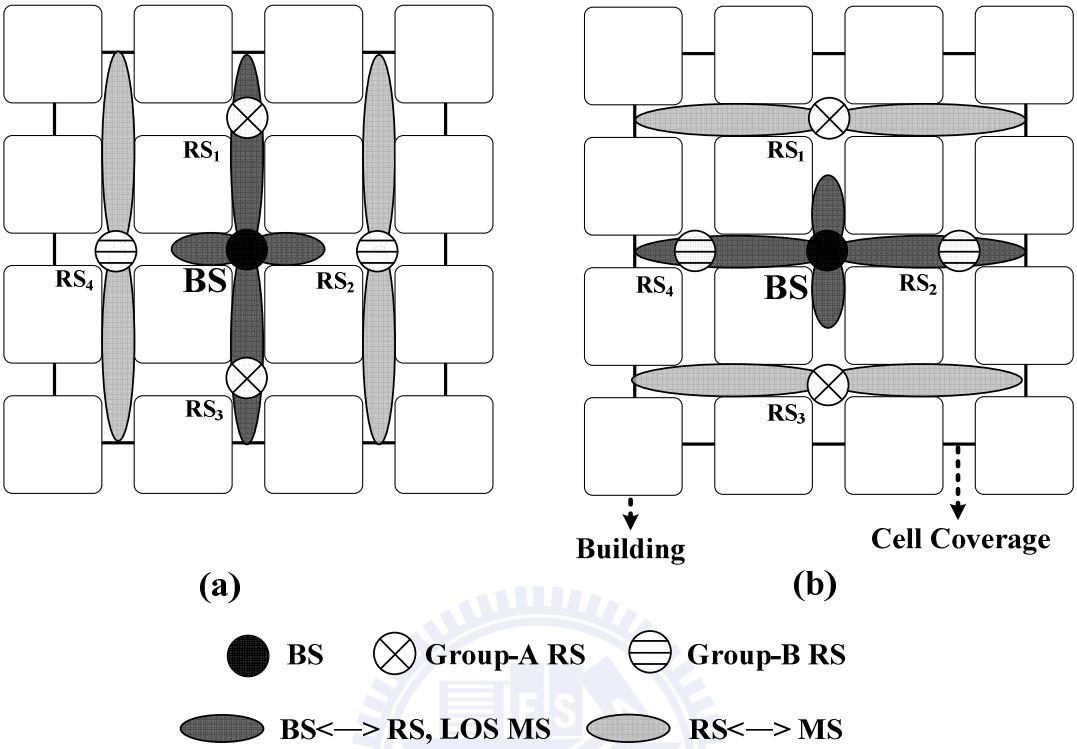

Figure 36. Two phases of transmissions in Method-2, (a) Phase 1 and (b) Phase 2.

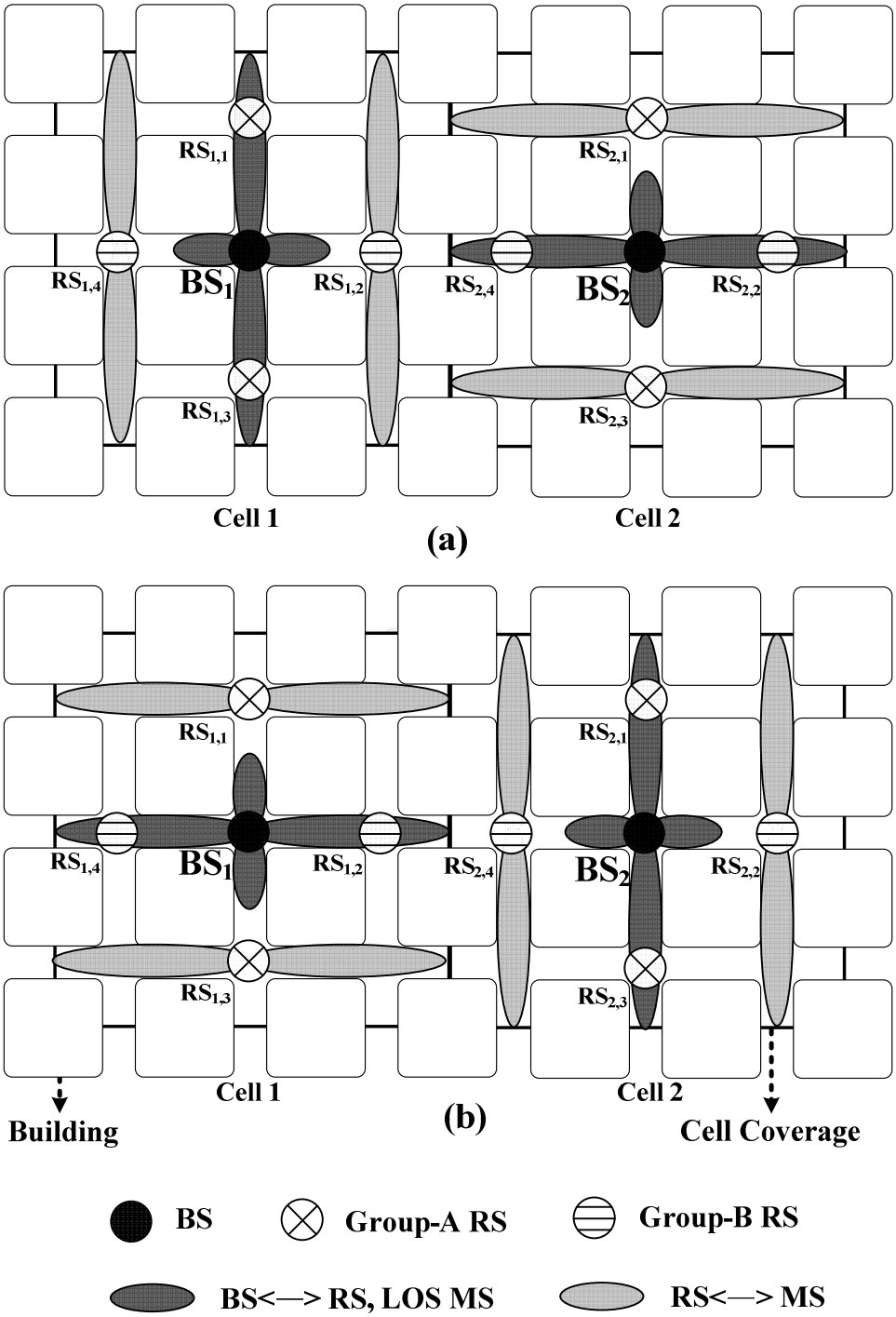

Figure 37. Two phases of transmissions of the neighboring cells in Method-2, (a) Phase 1 and (b) Phase 2.

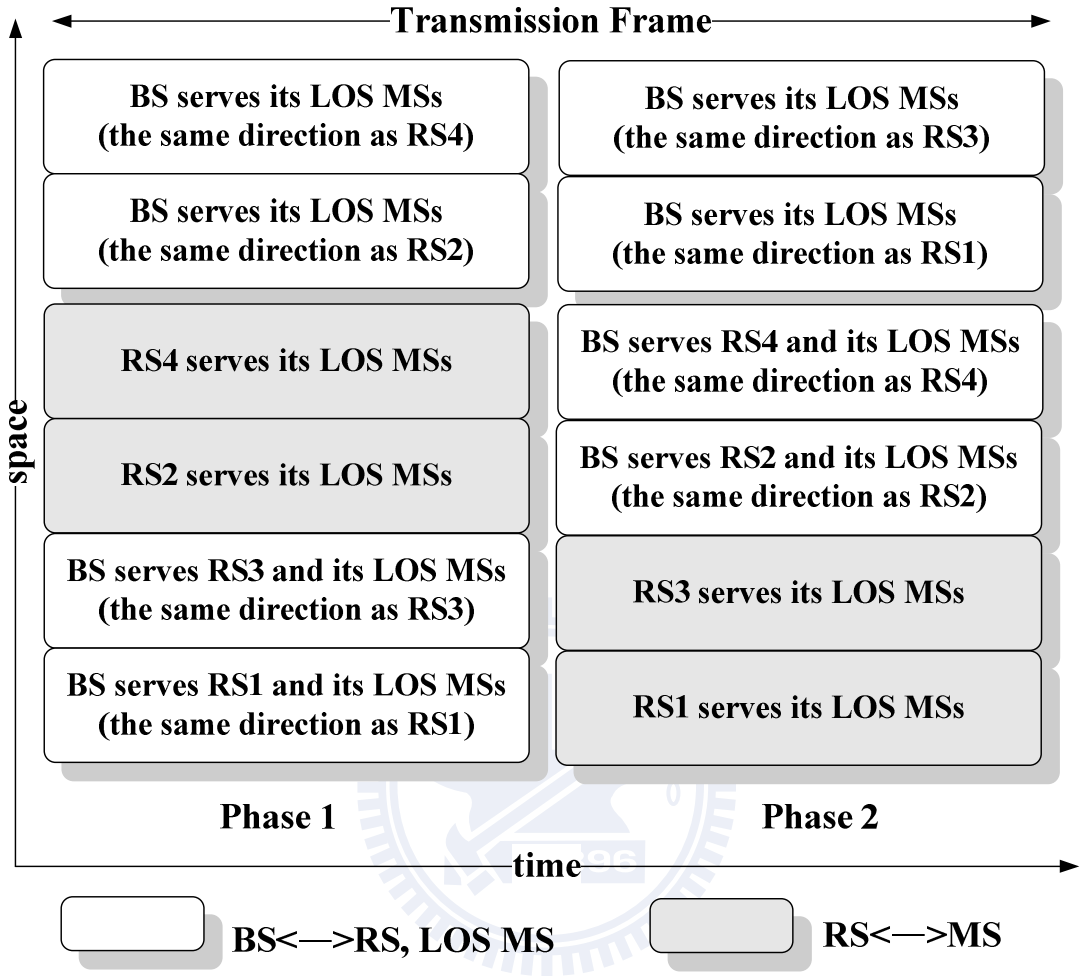

Figure 38. The frame structure of Method-2.

4.4 Numerical Results

The parameters of the simulated system are set according to the OFDMA mode in the IEEE 802.16 standard [14], [70], which are summarized in Table 9. The required SINRs to achieve 10^{-6} bit-error-rate (BER) for the various MCSs considered are given in Table 10 [70]. The scheduling method for the system with omni-directional antennas is also simulated to serve as the base-line scheme for performance comparisons. A multi-cell setup with two-tier interfering cells is considered. The locations of BS and RSs are fixed, while users are uniformly distributed within each cell. The data traffic of each user is full-buffer traffic model. A fixed transmission power is used in the downlink, and the adaptive rate control is executed every frame to select an appropriate modulation and coding scheme based on the perfect channel state information.

Figure 39 shows the simulated CDFs of SINR for different scheduling methods. To emphasize on the capacity gain obtained from the new scheduling methods, the transmission power in our simulation of the onmi-directional antenna case is increased to offset the antenna gain obtained with the directional antennas. Clearly, the scheduling scheme with omni-directional antennas has the best SINR performance, while Method-2 has the worst because it reuses the frequency spectrum more aggressive.

Table 9. OFDMA parameters for system-level simulation.

Parameter	Value
Carrier frequency	3.5 GHz
Bandwidth	6 MHz
FFT size	2048
Sub-carrier frequency spacing	3.348 kHz
OFDM symbol duration (including 1/8 cyclic-prefix)	336 μs
Duplexing	TDD
Frame duration	20 ms
Permutation mode of each sector	FUSC (full usage of sub-channels)
Number of sub-channels	32
Number of sub-carriers per sub-channel	48
Max. transmit power of BS /RS	100 mW
BS/RS antenna gain	14 dBi
MS antenna gain	0 dBi
MS/ BS noise figure	7 dB/ 5dB
Noise power	-174+10logB dBm
BS-to-BS distance	690 m
Number of Relay-assisted-cells (two-tier interfering cells)	25

Table 10. The used MCS.

Modulation	**Coding rate**	**Receiver SINR (dB) to achieve 10^{-6} BER**
BPSK	1/2	6.4
QPSK	1/2	9.4
	3/4	11.2
16-QAM	1/2	16.4
	3/4	18.2
64-QAM	2/3	22.7
	3/4	24.4

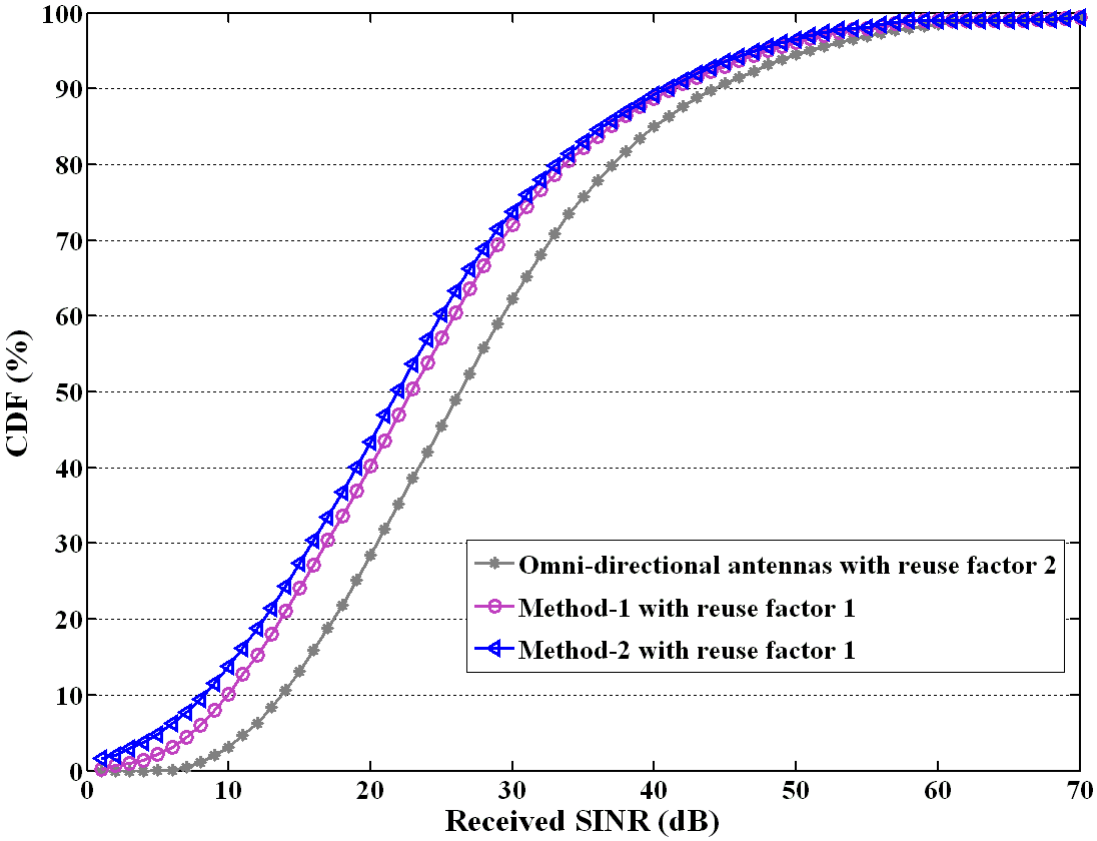

Figure 39. The CDF of SINR for different scheduling methods.

The capacity simulation result is shown in Figure 40. The cell capacity is increased enormously with the proposed methods. The capacity gain is approximately 6 and 12 times for Method-1 and Method-2, respectively, as compared with the system with the omni-directional antennas. The reason of the capacity gain can be simply explained as follows. First, as shown in Figure 34 and Figure 37, Method-1 and Method-2 can achieve frequency reuse factor of 1, while in Figure 29, the reuse factor of at least 2 (here the case of reuse factor 2 is simulated) is required for the system with omni-directional antennas. Hence, at least 2 times of capacity gain is obtained as compared to the omni-directional antenna case. Second, from Figure 32, only 2/3 of the transmission phases in a frame are used for the BS's transmission. On the other hand, 2 and 4 BS's transmissions in each phase are possible for Method-1 and Method-2 respectively, as shown in Figure 35 and Figure 38. That results in another 3 and 6 times of capacity gain over the case of the omni-directional antennas. Table 11 summaries where the capacity gains come from for Method-1 and Method-2 as compared with the omni-directional antenna case. However, due to the higher interference level observed in Figure 39, the simulated capacity gain of Method-1 over the system with omni-directional antennas is slightly less than 6 times, as our simplified analysis predicts. On the other hand, the simulated capacity gain of Method-2 over Method-1 is larger than 2 because the former provides more higher-data-rate connections.

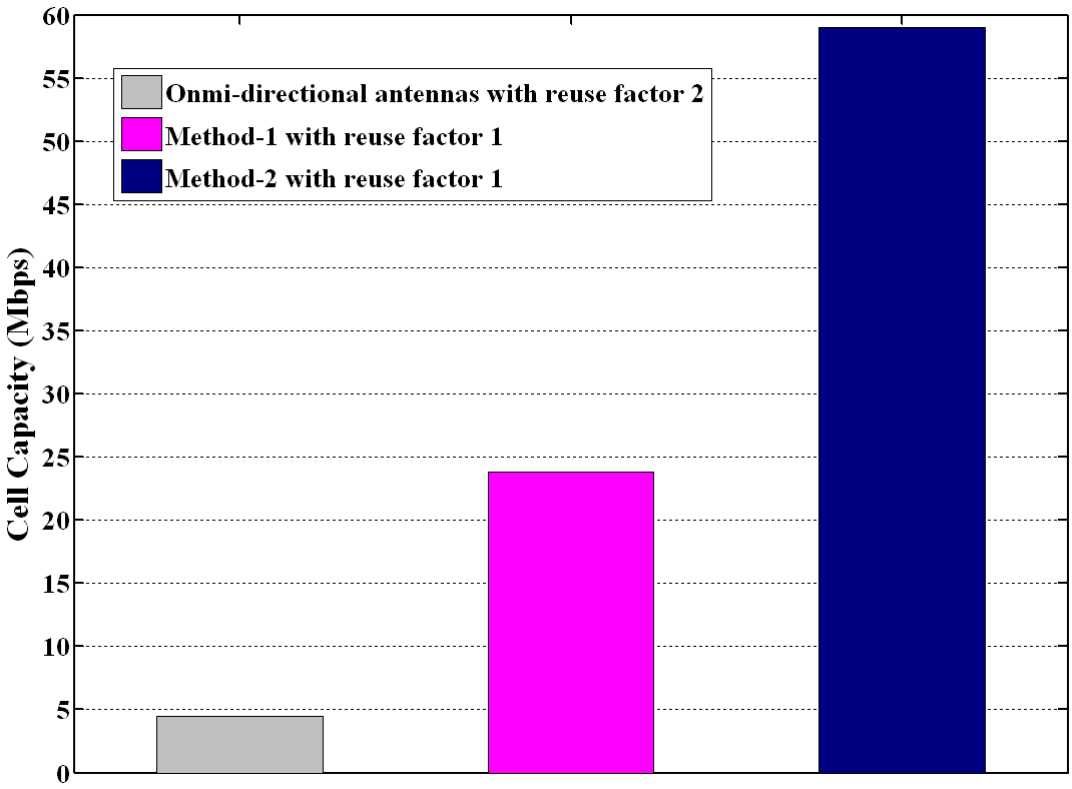

Figure 40. Comparisons of cell capacity between different scheduling methods.

Table 11. The analysis of the capacity gain.

Method	Reuse factor	Effective data frame transmitted in a frame	Anal sized capacity gain
Omni-directional antennas	2	2/3	1
Method-1	1	2	6
Method-2	1	4	12

4.5 Summary

Multi-hop relay (Relay-assisted) cell architecture is a promising candidate for the next generation wireless communication systems. It has been adopted as an amendment to IEEE 802.16e standard for cell coverage extension, user throughput improvement and/or system capacity enhancement. In this chapter, we investigate the important issue of resource scheduling for Relay-assisted networks in a Manhattan-like environment. The new resource scheduling methods are proposed for the Relay-assisted networks with directional antennas equipped at both the BSs and the RSs. By taking advantage of the effect of high degree shadowing in the Manhattan-like environment, the system throughput can be increased to nearly 6 and 12 times by the proposed Method-1 and Method-2, respectively, as compared to the system with omni-directional antennas.

Chapter 5
Conclusions

In this dissertation, the design and optimization of relay-assisted cellular networks are investigated from both theoretic and practical points of view.

We comprehensively evaluate the downlink theoretical performance of relay-assisted cellular networks in the multi-cell environment with various system configurations in the first part. A genetic algorithm (GA) based method is proposed for joint multi-cell optimization of system parameters including RS's positions, path selection, frequency-reuse pattern and resource allocation so as to maximize system SE. Numerical results show that (i) RSs provide significant improvement with respect to system SE and user throughput over the traditional cellular networks. (ii) Uniformity of user data rate comes at the expense of a large loss in system SE when FTA is employed. (iii) Somewhat surprising, the low-complexity SINR-based path selection performs nearly as good as the SE-based one for the no-reuse case while achieving slightly better performance in the frequency-reuse case.

In the second part, the uplink performance of relay-assisted cellular networks is investigated with optimized system parameters. The optimal RSs' positions, reuse pattern, path selection and bandwidth allocation are searched to achieve two goals: one is to minimize the MS's average transmit power to achieve a specified throughput, and the other is to maximize the uplink system SE by given a fixed MS transmit power. The advance formulation of each objective function is contributed. Genetic algorithm approach along with a multiple access interference estimation method designed for uplink performance evaluations are adopted to resolve the issues. Numerical results conclude that given a fixed allocated bandwidth to each MS, the average MS's transmit power is significantly reduced for a targeted throughput, and the user throughput as well as the system SE are largely enhanced for a fixed uplink transmit power with the assistance of RSs as compared to the conventional cellular systems.

In the third part, we investigate the important issue of resource scheduling for Relay-assisted networks in the Manhattan-like environment. New resource scheduling methods are proposed for the Relay-assisted networks with directional antennas equipped at both the base station and relay stations. By taking advantage of the effect of high degree shadowing in the Manhattan-like environment, the system throughput can be increased to nearly 6 and 12 times by the proposed Method-1 and Method-2, respectively, as compared to the system with omni-directional antennas.

In this dissertation, the theoretical performance in both downlink and uplink with general configurations in relay-assisted cellular networks is presented. The practical issues of resource scheduling of relay-assisted cellular networks in the Manhattan-like environment is also addressed. Not only the optimization methods but also performance limits of relay-assisted cellular networks are provided to the system designers. With comprehensively evaluations, we can conclude that a relay-assisted cellular system is with

the benefits to improve the system capacity and the user throughput, to save transmit power of an MS in the uplink, and to provide better coverage in the Manhattan-like environment with the optimized system parameters.

References

[1] V. H. MacDonald, “The Cellular Concept,” *Bell System Technical Journal*, vol. 58, no. 1, January 1979.

[2] Bell Labs, “High capacity Mobile Telephone System Technical Report,” *submitted to FCC*, Dec. 1971.

[3] J. S. Engle, “The Early History of Cellular Telephone,” *IEEE Communication Magazine*, pp. 27-29, August 2008.

[4] T. S. Rappaport, Wireless Communications Principles and Practices, *Prentice Hall*, 2002.

[5] J. Z. Sun, J. Sauvola, and D. Howie, “Features in Future: 4G Visions from a Technical Perspective,” in *Proc. IEEE GLOBECOM*, vol. 6, pp. 3533-3537, 2001.

[6] ITU-R M.816, “Framework for Services Supported on International Mobile Telecommunications-2000 (IMT-2000),” 1997.

[7] ITU-R M.1645, “Framework and Overall Objectives of the Future Development of IMT-2000 and Systems beyond IMT-2000,” 2003.

[8] ITU-R M.2134, “Requirements Related to Technical Performance for IMT-Advanced Radio Interface(s),” 2008.

[9] IEEE P802.16m/D4,” Part 16: Air Interface for Fixed and Mobile Broadband Wireless Access Systems,” February 2010.

[10] 3GPP TR36.814 V1.5.0, “Further Advancements for E-UTRA Physical Layer Aspects (Release 9),” November 2009.

[11] R. V. Nee and R. Prasad, OFDM for Wireless Multimedia Communications, *Artech House Publisher*, 2000.

[12] G. J. Foschini, “Layered Space-time Architecture for Wireless Communication in a Fading Environment When Using Multi-element Antennas,” *Bell Lab Technical Journal*, vol. 1, no. 2, pp. 41-59, 1996.

[13] M. Nohara et al, “IEEE 802.16 Tutorial: 802.16 Mobile Multihop Relay,” Official Document of IEEE 802.16 Mobile Multihop Relay Study Group: *IEEE 802.16mmr-06/006*, March 2006.

[14] “IEEE Standard for Local and Metropolitan Area Networks, Part 16: Air interface for fixed and mobile broadband wireless access systems, amendment for physical and medium access control layers for combined fixed and mobile operation in licensed bands,” *IEEE 802.16e-2005*, Feb. 2006.

[15] A. Host-Madsen and J. Zhang, “Capacity Bounds and Power Allocation for Wireless Relay Channel,” *IEEE Transaction on Information Theory,* vol. 51, pp. 2020-2040, June 2005.

[16] A. Host-Madsen, “On the Capacity of Wireless Relaying,” in *Proc. IEEE Vehicle Technology Conference*, vol. 3, pp. 1333-1337, September 2002.

[17] A. Ribeiro, X. Cai and G. B. Giannakis, “Symbol Error Probabilities for General Cooperative Links,” *IEEE Transaction on Wireless Communication,* vol. 4, pp. 1264-1273, May 2005.

[18] E. C. van der Meulen, “Three-terminal Communication Channels,” *Advances in Applied Probability*, vol. 3, pp. 120-154, 1971.

[19] H. Ochiai, P. Mitran and V. Tarokh, “Variable Rate Two Phase Collaborative Communication Protocols for Wireless Networks,” *IEEE Transaction on Information Theory,* vol. 52, pp. 4299-4313, September. 2006.

[20] J. N. Laneman, D. N. C. Tse, and G. W. Wornell, “Cooperative Diversity in Wireless Networks: Efficient Protocols and Outage Behavior,” *IEEE Transaction on Information Theory,* vol. 50, pp. 3062- 3080, December 2004.

[21] N. Ahmed, and B. Aazhang, “Throughput Gains Using Rate and Power Control in Cooperative Relay Networks,” *IEEE Transaction on Communication,* vol. 55, pp. 656 - 660, April 2007.

[22] R. U. Nabar, H. Bolcskei, and F.W. Kneubuhler, "Fading Relay Channels: Performance Limits and Space-time Signal Design," *IEEE Journal on Selected Areas in Communication*, vol. 22, pp. 1099-1109, August 2004.

[23] T. M. Cover and A. El Gamal, "Capacity Theorems for the Relay Channel," *IEEE Transaction on Information Theory*, vol. 25, pp. 572-584, September 1979.

[24] W. Su, A. K. Sadek, and K. J. Ray Liu, "Cooperative Communication Protocols in Wireless Networks: Performance Analysis and Optimum Power Allocation," *Wireless Personal Communication*, vol. 44, pp. 181-217, January 2008.

[25] D. R. Basgeet and Y. C. Chow, "Uplink Performance Analysis for a Relay Based Cellular System," in *Proc. IEEE VTC-2006 Spring*, pp. 132-136, May 2006.

[26] R. Pabst et al., "Relay-based Deployment Concepts for Wireless and Mobile Broadband Radio," *IEEE Communications Magazine*, vol. 42, issue 9, pp. 80- 89, September 2004.

[27] N. Esseling, B. Walke, and R. Pabst, "Performance Evaluation of A Fixed Relay Concept for Next Generation Wireless Systems," *Proc. of IEEE International Symposium on Personal, Indoor and Mobile Radio Communications*, vol. 2, pp.744-751, September 2004.

[28] A. Adinoyi and H. Yanikomeroglu, "Cooperative Relaying in Multi-antenna Fixed Relay Networks," *IEEE Transaction on Wireless Communication*, vol. 6, pp. 533-544, February 2007.

[29] A. Adinoyi et al, "Description of Identified New Relay Based Radio Network Deployment Concepts and First Assessment by Comparison Against Benchmarks of Well Known Deployment Concepts Using Enhanced Radio Interface Technologies," IST-2003-507581 *WINNER D3.2 V.1* , Feb. 2005.

[30] A. Nosratinia, T.E. Hunter and A. Hedayat, "Cooperative Communication in Wireless Networks," *IEEE Communication Magazine*, pp. 74-80, October 2004.

[31] A. Sendonaris, E. Erkip, and B. Aazhang, "User Cooperation Diversity - Part I: System Description," *IEEE Transaction on Communication*, vol. 51, pp. 1927-1938, November 2003.

[32] A. Sendonaris, E. Erkip, and B. Aazhang, “User Cooperation Diversity - Part II: Implementation Aspects and Performance Analysis,” *IEEE Transaction on Communication*, vol. 51, pp. 1939-1948, November 2003.

[33] D. Soldani and S. Dixit, “Wireless Relays for Broadband Access,” *IEEE Communication Magazine*, pp. 58-66, March 2008.

[34] https://www.ist-winner.org

[35] O. Oyman, J.N. Laneman, and S. Sandhu, “Multihop Relaying for Broadband Wireless Mesh Networks: from Theory to Practice,” *IEEE Communication Magazine*, pp.116-122, November 2007.

[36] Y. Yu, S. Murphy and L. Murphy, “Planning Base Station and Relay Station Locations in IEEE 802.16j Multi-hop Relay Networks,” in *Proc. IEEE CCNC’2008*, pp. 922-926, January 2008.

[37] H. Hu, H. Yanikomeroglu, D. D. Falconer and S. Periyalwar, “Range Extension without Capacity Penalty in Cellular Networks with Digital Fixed Relays,” in *Proc. IEEE Global Telecommunications Conference*, pp. 3053-3057, November, 2004.

[38] P. Li, et al., “Spectrum Partitioning and Relay Positioning for Cellular System Enhanced with Two-hop Fixed Relay Nodes,” *IEICE Transaction on Communication*, vol. E90-B, pp. 3181-3188, November 2007.

[39] E. Weiss, S. Max, O. Klein, G. Hiertz and B. Walke, “Relay-based vs. Conventional Wireless Networks: Capacity and Spectrum Efficiency,” in *Proc. IEEE PIMRC*, pp.1-5, September 2007.

[40] H. Zeng and C. Zhu, “System-level Modeling and Performance Evaluation of Multi-hop 802.16j Systems,” in *Proc. IEEE IWCMC*, pp. 354-359, August 2008.

[41] S-J. Kim, et al., “Multi-hop Relay Based Coverage Extension in the IEEE 802.16j Based Mobile WiMAX Systems,” in *Proc. IEEE Networked Computing and Advanced Information Management*, pp. 516-522, September 2008.

[42] C. Hoymann, M. Dittrich, and S. Goebbels, “Dimensioning Cellular Multihop WiMAX Networks,” in *Proc. IEEE Mobile WiMAX Symposium*, pp. 150-157, March

2007.

[43] J. Vidal, N. Marina and A. Host-Madsen, “Dimensioning Cellular Networks with Fixed Relay Stations,” in *Proc. IEEE ICT*, pp. 1-5, June 2008.

[44] B. Lin, et al, “Optimal Relay Station Placement in IEEE 802.16j Networks,” in *Proc. IEEE IWCMC*, pp. 25-30, August 2007.

[45] I. K. Fu, W. H. Sheen and F. C. Ren, “Shadow-assisted Resource Reuse for Relay-augmented Cellular Systems in Manhattan-like Environment,” *International Journal of Electrical Engineering*, vol. 14, No. 1, pp. 11-19, February 2007.

[46] J. Cho, and Z. J. Hass, “On the Throughput Enhancement of the Downstream Channel in Cellular Radio Networks through Multihop Relaying,” *IEEE Journal on Selected Areas in Communications*, vol. 22, No. 7, pp. 1206-1219, September 2004.

[47] R. Pabst, D. Schultz and B. Walke, “Performance Evaluation of a Relay-based 4G Network Deployment with Combined SDMA/OFDMA and Resource Partitioning,” in *Proc. IEEE VTC 2008-Spring*, pp. 2001-2005, May 2008.

[48] S. J. Lin, W. H. Sheen, I K. Fu and C. C. Huang, “Resource Scheduling with Directional Antennas for Multi-hop Relay Networks in a Manhattan-like Environment,” in *Mobile WiMAX*, John Wiley & Sons, April 2008. (ISBN: 9780470519417)

[49] S. J. Lin, W. H. Sheen, and C. C. Huang, “Downlink Performance and Optimization of Relay-assisted Cellular Networks”, in *Proc. IEEE WCNC*, pp.1-6, April 2009.

[50] W. H. Sheen, and S. J. Lin, ”Performance and Optimization of Relay-Assisted OFDMA Networks,” in *Orthogonal Frequency Division Multiple Access Fundamentals and Applications*, CRC Press, Taylor & Francis Group, April 2010. (ISBN: 9781420088243)

[51] W. H. Sheen, S. J. Lin, and C. C. Huang, “Downlink Optimization and Performance of Relay-assisted Cellular Networks in Multi-Cell Environments,” *IEEE Transaction on Vehicular Technology,* accepted January 2010.

[52] V. Genc, S. Murphy, Y. Yu and J. Murphy, “IEEE 802.16j Relay-based Wireless

Access Networks: an Overview," *IEEE Wireless Communications*, pp. 56-63, October 2008.

[53] S.W. Peters and R.W. Heath, "The Future of WiMAX: Multihop Relaying with IEEE 802.16j," *IEEE Communication Magazine*, pp. 104-111, January 2009.

[54] S. Mukherjee and H. Viswanathan, "Analysis of Throughput Gains From Relays in Cellular Networks," in *Proc. IEEE GLOBECOM*, vol. 6, 2005, pp. 3471–3476, December 2005.

[55] B. Walke, and R. Pabst, "Relay-based Deployment Concepts for Wireless and Mobile Broadband Cellular Radio," *WWRF/WG4 Relaying Subgroup White Paper*, June 2003.

[56] B. Walke, H. Wijaya, and D. Schultz, "Layer-2 Relays in Cellular Mobile Radio Networks," in *Proc. IEEE Vehicular Technology Conference*, vol. 1, pp. 81- 85, 2006.

[57] H. Viswanathan, and S. Mukherjee, "Performance of Cellular Networks with Relays and Centralized Scheduling," *IEEE Transaction on Wireless Communications*, vol. 4, issue 5, pp. 2318- 2328, September 2005.

[58] J. Sydir, R. Taori, "An Evolved Cellular System Architecture Incorporating Relay Stations," *IEEE Communication Magazine*, pp.115-121, June 2009.

[59] 3GPP TR 25.996 V6.1.0, "Spatial Channel Model for Multiple Input Multiple Output (MIMO) Simulations," September 2003.

[60] D. Tse and P. Viswanath, Fundamentals of Wireless Communication. *Cambridge University Press*, 2005.

[61] O. Oyman and S. Sandhu, "Non-Ergodic Power-Bandwidth Tradeoff in Linear Multi-hop Networks," in *Proc. IEEE ISIT*, pp. 1514-1518, July 2006.

[62] D. E. Goldberg, Genetic Algorithms in Search, Optimization, and Machine Learning. *Addison-Wesley*, 1989.

[63] R. L. Haupt and S. E. Haupt, Practical Genetic Algorithms. *John Wiley and Sons*, 2004.

[64] K. F. Man, K. S. Tang, and S. Kwong, “Genetic algorithms: concepts and applications,” *IEEE Transaction on Industrial Electronics*, vol. 43, pp. 519-534, October 1996.

[65] E. K. P. Chong and S. H. Zak, An introduction to optimization. *John Wiley and Sons*, 2001.

[66] A. Nix, and M. D. Vose, “Modeling genetic algorithms with Markov chains,” *Annals of Mathematics and Artificial Intelligence*, vol. 5, pp. 79-88, March 1992.

[67] O. Francois, “An Evolutionary Strategy for Global Minimization and its Markov Chain Analysis,” *IEEE Transaction on Evolutionary Computation*, vol. 2, pp. 77-90, September 1998.

[68] E. Visotsky, J. Bae, R. Peterson, R. Berry and M. L. Honig, “On the Uplink Capacity of an 802.16j System,” in *Proc. IEEE WCNC*, pp. 2657-2662, March-April, 2008.

[69] “Baseline Document for Draft Standard for Local and Metropolitan Area Networks, Part 16: Air Interface for Fixed and Mobile Broadband Wireless Access Systems: Multihop Relay Specification”, *IEEE 802.16j-06_026r3*, April 2007.

[70] “IEEE Standard for Local and Metropolitan Area Networks, Part 16: Air Interface for Fixed Broadband Wireless Access Systems,” *IEEE 802.16-2004*, October 2004.

[71] D. Schultz, R. Rabst and T. Irnich, “Multi-hop Radio Network Deployment for Efficient Broadband Radio Coverage,” in *Proc. of WPMC*, vol. 2, pp.377-381, October 2003.

[72] D. Schultz, B. Walke, R. Rabst and T. Irnich, “Fixed and Planned Based Radio Network Deployment Concepts,” in *Proc. of WWRF*, October 2003.

[73] T. Irnich, D. Schultz, R. Pabst, and P. Wienert, “Capacity of A Relaying Infrastructure for Broadband Radio Coverage of Urban Areas,” in *Proc. of IEEE Vehicular Technology Conference*, vol. 5, pp. 2886- 2890, October 2003.

[74] D. S. Baum et al, “Final Report on Link Level and System Level Channel Models” *IST-2003-507581 WINNER D5.4*, V. 1.00, September 2005.

Appendix

In this appendix, we prove the following two lemmas which state the conditions for the best bandwidth allocation in a two-hop path.

Lemma 1: For the fixed-bandwidth allocation w_t to each MS, the highest SE of a two-hop path is achieved with the following bandwidth allocation,

$$w_{B_i \to R_{i,j}}(\vec{m}) = \frac{S_{R_{i,j} \to M}(\vec{m})}{S_{B_i \to R_{i,j}}(\vec{m}) + S_{R_{i,j} \to M}(\vec{m})} \cdot w_t \tag{A.1}$$

and

$$w_{R_{i,j} \to M}(\vec{m}) = \frac{S_{B_i \to R_{i,j}}(\vec{m})}{S_{B_i \to R_{i,j}}(\vec{m}) + S_{R_{i,j} \to M}(\vec{m})} \cdot w_t \tag{A.2}$$

where $S_{B_i \to R_{i,j}}(\vec{m})$ and $S_{R_{i,j} \to M}(\vec{m})$ are the link SE of the $B_i \to R_{i,j}$ link and the $R_{i,j} \to M$ link, respectively.

Proof: Recall that for the fixed-bandwidth allocation, $w_t = w_{B_i \to R_{i,j}}(\vec{m}) + w_{R_{i,j} \to M}(\vec{m})$ for a two-hop path. Let

$$w_{B_i \to R_{i,j}}(\vec{m}) = \left(\frac{S_{R_{i,j} \to M}(\vec{m})}{S_{B_i \to R_{i,j}}(\vec{m}) + S_{R_{i,j} \to M}(\vec{m})} + \alpha \right) \cdot w_t \tag{A.3}$$

be the bandwidth allocated to the $B_i \to R_{i,j}$ link, where $0 \le \alpha \le 1$. Then, the bandwidth for the $R_{i,j} \to M$ link is

$$w_{R_{i,j}\to M}(\vec{m}) = \left(\frac{S_{B_i\to R_{i,j}}(\vec{m})}{S_{B_i\to R_{i,j}}(\vec{m}) + S_{R_{i,j}\to M}(\vec{m})} - \alpha \right) \cdot w_t \tag{A.4}$$

Thus, the throughput for the $B_i \to R_{i,j}$ link and the $R_{i,j} \to M$ link is given respectively by

$$t_{B_i\to R_{i,j}}(\vec{m}) = \left(\frac{S_{R_{i,j}\to M}(\vec{m})}{S_{B_i\to R_{i,j}}(\vec{m}) + S_{R_{i,j}\to M}(\vec{m})} + \alpha \right) \cdot w_t \cdot S_{B_i\to R_{i,j}}(\vec{m}) \tag{A.5}$$

and

$$t_{R_{i,j}\to M}(\vec{m}) = \left(\frac{S_{B_i\to R_{i,j}}(\vec{m})}{S_{B_i\to R_{i,j}}(\vec{m}) + S_{R_{i,j}\to M}(\vec{m})} - \alpha \right) \cdot w_t \cdot S_{R_{i,j}\to M}(\vec{m}) \tag{A.6}$$

Since $t_{B_i\to R_{i,j}\to M}(\vec{m}) = \min\left\{ t_{B_i\to R_{i,j}}(\vec{m}), t_{R_{i,j}\to M}(\vec{m}) \right\}$,

$$t_{B_i\to R_{i,j}\to M}(\vec{m}) \le \left(\frac{S_{B_i\to R_{i,j}}(\vec{m}) \cdot S_{R_{i,j}\to M}(\vec{m})}{S_{B_i\to R_{i,j}}(\vec{m}) + S_{R_{i,j}\to M}(\vec{m})} \right) \cdot w_t \tag{A.7}$$

The right side of (A-7) is obtained by setting $\alpha = 0$ in (A.1) and (A.2), i.e.,

$$w_{B_i\to R_{i,j}}(\vec{m}) = \frac{S_{R_{i,j}\to M}(\vec{m})}{S_{B_i\to R_{i,j}}(\vec{m}) + S_{R_{i,j}\to M}(\vec{m})} \cdot w_t \tag{A.8}$$

and

$$w_{R_{i,j}\to M}(\vec{m}) = \frac{S_{B_i\to R_{i,j}}(\vec{m})}{S_{B_i\to R_{i,j}}(\vec{m}) + S_{R_{i,j}\to M}(\vec{m})} \cdot w_t \tag{A.9}$$

With $\alpha = 0$, we have the maximum throughput of two-hop path

$$t_{B_i\to R_{i,j}\to M}(\vec{m}) = t_{B_i\to R_{i,j}}(\vec{m}) = t_{R_{i,j}\to M}(\vec{m}) = \frac{S_{B_i\to R_{i,j}}(\vec{m}) \cdot S_{R_{i,j}\to M}(\vec{m})}{S_{B_i\to R_{i,j}}(\vec{m}) + S_{R_{i,j}\to M}(\vec{m})} \cdot w_t \tag{A.10}$$

Lemma 2: For the fixed-throughput allocation, the highest SE of a two-hop path to achieve the target throughput t_t is obtained with the following bandwidth allocation,

$$w_{B_i \to R_{i,j}}(\vec{m}) = \frac{t_t}{S_{B_i \to R_{i,j}}(\vec{m})} \tag{A.11}$$

and

$$w_{R_{i,j} \to M}(\vec{m}) = \frac{t_t}{S_{R_{i,j} \to M}(\vec{m})} \tag{A.12}$$

Proof: Since $t_{B_i \to R_{i,j} \to M}(\vec{m}) = \min\left\{t_{B_i \to R_{i,j}}(\vec{m}), t_{R_{i,j} \to M}(\vec{m})\right\}$, one needs to have

$$t_{B_i \to R_{i,j}}(\vec{m}) = S_{B_i \to R_{i,j}}(\vec{m}) \cdot w_{B_i \to R_{i,j}}(\vec{m}) \geq t_t \tag{A.13}$$

and

$$t_{R_{i,j} \to M}(\vec{m}) = S_{R_{i,j} \to M}(\vec{m}) \cdot w_{R_{i,j} \to M}(\vec{m}) \geq t_t \tag{A.14}$$

The proof follows immediately from (A.13) and (A.14).

Vita

Shiang-Jiun Lin was born in Taichung, Taiwan. She received the B.S. degree in computer science and information engineering and the M.S. and Ph.D. degrees in communication engineering from the National Chiao Tung University, Hsinchu, Taiwan, in 2000, 2002, and 2010, respectively.

In 2007, she was a summer intern in the Communication Networks (ComNets) Research Group at RWTH Aachen University in Germany. In 2008, she was a Visiting Scholar with the Department of Electrical Engineering, University of Washington, Seattle, WA, USA. Her research interests include wireless communication networks, relaying communication technology, and optimizations for wireless communication systems.